VARIATIONAL BOUSSINESQ MODELLING OF SURFACE GRAVITY WAVES OVER BATHYMETRY

Gert Klopman

The research presented in this thesis has been performed within the group of Applied Analysis and Mathematical Physics (AAMP), Department of Applied Mathematics, University of Twente, PO Box 217, 7500 AE Enschede, The Netherlands.

Cover design by Esther Ris, www.e-riswerk.nl

Printed by Wöhrmann Print Service, Zutphen, The Netherlands.

ISBN 978-90-365-3037-8

DOI 10.3990/1.9789036530378

VARIATIONAL BOUSSINESQ MODELLING OF SURFACE GRAVITY WAVES OVER BATHYMETRY

PROEFSCHRIFT

ter verkrijging van
de graad van doctor aan de Universiteit Twente,
op gezag van de rector magnificus,
prof. dr. H. Brinksma,
volgens besluit van het College voor Promoties
in het openbaar te verdedigen op
donderdag 27 mei 2010 om 13.15 uur

door

Gerrit Klopman

geboren op 25 februari 1957
te Winschoten

Dit proefschrift is goedgekeurd door de promotor
prof. dr. ir. E.W.C. van Groesen

Aan mijn moeder

Contents

Samenvatting

Golven, zichtbaar aan het wateroppervlak van zeeën en oceanen, worden opgewekt door de wind. Onder het golvende oppervlak is het water in een oscillerende beweging, en wel het sterkst dichtbij het wateroppervlak. Het water wordt teruggedrongen naar de evenwichtsstand – een horizontaal glad oppervlak – door de zwaartekracht.[1]

De zwaartekrachtsversnelling verandert de snelheid van het water. Hierbij sluit de onsamendrukbaarheid van het water bewegingen uit, die leiden tot volumeveranderingen van de waterpakketjes. De massatraagheid van het water leidt ertoe dat het wateroppervlak door de evenwichtsstand heenschiet, waarna de zwaartekracht de verticale waterbeweging vertraagt. Totdat de verticale snelheid van een waterpakketje momentaan nul is (in een verticale positie uit de evenwichtsstand) en er een nieuwe cyclus begint.

Zolang ze niet breken, is de demping van (langere) zeegolven zeer klein (zie de inleiding in hoofdstuk 1). In goede benadering is de Hamiltoniaan – de totale energie, zijnde de som van de potentële en kinetische energie – dan constant. Voor een wrijvingsvrije stroming kan de waterbeweging worden gemodelleerd met behulp van een Hamiltoniaanse beschrijving. Hierin is de potentiële energie ten gevolge van de zwaartekracht eenvoudig exact te modelleren, maar de (dieptegeïntegreerde) kinetische energie kan alleen via benaderingen beschreven worden. Deze benaderingen van de kinetische energie leiden gemakkelijk tot formuleringen waarbij de energie niet meer gegarandeerd positief is. En dat kan aanleiding geven tot ongewenste niet-fysische instabiliteiten in de resulterende modellen.

In dit proefschrift wordt een methode beschreven om te komen tot een variationeel model met gegarandeerd positieve Hamiltoniaan (som van kinetische en potentiële energie). Hierbij wordt de waterbeweging onder het wateroppervlak benaderend beschreven, door het maken van aannames over de verticale structuur van de stroomsnelheden, op een wijze zoals voor het eerst toegepast door Joseph Valentin Boussinesq (1842–1929) voor vrij lange oppervlaktegolven in ondiepe zeeën. De daarna gebruikte integratie over de diepte van het water leidt tot een vereenvoudiging van de modellen: in plaats van een drie-dimensionale beschrijving resulteert een tweedimensionaal model in het horizontale vlak, oftewel in de golfvoortplantingsruimte.

In het proefschrift wordt de methodiek uitgelegd, die leidt tot een benaderende en positieve Hamiltoniaan, alsmede de (lineaire) voortplantings- en reflectie-eigenschappen

[1] En voor korte rimpelingen wordt het wateroppervlak ook in grote mate naar een recht vlak getrokken door de oppervlaktespanning (capillariteit), maar zulke capillaire golven vallen buiten het onderwerp van dit proefschrift).

van de resulterende golfmodellen. Deze golfmodellen voldoen aan dieptegeïntegreerd behoud van zowel massa als energie. En voor een horizontale bodem ook aan dieptegeïntegreerd behoud van horizontale impuls. Tevens is er behoud van golfactie, als een direct gevolg van de variationele beschrijvingswijze.

De eigenschappen van het volledig niet-lineaire model – zonder benaderingen ten aanzien van de grootte van de golfhoogte – worden beschouwd door het uitvoeren van numerieke simulaties. Vergelijking met de resultaten uit andere modellen, alsmede uit laboratoriumexperimenten, toont de niet-lineaire kwaliteiten van de variationele Boussinesq modellering. De modelsimulaties blijken bovendien allen (numeriek) stabiel te zijn, hetgeen kan worden toegeschreven aan de gegarandeerde positiviteit van de golfenergie (Hamiltoniaanse dichtheid).

Summary

Waves, as visible on the surface of seas and oceans, are generated by wind. Below the wavy surface the water is in an oscillatory motion, which is strongest nearer to the surface. The water is forced back towards its equilibrium position – a smooth horizontal surface – by gravity.[2]

The gravitational acceleration changes the fluid flow velocity. The incompressibility of the water constraints the motion to those which do not result in volume changes of the fluid parcels. The fluid's inertia results in the water surface flipping through its equilibrium position. After which gravity decelerates the vertical fluid motion. Until the vertical velocity of a fluid parcel is momentarily zero (in a non-equilibrium vertical position) and a new cycle starts.

Without breaking, the attenuation of (longer) sea waves is very small (see the introduction in Chapter 1). To good approximation the Hamiltonian – the total energy, *i.e.* the sum of potential and kinetic energy – is a constant in the non-breaking wave case. For a frictionless flow the water motion can be modelled through a Hamiltonian description. The exact modelling of gravity's potential energy is easily performed, but (depth-integrated) kinetic energy can only be described trough using approximations. These kinetic-energy approximations easily result in formulations which no longer guarantee the positivity of the energy. Which may result in spurious non-physical instabilities of the such-derived models.

In this thesis a method is presented to construct a variational model with an always positive Hamiltonian (sum of kinetic and potential energy). In this methodology the fluid motion beneath the surface is approximated, by making assumptions on the vertical structure of the flow velocities, in a fashion as first applied by Joseph Valentin Boussinesq (1842–1929) for the description of fairly-long surface waves in shallow water. The subsequent integrations over the total water depth result in simplified models: instead of a three-dimensional description, the result is a two-dimensional model in the horizontal plane, denoted as the propagation space.

The thesis presents the methodology resulting in an approximate and positive Hamiltonian, as well as the (linear) propagation and reflection characteristics of the associated wave models. These models conserve depth-integrated mass and energy. And in case of a horizontal sea bed, also depth-integrated horizontal momentum is conserved. Besides, wave action is conserved as a direct consequence of the variational description of the flow.

[2] In case of short ripples the surface is also straightened by surface tension, but capillary waves are outside the scope of this thesis.

The properties of the fully non-linear model – without assumptions regarding the relative wave height – are studied through numerical simulations. Comparison with the results from other models, as well as from laboratory experiments, show the non-linear capacities of the variational Boussinesq modelling. Besides, model simulations are all numerically stable, which may be attributed to the guaranteed positivity of the wave energy (Hamiltonian density).

Acknowledgements

This thesis is based on work performed at the group of Applied Analysis and Mathematical Physics (AAMP) of the Department of Applied Mathematics at the University of Twente. Which work is in part funded by the University of Twente and by LabMath Indonesia, and I am very grateful for the research opportunities offered.

I deeply appreciate the support, stimulation and guidance of Brenny van Groesen during this research, as well as all the support from and discussions with staff and students of the groups of AAMP and NACM at the University. The discussions with colleagues at Witteveen+Bos Rotterdam, MARIN Wageningen, Deltares and Alkyon during the course of this research are highly appreciated.

Further I like to express my gratitude to Kees Vreugdenhil, Eco Bijker, Walt Massie, Jan Karel Kostense, Maarten Dingemans and Marcel Stive for teaching me the profession. And to my parents for their support during my education.

Many thanks go to my friends and family, for their support during this research as well as everywhere else. Especially, I deeply thank Carmen Comvalius for her stimulation to finish this project. And many thanks to Esther Ris for designing the cover, which I like very much.

Chapter 1

Introduction

1.1 General

Waves at the water surface of the oceans, seas and lakes are generated by the wind, in general. The waves propagate under the influence of the Earth's gravity.[1] While propagating, surface gravity waves only decay slowly due to viscous effects (Lighthill, 1978, pp. 232–235), as can be seen in Figure 1.1. For instance, a periodic wave with 10 metre wavelength has been reduced to 61% of its original amplitude after travelling over a distance of 125 thousand wavelengths. Further, the main interest of this thesis *are* the energetic waves, as occurring in the sea and near the coast, with wavelengths in excess of a metre. So, while propagating in deep water, dissipation is very small: mainly being due to whitecapping in steep waves. In shallower water, with water depths less than half the wavelength, dissipation is enhanced by bottom friction, but still very small. Only near the coast – in the surf zone – waves decay rapidly by dissipation due to wave breaking.

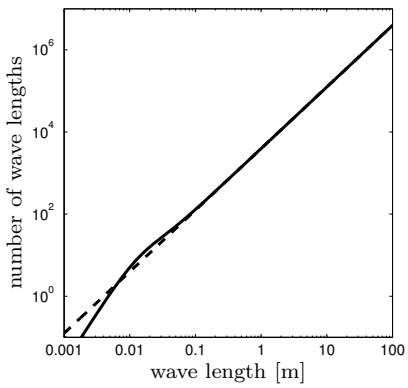

Figure 1.1: Number of wavelengths after which the wave energy-density of gravity–capillary waves in water of infinite depth has attenuated by a factor of $1/e \approx 0.37$, and equivalently the wave amplitude is reduced by a factor of $1/\sqrt{e} \approx 0.61$.

When using mathematical physics to model the propagation and transformation of water waves, the smallness of the dissipation – as encountered in many situations – has to be reflected in the wave model, for it to be of practical value. The approach used within this thesis is based on the application of variational methods, and posing a priori that wave energy is conserved.

Water wave models, at the present moment, can largely be classified into three categories, based on the proportions of the specific problem under consideration:

[1] Except for very short wave-components – with wavelengths less than a few decimetres – which are influenced by surface tension effects.

Three-dimensional wave modelling: as required when the dimensions of the objects under consideration are of the order of the wavelength. An example is the study of ship motion by sea waves.

Wave-energy models: which describe the generation and propagation of phase-averaged energy-density in two horizontal dimensions. These are applicable in situations where the wavelength is small compared to the typical distances over which the bathymetry (sea-bed topography) varies. This is typical for studying the transformation of the wave conditions from the open sea to near the coast.

Phase-resolving wave models: for two-dimensional horizontal (2DH) propagation and transformation of the waves. The effects of the vertical structure of the flow underneath the free surface are captured in an enhanced 2DH description – as compared to the shallow water equations, valid for very long waves like *e.g.* tidal motion. For this category of models to be applicable, the wavelength has to be of the same order (or smaller) as the typical length scales over which bathymetry, coastline and man-made structures significantly vary. Boussinesq-like wave models, as often applied for instance in the computation of wave motion in and near harbours and coasts, are within this category.

The first category considers three-dimensional wave modelling, while the second and third contain 2DH models. Further, the first and third category involve phase-resolving water-wave models, while the second category is phase averaged. In phase averaging, the details – of the time series for the wave motion – are lost.

This thesis focusses on Boussinesq-like models, which are within the last category of 2DH phase-resolving models. The motivation for their derivation lies in the fact, that often water waves propagate horizontally, while the vertical structure of the flow is not wave like. The horizontal space is then called the *propagation space*, while the vertical space is called the *cross space*. In Boussinesq-like models an approximate vertical structure of the flow is used to eliminate the cross space. The result is a 2DH model in propagation space. Main challenges when deriving a Boussinesq-like wave model come from the following issues:

Frequency dispersion: water waves exhibit frequency dispersion, *i.e.* wave components with different wavelength travel at different propagation speeds. Classical Boussinesq-like models are limited to long waves – having wavelengths much longer than the water depth. Starting with Witting (1984), there is an ongoing search for Boussinesq-like models applicable to waves in deeper water.

Non-linearity: especially in shallower water, the waves exhibit strong non-linearity, visible in flat troughs and sharp wave crests, see Figure 1.2. While in classi-

Figure 1.2: A periodic wave solution to the variational Boussinesq model (VBM), Eqs. (1.14) with a parabolic shape function (1.9) for the vertical flow structure. The mean water depth is 5 m, the wave height is 1.8 m and the period is 6 s.

cal Boussinesq-like models there are approximations regarding the non-linear terms, there are also models now without these approximations.

Mass, momentum and energy conservation: if dissipation is neglected, the Euler equations for fluid flow are conserving mass, momentum and energy. Preferably these characteristics are also transferred to the Boussinesq-like model under the approximations imposed in the process of constructing the model. Note that in a 2DH model depth-integrated horizontal momentum is only conserved in case of a horizontal sea bed.

High-order spatial derivatives: as often encountered in Boussinesq-like models may pose problems for the numerical implementation of the model. Their order should be as low as possible from the point of view of practical application of the model.

Mixed space–time derivatives: regularly occur in such models. Their treatment can put challenges for the numerical modelling of the system.

Stability: the model stability is an important issue for its applicability. One important mathematical–physical factor regarding stability is that the energy (Hamiltonian) in the model is positive definite – *i.e.* positive for all possible values of the constituent variables. Several forms of Boussinesq-like models exist which have negative energy for wave components of very short wavelength, being unstable when in numerical implementations the grid spacing is refined.

Bottom slopes: are often mild in coastal regions, which allow for associated approximations in the modelling. However, also steeper slope may occur. The bathymetry also introduces reflections; the correct predictions of these are also influenced by the approximate treatment of the bottom slope in the model.

Numerical treatment: although not a direct part of the mathematical–physical model, both the amenability of the Boussinesq-like model to numerical implementation – as well as the numerical modelling itself – are of importance for the practical application of the model.

These aspects are treated in the remainder of this thesis, especially with respect to the present variational approach for Boussinesq-like wave models with positive-definite Hamiltonian. The latter property is important since it contributes to the good dynamical behaviour of the resulting model equations.

In this introduction we first discuss the variational principles for surface gravity waves (§1.2). Thereafter, in §1.3, an overview is given of the present contributions with respect to the use of variational principles for Boussinesq-like wave modelling with positive-definite Hamiltonian. In §1.4 these present contributions are set within the context of surface gravity wave modelling. And in §1.5 an outline is given on the other chapters in this thesis.

1.2 Variational principles for water waves

As discovered by Zakharov (1968), and rediscovered by Broer (1974) and Miles (1977), the mathematical–physical description of waves on the surface of a homogeneous fluid – performing an incompressible and irrotational flow – has a Hamiltonian structure. Besides gravity *e.g.* surface tension can be considered as a restoring force. But here only gravity is taken into account, since the primary interest is in coastal and ocean engineering applications.

Because the waves propagate horizontally, the Cartesian coordinate system which is used distinguishes between a horizontal coordinate vector $\boldsymbol{x}$ (with components x_1 and x_2) and vertical coordinate z. The positive z-direction is upward, *i.e.* opposite to the direction of the gravitational acceleration vector – which has length g. The fluid region is bounded below by an impermeable bed at $z = -h_0(\boldsymbol{x})$, and above by the free surface located at $z = \zeta(\boldsymbol{x}, t)$. Further t denotes time.

As said, the fluid is assumed to be incompressible and homogeneous, so its density ρ is a constant. The irrotational flow can be described with a velocity potential $\Phi(\boldsymbol{x}, z, t)$: the horizontal velocity is $\boldsymbol{\nabla}\Phi$ with $\boldsymbol{\nabla}$ the horizontal gradient operator, and $\partial_z\Phi$ is the vertical velocity component with ∂_z denoting the partial derivative with respect to z (and likewise ∂_t with respect to time t).

The Hamiltonian density H is the sum of the kinetic and potential energy per unit of horizontal area, and the Hamiltonian $\mathscr{H}$ is the integral of H over horizontal space:[2]

$$H = \rho \int_{-h_0}^{\zeta} \frac{1}{2} \left\{ (\boldsymbol{\nabla}\Phi)^2 + (\partial_z\Phi)^2 \right\} \mathrm{d}z \; + \; \frac{1}{2}\rho\, g\, \zeta^2 \quad \text{and} \quad \mathscr{H} = \iint H \, \mathrm{d}\boldsymbol{x}, \tag{1.1}$$

where with $(\boldsymbol{\nabla}\Phi)^2$ is meant the dot product $(\boldsymbol{\nabla}\Phi) \cdot (\boldsymbol{\nabla}\Phi)$. Under the constraints that:

- the velocity potential $\Phi(\boldsymbol{x}, z, t)$ satisfies the Laplace equation $\boldsymbol{\nabla}\cdot\boldsymbol{\nabla}\Phi + \partial_z^2\Phi = 0$ in the fluid interior – because of the incompressible and irrotational flow – as well as
- the impermeability condition $\partial_n\Phi = 0$ for the velocity component normal to the bed at $z = -h_0(\boldsymbol{x})$, and provided
- the velocity potential at the free surface is equal to $\varphi(\boldsymbol{x}, t) = \Phi(\boldsymbol{x}, \zeta(\boldsymbol{x}, t), t)$,

the Hamiltonian $\mathscr{H}(\zeta, \varphi)$ is a functional of the surface elevation $\zeta(\boldsymbol{x}, t)$ and the surface potential $\varphi(\boldsymbol{x}, t)$. These constraints follow directly from requiring the variational derivative to satisfy

$$\frac{\delta\mathscr{H}}{\delta\Phi} = 0 \tag{1.2}$$

[2] The potential energy density per unit of horizontal area is

$$\int_{-h_0}^{\zeta} \rho\, g\, z \, \mathrm{d}z = \tfrac{1}{2}\rho\, g\, (\zeta^2 - h_0^2).$$

But since the zero-level of the potential energy does not influence the dynamics – forces being the gradient of the potential energy – the term with h_0^2 is dynamically insignificant.

for arbitrary variations $\delta\Phi$ in the fluid interior and along the bed, while specifying $\Phi(\boldsymbol{x}, \zeta, t) = \varphi$ at the free surface.

Now – under the above side conditions – the dynamics of the canonical variables $\zeta(\boldsymbol{x}, t)$ and $\varphi(\boldsymbol{x}, t)$ is given by (Zakharov, 1968; Broer, 1974; Miles, 1977):

$$\rho\,\partial_t\zeta - \frac{\delta\mathscr{H}}{\delta\varphi} = 0 \qquad \text{and} \tag{1.3a}$$

$$\rho\,\partial_t\varphi + \frac{\delta\mathscr{H}}{\delta\zeta} = 0, \tag{1.3b}$$

As shown by Miles (1977) (see also Milder, 1977), there is a direct correspondence between the above Hamiltonian representation and the variational formulation in terms of a Lagrangian $\mathscr{L}(\zeta, \Phi)$ by Luke (1967):

$$\mathscr{L} = -\rho \int \iint \left\{ \int_{h_0}^{\zeta} \left[\partial_t\Phi + \frac{1}{2}\left(\boldsymbol{\nabla}\Phi\right)^2 + \frac{1}{2}\left(\partial_z\Phi\right)^2 + g\,z \right] \mathrm{d}z \right\} \mathrm{d}\boldsymbol{x}\;\mathrm{d}t. \tag{1.4}$$

Luke (1967) shows that both the Laplace equation in the fluid interior and the boundary conditions at the free surface and bed follow from the variations of $\mathscr{L}$ with respect to Φ and ζ. By using the Bernoulli equation[3] the Lagrangian $\mathscr{L}$ can be shown to be equal to the integral of the fluid pressure $p(\boldsymbol{x}, z, t)$. This observation has before been made by Bateman (1929) for the (rotational) Euler equations, but without a free surface.

The correspondence between Luke's Lagrangian formulation and the Hamiltonian one becomes clear by expressing the Lagrangian (1.4) – integrating out the $\partial_t\Phi$ term to the boundary of the time domain using Leibnitz integral rule – as (Miles, 1977):

$$\mathscr{L} = \int \left[\rho \iint \left(\varphi\,\partial_t\zeta\right)\,\mathrm{d}\boldsymbol{x} \;-\; \mathscr{H} \right] \mathrm{d}t, \tag{1.5}$$

dropping the dynamically uninteresting terms, *i.e.* the volume integral of Φ itself and the horizontal-space integral of $-\frac{1}{2}\rho g h_0^2$. The variation of $\mathscr{L}$ with respect to ζ and Φ now directly leads to the Hamiltonian system (1.3), as well as the Laplace equation for Φ in the fluid interior and the impermeability boundary condition at the bed $z = -h_0$.

Further information on Hamiltonian dynamics and water waves can be found in several reviews and the references therein, *e.g.* Radder (1999), Dingemans (1997, §5.6), van Groesen & de Jager (1994, Part I), Shepherd (1990), Salmon (1988*a*) and Benjamin & Olver (1982).

[3]The Bernoulli equation for this unsteady potential flow is:

$$\partial_t\Phi + \tfrac{1}{2}\left(\boldsymbol{\nabla}\Phi\right)^2 + \tfrac{1}{2}\left(\partial_z\Phi\right)^2 + \frac{p}{\rho} + gz = 0.$$

1.3 Present contributions

1.3.1 Motivation

My inspiration for and interest into a variational description of Boussinesq-type wave models with positive-definite Hamiltonian has been triggered by the work described in Dingemans (1997, §5.6) (see also Radder, 1999; Mooiman & Verboom, 1992). The described Hamiltonian approach expands on the method as founded by Broer (1974, 1975), Broer *et al.* (1976) and van Groesen (1978). My feeling and hope then – in the 1990's – was that a more systematic and simpler approach should be possible to construct such a model.

When looking into the paper of Miles (1977) on deriving the Hamiltonian dynamics of surface waves in late 2004, his Lagrangian formulation (Miles, 1977, Eq. (1.2), see above Eq. (1.5)) – equivalent to Luke's variational principle (1.4) – brought up the idea to directly apply a Ritz method to the vertical structure of the velocity potential $\Phi(\boldsymbol{x}, z, t)$. In the Ritz method, a limited number of trial functions with parameters is used for the description of the flow:

$$\begin{aligned}\Phi(\boldsymbol{x}, z, t) &= f_0(z)\,\psi_0(\boldsymbol{x}, t) + f_1(z)\,\psi_1(\boldsymbol{x}, t) + \cdots + f_M(z)\,\psi_M(\boldsymbol{x}, t) \\ &= \sum_{m=0}^{M} f_m(z)\,\psi_m(\boldsymbol{x}, t),\end{aligned} \tag{1.6}$$

with specified shape functions f_m and yet to be determined parameters $\psi_m(\boldsymbol{x}, t)$, $m = 0, 1, \cdots, M$. If this approximation is used directly into the variational principle, the positivity of the Hamiltonian $\mathscr{H}$ will be retained. The Hamiltonian now has to fullfill, instead of $\delta\mathscr{H}/\delta\Phi = 0$, the additional constraints:

$$\frac{\delta\mathscr{H}}{\delta\psi_m} = 0, \qquad \text{for } m = 0, 1, \cdots, M. \tag{1.7}$$

However, in general the Ritz method will also lead to the appearance of time derivatives of all parameters $\psi_m(\boldsymbol{x}, t)$, $m = 0, 1, \cdots, M$ in the resulting dynamical equations. As a result, the canonical structure of the Hamiltonian system is lost. However, if **all but one** – say for $m = 0$ – of the shape functions f_m are taken to be zero at the free surface, then the canonical structure (1.3) is regained, with $\varphi(\boldsymbol{x}, t) = \psi_0(\boldsymbol{x}, t)$ provided $f_0(\zeta) = 1$ is demanded (without loss of generality) at the free surface $z = \zeta(\boldsymbol{x}, t)$.

An important conservation law is the conservation of mass. If one only takes one shape function f_0, so $M = 0$, *e.g.* like in the Hamiltonian approach to derive the so-called mild-slope equation of Eckart (1952) and Berkhoff (1972, 1976) (see Dingemans, 1997, pp. 250–255), the resulting equations are in general not mass conserving, in a depth averaged sense. For surface gravity waves on a potential flow, mass conservation follows from invariance with respect to the base level of the velocity potential (Benjamin & Olver, 1982; Radder, 1999), by Noether's theorem. Hence, this property has to be retained, when applying the Ritz method, to obtain depth-averaged mass conservation. This requires that the approximations to the

flow velocity $(\boldsymbol{\nabla}\Phi, \partial_z\Phi)$ – as applied in the variational principle – do not depend on $\psi_0 \equiv \varphi$ itself, but only on its derivatives. As a result, **one has to take $f_0 = 1$** in order to transfer depth-averaged mass conservation to the approximate flow model. Now the case $M = 0$ gives the shallow water equations, which is very often inadequate for the description of surface gravity waves.

1.3.2 Variational Boussinesq-type model for one shape function

The simplest model of practical interest has one additional shape function ($M = 1$):

$$\Phi(\boldsymbol{x}, z, t) = \varphi(\boldsymbol{x}, t) + f(z; h_0, \zeta, \kappa)\, \psi(\boldsymbol{x}, t), \tag{1.8}$$

dropping the index 1 from f and ψ, for ease of notation. In order to accomodate the propagation of waves over water layers of varying depth, the vertical structure f is taken to be also a function of depth h_0, surface elevation ζ and possibly an additional parameter κ. All three vary with horizontal space $\boldsymbol{x}$, and at least the surface elevation also varies with time t. The additional parameter $\kappa(\boldsymbol{x})$ can for instance be a characteristic wave number of the (anticipated) solution (ζ, φ, ψ) determining the curvature of the shape function (*e.g.* in case f has a hyperbolic cosine form as occurring in Airy wave theory). Normally, the shape function will be of the form $f(z + h_0; h_0 + \zeta, \kappa)$, only dependent on the distance $h_0 + z$ above the bed, the total water depth $h_0 + \zeta$ and the shape parameter κ. The two forms considered into more detail in this thesis are, first, the parabolic shape function:

$$f^{(p)} = \frac{1}{2}\,\frac{(h_0 + z)^2 - (h_0 + \zeta)^2}{h_0 + \zeta} = \frac{1}{2}\,(z - \zeta)\,\frac{2h_0 + z + \zeta}{h_0 + \zeta}, \tag{1.9}$$

inspired by the parabolic shape function of classical Boussinesq theory, as valid for long waves. And second, the hyperbolic cosine based on Airy wave theory:

$$f^{(c)} = \cosh\left[\kappa\,(h_0 + z)\right] - \cosh\left[\kappa\,(h_0 + \zeta)\right], \tag{1.10}$$

with κ a shape parameter, characterizing the curvature of the shape function. Both forms – parabolic and hyperbolic cosine – are chosen in accordance with the homogeneous case of a horizontal bed, *i.e.* $\partial_z f = 0$ at $z = -h_0$.

The approximate horizontal and vertical flow velocities become, using (1.8):

$$\boldsymbol{\nabla}\Phi \approx \boldsymbol{\nabla}\varphi + f\,\boldsymbol{\nabla}\psi + \Big[\,(\partial_\zeta f)\;\boldsymbol{\nabla}\zeta + \big(\partial_{h_0} f\big)\;\boldsymbol{\nabla}h_0 + (\partial_\kappa f)\;\boldsymbol{\nabla}\kappa\Big]\;\psi, \tag{1.11a}$$

$$\partial_z\Phi \approx (\partial_z f)\;\psi. \tag{1.11b}$$

These are thereafter applied in the Hamiltonian (1.1). Note that additional approximations can be made to the velocities (1.11), before inserting them into the Hamiltonian, without losing its postive definiteness. Approximations made afterwards – to the Hamiltonian or the resulting dynamical equations – will easily lead to loss of positivity of $\mathscr{H}$. The dynamical equations resulting from the Hamiltonian description become simpler when a quasi-homogeneous approximation is made, neglecting the effects of bed slope $\boldsymbol{\nabla}h_0$ and parameter variations $\boldsymbol{\nabla}\kappa$:

$$\boldsymbol{\nabla}\Phi \approx \boldsymbol{\nabla}\varphi + f\,\boldsymbol{\nabla}\psi + (\partial_\zeta f)\,\psi\,\boldsymbol{\nabla}\zeta \qquad \text{and} \qquad \partial_z\Phi \approx (\partial_z f)\;\psi, \tag{1.12}$$

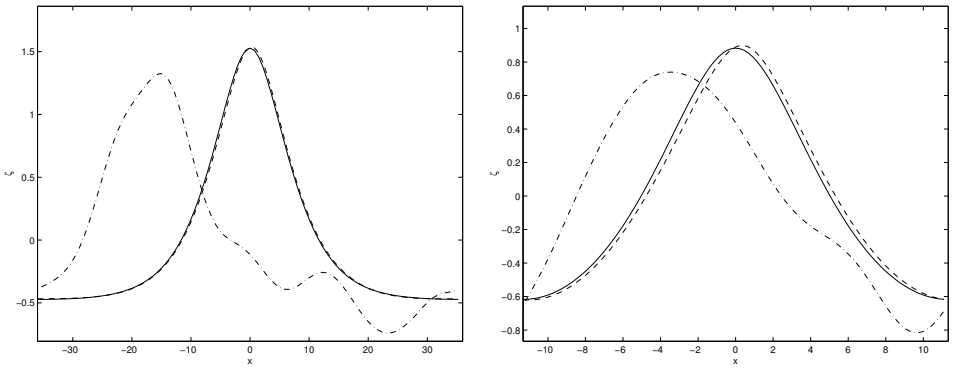

(a) $\tau = 10$ s, $H_w = 2.0$ m. **(b)** $\tau = 4$ s, $H_w = 1.5$ m.

Figure 1.3: Snapshots of the free-surface elevation $\zeta(x, 5\tau)$ for periodic waves above a horizontal bed after five periods. The results are for the fully non-linear model (dash–dash line), the weakly non-linear model (dash–dot line, neglecting $\boldsymbol{\nabla}\zeta$ in the velocity (1.12)) and the high-accuracy Rienecker & Fenton (1981) solution (solid line). The mean water depth is 5 m, gravitational acceleration is $g = 9.81$ m/s^2, τ is the period and H_w is the wave height.

In the remainder, this quasi-homogeneous approximation is referred to as 'mild-slope approximation'. Additional neglect of the free-surface slope $\boldsymbol{\nabla}\zeta$ leads to an unsatisfactory performance of the resulting equations for waves of higher amplitude (Klopman *et al.*, 2005), see Figure 1.3. The use of (1.12) produces a Boussinesq-type model which is fully non-linear: in the sense that no approximations are made with respect to surface slope and excursions.

The resulting positive-definite Hamiltonian density, using Eqs. (1.1) and (1.12), is (Klopman *et al.*, 2010):

$$\begin{aligned}\frac{1}{\rho}\,H = \frac{1}{2}\,(h_0+\zeta)\,(\boldsymbol{\nabla}\varphi)^2 + \frac{1}{2}\,g\,\zeta^2 + \frac{1}{2}\,F\,(\boldsymbol{\nabla}\psi)^2 + \frac{1}{2}\,\Big[K + G\,(\boldsymbol{\nabla}\zeta)^2\Big]\,\psi^2 \\ + P\,(\boldsymbol{\nabla}\psi)\cdot(\boldsymbol{\nabla}\varphi) + Q\,\psi\,(\boldsymbol{\nabla}\varphi)\cdot(\boldsymbol{\nabla}\zeta) + R\,\psi\,(\boldsymbol{\nabla}\psi)\cdot(\boldsymbol{\nabla}\zeta)\,,\end{aligned} \tag{1.13}$$

with integral parameters $F(\zeta, h_0; \kappa)$, $G(\zeta, h_0; \kappa)$, $K(\zeta, h_0; \kappa)$, $P(\zeta, h_0; \kappa)$, $Q(\zeta, h_0; \kappa)$ and $R(\zeta, h_0; \kappa)$ – given in the Appendix of Klopman *et al.* (2010), see Chapter 2 – all dependent on the surface elevation $\zeta(\boldsymbol{x}, t)$, which is important when taking the variations. The first two terms on the right are the familiar ones for the shallow water equations. For the parabolic shape function, Eq. (1.9), the positive-definiteness of the resulting Hamiltonian density can directly be made visible by writing it as a sum of squares, see Eq. (2.10).

Variation of $\mathscr{H}$ with respect to ζ, φ and ψ then gives the approximate dynamical equations for the variational Boussinesq model (VBM), using (1.3) and (1.2):

$$\partial_t\zeta + \boldsymbol{\nabla}\left[(h_0+\zeta)\,\boldsymbol{\nabla}\varphi + P\,\boldsymbol{\nabla}\psi + Q\,\psi\,\boldsymbol{\nabla}\zeta\right] = 0, \tag{1.14a}$$

$$\partial_t\varphi + \frac{1}{2}\,(\boldsymbol{\nabla}\varphi)^2 + g\,\zeta + \mathcal{R} = 0 \qquad \text{and} \tag{1.14b}$$

$$\left[K + G\,(\boldsymbol{\nabla}\zeta)^2\right]\,\psi + Q\,(\boldsymbol{\nabla}\varphi)\cdot(\boldsymbol{\nabla}\zeta) + R\,(\boldsymbol{\nabla}\psi)\cdot(\boldsymbol{\nabla}\zeta) - \boldsymbol{\nabla}\cdot\left[F\,\boldsymbol{\nabla}\psi_0 + P\,\boldsymbol{\nabla}\varphi + R\,\psi\,\boldsymbol{\nabla}\zeta\right] = 0, \tag{1.14c}$$

with (a prime denotes variation with respect to ζ, *e.g.* $K' \equiv \delta K/\delta\zeta$):

$$\mathcal{R} = \frac{1}{2}F'\,(\boldsymbol{\nabla}\psi)^2 + \frac{1}{2}\left[K' + G'\,(\boldsymbol{\nabla}\zeta)^2\right]\,\psi^2 + [P'\,\boldsymbol{\nabla}\psi + Q'\,\psi\,\boldsymbol{\nabla}\zeta]\cdot\boldsymbol{\nabla}\varphi + R'\,\psi\,(\boldsymbol{\nabla}\psi)\cdot(\boldsymbol{\nabla}\zeta) - \boldsymbol{\nabla}\cdot\left[G\,\psi^2\,\boldsymbol{\nabla}\zeta + Q\,\psi\,\boldsymbol{\nabla}\varphi + R\,\psi\,\boldsymbol{\nabla}\psi\right]. \tag{1.14d}$$

The third equation (1.14c) is – for given ζ and φ – a linear elliptic equation in terms of ψ. Forms of Boussinesq equations where additional elliptic equations have to be solved are not new, see *e.g.* Whitham (1967*b*)[4], Broer (1975), Mooiman & Verboom (1992), Borsboom *et al.* (2001). Note that the highest-order spatial derivatives in all equations are of second order.

A Hamiltonian system in terms of the 'velocity' $\boldsymbol{u}(\boldsymbol{x},t) \equiv \boldsymbol{\nabla}\varphi$ is equally well possible.[5] Replacing $\boldsymbol{\nabla}\varphi$ with $\boldsymbol{u}$ in the Hamiltonian (1.13), the dynamics for irrotational flow are given by:

$$\partial_t\zeta + \boldsymbol{\nabla}\cdot\left(\frac{\delta\mathscr{H}}{\delta\boldsymbol{u}}\right) = 0, \tag{1.15a}$$

$$\partial_t\boldsymbol{u} + \boldsymbol{\nabla}\left(\frac{\delta\mathscr{H}}{\delta\zeta}\right) = \boldsymbol{0} \tag{1.15b}$$

and $\delta\mathscr{H}/\delta\psi = 0$.

The vertical component of 'vorticity' $\boldsymbol{\nabla}\times\boldsymbol{u}$ can easily be introduced. The (non-canonical) Hamiltonian description for such a rotational flow can be given through (Shepherd, 1990, Eq. (4.45)):

$$\partial_t\zeta + \boldsymbol{\nabla}\cdot\left(\frac{\delta\mathscr{H}}{\delta\boldsymbol{u}}\right) = 0, \tag{1.16a}$$

$$\partial_t\boldsymbol{u} + \boldsymbol{\nabla}\left(\frac{\delta\mathscr{H}}{\delta\zeta}\right) + \boldsymbol{\varpi}\times\left(\frac{\delta\mathscr{H}}{\delta\boldsymbol{u}}\right) = \boldsymbol{0} \qquad \text{with} \qquad \boldsymbol{\varpi} = \frac{\boldsymbol{\nabla}\times\boldsymbol{u}}{h_0+\zeta} \tag{1.16b}$$

the potential vorticity. By use of the vector identity $\boldsymbol{\nabla}(\frac{1}{2}\boldsymbol{u}\cdot\boldsymbol{u}) + (\boldsymbol{\nabla}\times\boldsymbol{u})\times\boldsymbol{u} = \boldsymbol{u}\cdot\boldsymbol{\nabla}\boldsymbol{u}$, see *e.g.* Batchelor (1967, p. 382), this directly leads – among others – to the appearance of the well-known convection term $\boldsymbol{u}\cdot\boldsymbol{\nabla}\boldsymbol{u}$ in the evolution equation for $\boldsymbol{u}(\boldsymbol{x},t)$.

The performance of the VBM model (1.14) has been assessed through both an analytical study of the linearised model, as well as through numerical verification using

[4] Eqs. (14) of the Lagrangian variational model of Whitham (1967*b*) lead to: $\partial_t h + \boldsymbol{\nabla}\cdot(h\boldsymbol{\nabla}\phi) = 0$, $\partial_t\xi + \frac{1}{2}(\boldsymbol{\nabla}\phi)^2 + g(h-h_0) = 0$ with $\xi = \phi + \frac{1}{3}h_0\partial_t h = \phi - \frac{1}{3}h_0\,\boldsymbol{\nabla}\cdot(h\boldsymbol{\nabla}\phi) = 0$. The latter is an elliptic equation for the potential ϕ.

[5] Note that $\boldsymbol{u}(\boldsymbol{x},t)$ is not the horizontal velocity $\boldsymbol{\nabla}\Phi$ at the free surface, but equal to $\boldsymbol{u} = [\boldsymbol{\nabla}\Phi]_{z=\zeta} + \boldsymbol{\nabla}\zeta\,[\partial_z\Phi]_{z=\zeta}$.

the non-linear model. The study of the linearised model involves the linear dispersion characteristics and shoaling by depth changes (Klopman *et al.*, 2010), as well as reflections by bathymetry (Klopman & Dingemans, 2010; Dingemans & Klopman, 2009).

1.3.3 Dispersion relation for linear waves

For linear waves of infinitesimal amplitude – propagating on a layer of constant mean depth h_0 and without mean current – the angular frequency $\omega \equiv 2\pi/\tau$ of a periodic wave is related of the wave number $k \equiv 2\pi/\lambda$, where λ is the wavelength and τ the period. This is known as the dispersion relation, and is of the form:

$$\omega^2 = \Omega^2(k). \tag{1.17}$$

For the one-parameter case – the parabolic and hyperbolic-cosine VBM, as described in §1.3.2 – the linear dispersion relation of waves on a layer of constant mean depth becomes (Klopman *et al.*, 2010, Eq. (5.14)):

$$\begin{aligned} \frac{\Omega^2(k)\,h_0}{g} &= (kh_0)^2\ \frac{\overline{K}\,h_0^3 + \left(\overline{F}\,h_0 - \overline{P}^2\right)\,(kh_0)^2}{\overline{K}\,h_0^3 + \overline{F}\,h_0\,(kh_0)^2} \\ &\equiv (kh_0)^2\ \frac{1+\gamma_{\text{num}}\,(kh_0)^2}{1+\gamma_{\text{den}}\,(kh_0)^2}, \end{aligned} \tag{1.18a}$$

with

$$\begin{aligned} &\overline{F} = \int_{-h_0}^{0} f^2\,\mathrm{d}z, \qquad \overline{P} = \int_{-h_0}^{0} f\,\mathrm{d}z \quad \text{and} \quad \overline{K} = \int_{-h_0}^{0} (\partial_z f)^2\,\mathrm{d}z, \\ &\gamma_{\text{num}} \equiv \frac{\overline{F}\,h_0 - \overline{P}^2}{\overline{K}\,h_0^3} \quad \text{and} \quad \gamma_{\text{den}} \equiv \frac{\overline{F}}{\overline{K}\,h_0^2}, \end{aligned} \tag{1.18b}$$

Because of the Cauchy–Schwartz inequality

$$\left|\int_{-h_0}^{0} f\cdot 1\,\mathrm{d}z\right|^2 \le \int_{-h_0}^{0} |f|^2\,\mathrm{d}z \cdot \int_{-h_0}^{0} |1|^2\,\mathrm{d}z, \tag{1.19}$$

there is $\overline{P}^2 \le \overline{F}\,h_0$ (Lakhturov & van Groesen, 2010). Consequently, in the dispersion relation (1.18a) both coefficients are non-negative: $\gamma_{\text{den}} \ge \gamma_{\text{num}} \ge 0$, as a direct consequence of our positive-definite Hamiltonian. The phase speed $C \equiv \Omega(k)/k$ is

$$\frac{C^2}{g\,h_0} = \frac{1+\gamma_{\text{num}}\,(kh_0)^2}{1+\gamma_{\text{den}}\,(kh_0)^2}, \tag{1.20}$$

which is well behaved for high wave numbers (small wavelengths), with limiting value $C/\sqrt{(g\,h_0)} \to \sqrt{(\gamma_{\text{num}}/\gamma_{\text{den}})} \le 1$ for $k\,h_0 \to \infty$. Further, the group velocity $V \equiv \partial_k\Omega$ is also well behaved: it is always in the same direction as the phase

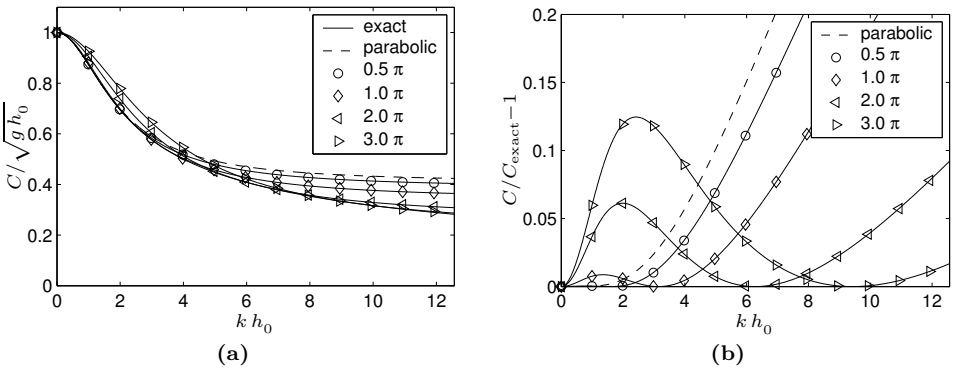

Figure 1.4: Linear dispersion characteristics of the parabolic and cosh structure model as a function of kh_0. (a) Phase speed $C/\sqrt{g\,h_0}$ (with $C \equiv \Omega/k$) in the cosh structure model (solid lines with markers) *vs* the exact linear phase speed (solid line, lowest curve) and the parabolic structure model (dashed line). (b) Relative error $C/C_{\rm exact} - 1$ (on a linear scale) in the phase speed of the cosh structure model (solid lines) and the parabolic structure model (black dashed line). The markers are for different values of κh_0: $\frac{1}{2}\pi$ (–○–), π (–◇–), 2π (–◁–) and 3π (–▷–).

velocity C, for given (real) wave number k. Note that for given angular frequency ω the dispersion relation (1.18a) has four solutions for the wave number k: two real ones of equal magnitude and opposite sign, corresponding with propagating waves, and two pure imaginary ones – also of equal magnitude and opposite sign – which are so-called evanescent modes.

For the parabolic shape function (1.9) the linear dispersion characteristics ($\gamma_{\rm num} = \frac{1}{15}$, $\gamma_{\rm den} = \frac{2}{5}$) are equal to those of the model of Madsen & Sørensen (1992), as well as the second-order model of Witting (1984). The dispersion characteristics of the hyperbolic-cosine (cosh) model (1.10) are tuned to the value of the shape parameter κ. At the wave number $k = \kappa$ both the phase velocity C and the group velocity V have the exact values, in accordance with Airy wave theory, see Figure 1.4. The parabolic shape function may be regarded as a special case of the cosh model, tuned for $\kappa \to 0$. In all cases the solutions of the parabolic and cosh models propagate faster than than the exact linear phase speed.

Some shortcomings of the VBM models with one shape function appear when looking into the second derivative $\partial_k^2\Omega(k)$ of the dispersion equation (1.18a), see Figure 1.5. The relative errors in $\partial_k^2\Omega(k)$ become easily large for larger kh_0. This curvature of the dispersion curve is an essential parameter in the description of non-linear wave stability on deeper water ($kh_0 > 1.36$, Benjamin, 1967), as well as deeper-water non-linear wave groups. Better characteristics with respect to $\partial_k^2\Omega(k)$ can only be obtained by using a VBM with two or more shape functions.

1.3.4 Linear wave shoaling

The analysis of linear wave shoaling by depth changes is very easy, due to the variational principles underlying the VBM. Direct use can be made of the average Lagrangian method of Whitham (1974), resulting in conservation of wave action

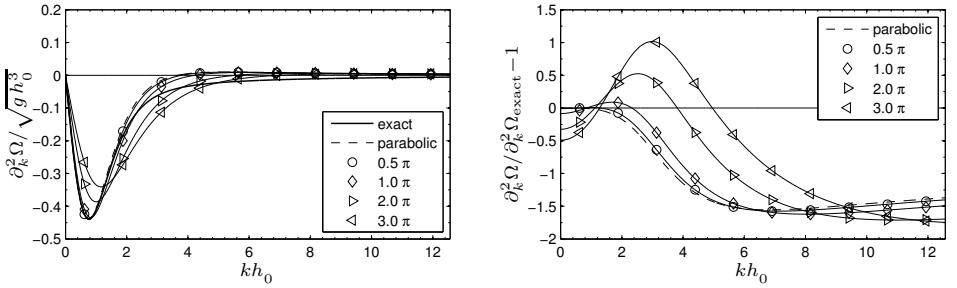

(a) **(b)**

Figure 1.5: Curvature of the linear dispersion equation for the parabolic VBM and cosh VBM as a function of kh_0. (a) Dispersion relation curvature $\partial_k^2\Omega/\sqrt{g\,h_0^3}$ in the parabolic structure model (thin dashed line) and the cosh structure model (thin solid lines with markers) *vs* the exact linear phase speed (thick solid line). (b) Relative error $\partial_k^2\Omega/\partial_k^2\Omega_{\rm exact}-1$ in the curvature of the dispersion relation $\Omega(k)$ for the parabolic structure model (dashed line) and cosh structure models (solid lines with markers). The markers are for different values of κh_0: $\frac{1}{2}\pi$ (–○–), π (–◇–), 2π (–◁–) and 3π (–▷–).

both for linear and non-linear waves (Hayes, 1970*a*, 1973). Consequently, for the one-dimensional wave propagation case for linear waves of constant frequency ω the wave energy flux at each location is a constant (Klopman *et al.*, 2010):

$$V\,\left(\tfrac{1}{2}\,\rho\,g\,a^2\right) = \text{constant}, \tag{1.21}$$

with $a(x)$ the wave amplitude and $V(x) \equiv \partial_k\Omega$ the group velocity. This is a *global* shoaling relation, relating the wave amplitudes $a(x_A)$ and $a(x_B)$ between different locations x_1 and x_2, and is a direct consequence of the underlying variational principle. For other Boussinesq-like models – using a WKBJ approach and with much more efforts (see *e.g.* Dingemans, 1997, pp. 545–559 & 569–571) – *local* shoaling relations between $(\mathrm{d}a/\mathrm{d}x)'/a$ and $(\mathrm{d}h/\mathrm{d}x)/h$ are obtained. Chen & Liu (1995) obtain global shoaling characteristics for their model by integration of the local shoaling relationships, but their is no guarantee that this is possible for every (non-variational) Boussinesq-type of model. The parabolic VBM has the same shoaling characteristics as the Madsen & Sørensen (1992) model, which is not surprising since it also has the same dispersion characteristics. The cosh VBM has exact linear shoaling for monochromatic waves of frequency ω, provided $\kappa(x)$ is chosen at each depth $h_0(x)$ according to the dispersion relation of Airy wave theory. This is due to the fact that in the cosh VBM the group velocity V has the exact value at $k = \kappa$.

1.3.5 Linear wave reflection by bathymetry

The reflection characteristics of linear monochromatic waves for the parabolic and cosh VBM have been studied for a plane slope connecting two regions of constant but different depth (Klopman & Dingemans, 2010). For this test case by Booij (1983) – with waves propagating from a deep part with dimensionless depth $\omega^2 h_0/g = 0.6$ ($k_{\rm exact}\,h_0 \approx 0.861$) into a shallow part with $\omega^2 h_0/g = 0.2$ ($k_{\rm exact}\,h_0 \approx 0.463$) – there are accurate numerical results for the full potential-flow problem by Porter & Porter

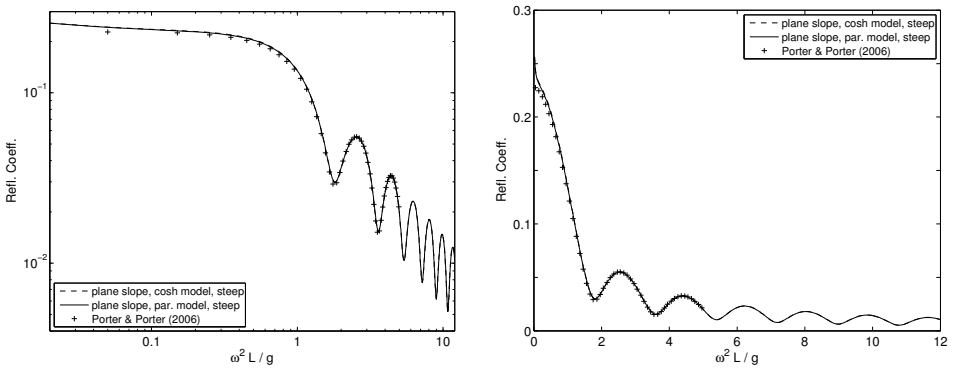

(a) **(b)**

Figure 1.6: Reflection coefficients as a function of $\omega^2 L/g$ for a plane slope (Booij, 1983, test case): parabolic and cosh models with velocity approximation (1.11). Solid lines: parabolic VBM; dashed lines: cosh VBM; +: Porter & Porter (2006). (a) Double logarithmic axes; (b) the same with linear axes.

(2006). For the approximation (1.11) of the vertical velocity structure (called 'steep slope' models in Klopman & Dingemans (2010)) both the parabolic and cosh models give accurate results for a varying width L of the slope region, see Figure 1.6. Up to slopes of steepness 2:5 ($\Delta h_0/L < 0.4$, $\omega^2 L/g > 1$.) the reflection characteristics compare well with the theoretical ones, despite that the used shape functions f have $\partial_z f = 0$ athe sea bed, as only valid for waves above a horizontal bed.

However, when the quasi-homogeneous approximation (QH) (1.12) is used, neglecting the terms with $\boldsymbol{\nabla} h_0$ and $\boldsymbol{\nabla}\kappa$ in the horizontal flow velocity – denoted by 'mild slope' approximation in Klopman & Dingemans (2010) – the parabolic and cosh model perform not so well, see Figure 1.7. Also the Eckart–Berkhoff mild-slope equation does not perform well with respect to reflection, which in that case can be remedied by the inclusion of bottom-slope effects (Dingemans, 1985, pp. 9–10; Dingemans, 1997, §3.1.1; Chamberlain & Porter, 1995).

Observe, that the parabolic QH-VBM follows the reflection coefficient undulations with $\omega^2 L/g$ more than the cosh VBM. The main difference being, in this test case with $kh_0 < 0.86$, the different normalisations used in the shape functions $f^{(p)}(z)$, Eq. (1.9), and $f^{(c)}(z)$, Eq. (1.10). As a result, $\psi(\boldsymbol{x}, t)$ also has different dimensions for the two models: it is the vertical velocity at the free surface for the parabolic QH-VBM, and has the dimensions of a velocity potential in the cosh QH-VBM.

This observation has raised the question whether it is possible to improve the performance of the parabolic and cosh QH-VBM by optimisation of the normalisation used. The normalisation affects the size of the neglected terms in the Hamiltonian – and thus the resulting dynamical equations – and our aim (Dingemans & Klopman, 2009; Klopman & Dingemans, 2010) is to minimize the neglected terms. This minimization has been done in a heuristic way: minimizing the simplest of these terms and observing, as expected, that the other terms reduce as well. For the parabolic QH-VBM this term can be made exactly equal to zero by the correct norm in terms

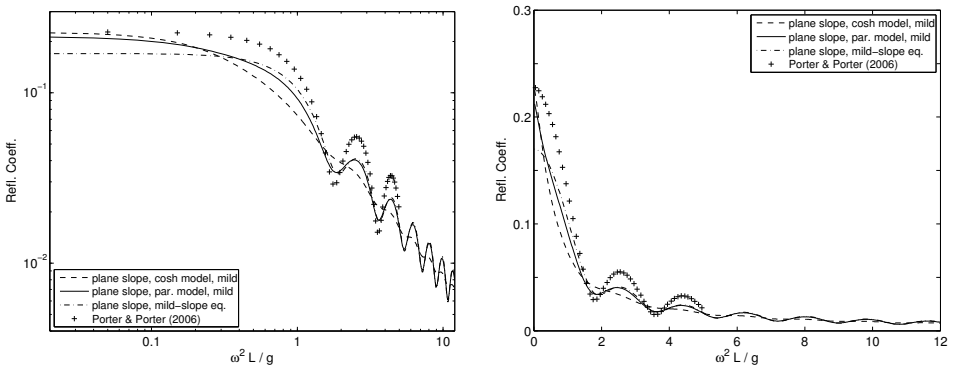

(a) **(b)**

Figure 1.7: Reflection coefficients as a function of $\omega^2 L/g$ for a plane slope: mild-slope models with quasi-homogeneous velocity approximation (1.12). Solid lines: parabolic QH-VBM in the mild-slope approximation; dashed lines: cosh QH-VBM in the mild-slope approximation, dash-dot lines: Eckart–Berkhoff mild-slope equation; +: Porter & Porter (2006).

of depth h_0. For the cosh QH-VBM this is not possible, and an approximate min–max normalisation was obtained from the desired asymptotic behavior of the norm for $\kappa h_0 \to 0$ and $\kappa h_0 \to \infty$, as well as by a trial-and-error postulation of formulations matching both κh_0 asymptotes.

With these normalisations, both the parabolic and cosh QH-VBM perform as well with respect to reflection – for the Booij test case – as the corresponding models without the quasi-homogeneity approximation. While the simpler structure of the flow equations is retained, as obtained by the neglect of the gradient terms in h_0 and κ in the velocities (1.11) used in the Hamiltonian $\mathscr{H}$, Eq. (1.1).

1.3.6 Numerical modelling and verification

The quasi-homogeneous flow equations, Eqs. (1.15), in terms of the free-surface potential gradient $\boldsymbol{u} \equiv \boldsymbol{\nabla}\varphi$, are used for numerical tests on the performance of the variational Boussinesq models (Klopman *et al.*, 2005, 2007, 2010). The method of lines is used: by using a pseudo-spectral Fourier-series method in horizontal space – either one-dimensional (1DH) or two-dimensional (2DH) – the partial differential equations for surface elevation $\zeta(\boldsymbol{x},t)$ and surface potential gradient $\boldsymbol{u}(\boldsymbol{x},t) \equiv \boldsymbol{\nabla}\varphi$ transform into a series of ordinary differential equations (ODE's) for their values at the equi-distant grid nodes.[6] This set of ordinary differential equations is solved by a high-order ODE'solver with adaptive time-step adjustment (in order to meet a user-defined error criterium). No artificial damping has been used: only a very small numerical damping – inherent to the used ODE solvers – is present.

Before $\zeta(\boldsymbol{x},t)$ and $\boldsymbol{u}(\boldsymbol{x},t)$ can be advanced in time, the parameter field $\psi(\boldsymbol{x},t)$ has to be known. This is obtained by solving the elliptic equation (1.14c), which is

[6]Note that the 1DH computations of wave reflection for monochromatic waves, Chapter 4, have been done with a different method, only requiring the solution of ODE's with boundary values.

linear in ψ for given ζ and $\boldsymbol{u}$. A preconditioned conjugate gradient method – well-suited since the positive-definite Hamiltonian guarantees a symmetric and positive system matrix – is used. In practice the system matrix is not needed, but only the residue of the system of equations, *i.e.* the left-hand side of Eq. (1.14c). This is also computed with a pseudo-spectral method. The solution of the elliptic equation for $\psi(\boldsymbol{x},t)$ in general only takes two to ten iterations, since a good initial guess for $\psi(\boldsymbol{x},t)$ is available from the previous time steps. Overall, the solution of the elliptic equation takes 30% to 50% of the computing time, *i.e.* the computing time is about one-and-a-half to twice the time needed for advancing the surface elevation ζ and velocity $\boldsymbol{u}$ in time.

The advantage of the pseudo-spectral method is its accurate computation of spatial derivatives, which is beneficial in our aim to test the performance of the VBM without effects of numerical discretisation. Disadvantages are the requirement of periodic spatial domains for performing the fast Fourier transforms (FFT's), and the inability to represent shock waves. However, in the present verifications of the Boussinesq-type models these disadvantages are of minor concern. Wave conditions are specified as initial conditions on a flat-bed region, and the extend of the spatial domains has been chosen large enough to prevent unwanted effects from the domain periodicity. All computational modelling reported below has been done using MATLAB for programming and computing. In other applications of different versions of VBM – outside the scope of this thesis – experience has been gained with finite difference and finite element discretisations, both for formulations in terms of velocity potential φ as well as in terms of its gradient $\boldsymbol{u}$.

The numerical experiments show – both for one dimensional (1DH) wave propagation (Klopman *et al.*, 2005, 2010; Chapter 2) as well as in two horizontal dimensions (Klopman *et al.*, 2007; Chapter 3) – the capacities of the parabolic VBM regarding the propagation of non-linear waves over bathymetry.

The cosh VBM has even higher capacities than the parabolic VBM. As an example, consider the propagation of highly non-linear solitary waves, see Figure 1.8. The maximum solitary wave height is $H_w \approx 0.83\,h_0$ (see *e.g.* Longuet-Higgins & Fenton, 1974; Williams, 1981). The solitary waves have, after a dimensionless time $t\sqrt{(g/h)} = 50$ propagated over a distance of $62.5\,h_0$ and $64.3\,h_0$, for the case $H_w/h_0 = 0.60$ and 0.73, respectively. In both cases the cosh model performs well, hardly to be distinguished from Tanaka's solution in these plots. The parabolic model also performs quite well for $H_w/h_0 = 0.60$, changing form a bit and traveling somewhat too fast. For higher waves, the solitary wave deforms strongly[7] for the parabolic model (not shown in Fig. 1.8(b)), while the cosh model still performs very well. The solitary wave in the cosh model breaks for $H_w/h_0 = 0.75$.

[7] The wave front steepens, and thereafter a Gibbs overshoot phenomenon occurs due to the pseudo-spectral method used, after which the numerical model is no longer capable to accurately reproduce the wave.

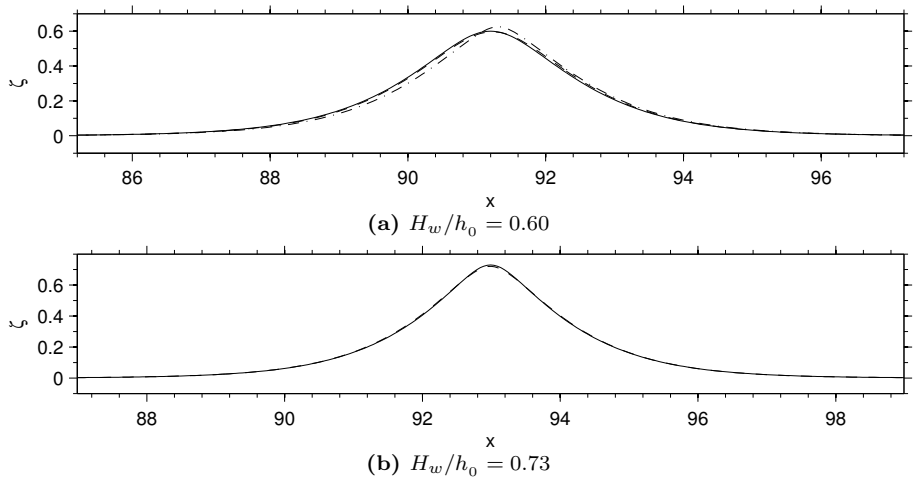

(a) $H_w/h_0 = 0.60$

(b) $H_w/h_0 = 0.73$

Figure 1.8: Propagation of a solitary wave over a horizontal bed. Snapshot of the surface elevation ζ as a function of x after a propagation time of $t = 50\sqrt{(h_0/g)}$. The solid line is an accurate numerical solution of the solitary wave (Tanaka, 1986), also used to provide the initial values of ζ and φ. The dash–dot line is for the parabolic VBM (only results for $H_w/h_0 = 0.6$) and the dashed line is for the cosh VBM (with $\kappa h_0 = \frac{1}{2}\pi$).

1.4 Context

The present contributions are put within the wider context of the modelling of surface gravity waves in the time domain. This is quite a wide field of research, so this overview will be far from complete. It is a sketch of the present modelling approach within the landscape of other efforts during the past three or four decades, with emphasis on Boussinesq-like models and wave propagation over bathymetry. For reviews on Boussinesq-type wave modelling, see Madsen & Schäffer (1999), and Chapter 5 of Dingemans (1997); as well as Peregrine (1972) for earlier developments.

The focus will be on three aspects of surface gravity waves, namely: frequency dispersion, non-linearity and the incorporation of bathymetry. For structuring purposes, a classification of the models is made by using their linear frequency dispersion characteristics, for linear waves propagating above a horizontal sea bed.

To start with: in $\omega^2 = \Omega^2(k)$, Eq. (1.17), the exact dispersion relation $\Omega_{\text{exact}}(k)$ according to Airy wave theory is

$$\Omega_{\text{exact}}(k) = \sqrt{g\,k\,\tanh\,(k\,h_0)}, \tag{1.22}$$

with k the wave number and h_0 the mean water depth, see also Figure 1.9. The shallow water behaviour is

$$\Omega^2_{\text{exact}} \to \frac{g}{h_0}\left(k^2\,h_0^2 - \frac{1}{3}\,k^4\,h_0^4 + \frac{2}{15}\,k^6\,h_0^6 + \cdots\right) \qquad \text{for } kh_0 \to 0. \tag{1.23}$$

Corresponding with k^2 is the operator $-\boldsymbol{\nabla}^2$ (minus the Laplace operator) in physical $\boldsymbol{x}$-space. This is exploited with advantage in many wave models, which use a rational

function approximation in terms of k^2 to the dispersion relation, *e.g.* by use of a Padé approximation in terms of k^2 to the Taylor series expansion of $\Omega^2(k)$. The Laplace operator and its powers – as well as their generalisations for non-homogeneous media – lend themselves well for numerical treatment in practical applications by using finite element, finite volume or finite difference methods.

The deep water limit of the dispersion relation (1.22) is:

$$\Omega_{\text{exact}} \to \sqrt{g\,k} \qquad \text{for } kh_{_0} \to \infty \tag{1.24}$$

which is not a rational function of k. If one wants to retain exact linear dispersion, this deep-water behaviour cannot be incorporated in terms of *local* operators in space, like the Laplace operator. An approach using *global* operators is needed, for instance by using integral equations or the fast Fourier transform (FFT), in order to obtain exact frequency dispersion in a wave model.

1.4.1 Exact linear frequency dispersion

Using Zakharov's (1968) Hamiltonian formulation, several models have been developed incorporating exact linear dispersion. These developments start with West *et al.* (1987) (based on Watson & West, 1975) and Dommermuth & Yue (1987). The approximations in these models are with respect to non-linearity, by using series expansions around a reference level, normally the mean-surface elevation. This series expansion results in a loss of the positive-definiteness of the Hamiltonian in these models, which may introduce high wave-number instabilities (Milder, 1990). For high waves, these methods do not converge.

These convergence problems are overcome by Clamond & Grue (2001): they introduce a rapidly converging iteration scheme – using fast Fourier transforms – for the solution of the Laplace equation in the fluid interior through integral equations (see also Clamond & Grue, 2001; Fructus *et al.*, 2005*a*,*b*). The technique can also be used for waves propagating over bathymetry (Fructus & Grue, 2007).

Other Hamiltonian approaches to non-linear waves with exact linear dispersion include Craig & Sulem (1993), Guyenne & Nicholls (2007), and Otta *et al.* (1996) (see also Radder, 1999).

The description of uni-directional water waves has its roots in the Korteweg–de Vries (KdV) equation. However, the KdV equation is without exact dispersion and only valid for fairly long waves. On the other side, deep-water waves with a narrow-band carrier-wave spectrum can be described using the (modified) non-linear Schrödinger (NLS) equation (Zakharov, 1968; Dysthe, 1979), also with approximate dispersion and uni-directionalisation.[8] The Dysthe equation has been extended with exact linear dispersion by Trulsen *et al.* (2000) (see also Trulsen, 2007), but retaining the weak non-linearity of the NLS and Dysthe models. Janssen *et al.* (2006) use a weak

[8]Here, uni-directional – for the 2DH case – means that the waves mainly propagate in one direction. That is, when the wave field is thought of as the sum of many plane (long-crested) propagating waves, the wave number vectors fall within a sector of $\pm 90^\circ$ around some pre-chosen direction.

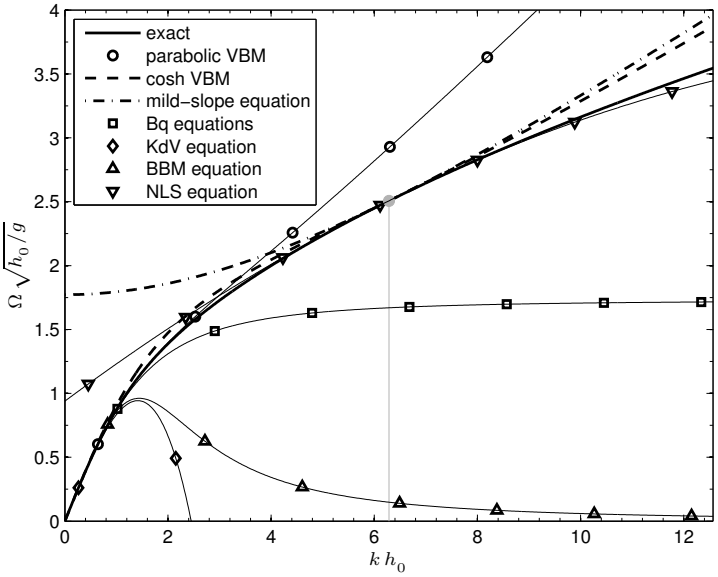

Figure 1.9: The frequency dispersion relationship $\Omega(k)\sqrt{h_0/g}$ as a function of kh_0 for linear waves in various wave models. The cosh VBM, Eckart–Berkhoff mild-slope equation and non-linear Schrödinger (NLS) equation are all tuned – in the shown example – at $\kappa h_0 = 2\pi$, *i.e.* for a wavelength λ equal to the water depth h_0. The Boussinesq (Bq) equations correspond with the system in Eq. (5.107) of Dingemans (1997); and the time-dependent mild-slope equation is given in Eq. (3.20), *ibid.* The NLS equation uses the first three terms (*i.e.* a parabolic approximation) from the Taylor-series expansion of $\Omega_{\text{exact}}(k)$ around $k = \kappa$.

non-linear description of uni-directional waves propagating over bathymetry, with exact linear frequency dispersion.

By direct approximations to the Hamiltonian, van Groesen & Andonowati (2007) derive a uni-directional wave equation for arbitrary constant depth. Very high deep-water waves – near the highest wave height – can be described accurately with this uni-directional variational approach (van Groesen *et al.*, 2010). The extension to mainly uni-directional wave propagation in two horizontal dimensions is made by She Liam & van Groesen (2010).

I will now turn to non-linear wave models with approximations to the frequency dispersion. This is the class within which the variational Boussinesq models reside.

1.4.2 Frequency dispersion approximations

The focus here will be on Boussinesq-like equations, with Boussinesq-like meaning that some approximations are made with respect to the vertical flow structure, in order to be able to remove the cross-space (the vertical z-direction) and end up with an equation in propagation space (the horizontal $\boldsymbol{x}$-plane). When appropriate, comments relating to the present VBM approach will be added.

Variational formulations, for the 'classical' Boussinesq equations and the Korteweg–de Vries equation are given by Whitham (1967*b*). The related dispersion curves are shown in Figure 1.9. As can be seen, the KdV equation becomes unstable for $kh_0 > \sqrt{6}$. This stability problem is remedied in the Benjamin–Bona–Mahony (BBM) equation (Benjamin *et al.*, 1972).

Improved frequency dispersion characteristics – as compared with 'classical' Boussinesq equations – are obtained by Witting (1984) for waves over a horizontal bed, by introducing implicit relations (elliptic equations) between the free-surface 'velocity' $\boldsymbol{u} = \boldsymbol{\nabla}\varphi$ and the depth-averaged velocity $\boldsymbol{U}$. The resulting dispersion relations of the linearised model are rational functions (Padé approximations) in terms of $k^2 h_0^2$, *i.e.* the relative water depth squared:

$$\Omega^2_{[M,N]}(k) = \frac{g}{h_0}\left(k^2\, h_0^2\right) \frac{1 + \sum_{m=1}^{M} \alpha_m \left(k^2\, h_0^2\right)^m}{1 + \sum_{n=1}^{N} \beta_n \left(k^2\, h_0^2\right)^n}. \tag{1.25}$$

This approach is taken up in Madsen *et al.* (1991) and Madsen & Sørensen (1992), who extended the form with $M = 1$ and $N = 1$ to two horizontal dimensions with bathymetry, and further optimised with respect to numerical implementation. A conservative formulation is given in Borsboom *et al.* (2001), requiring the additional solution of an elliptic equation (but a different one as used in the parabolic VBM). Later, in Agnon, Madsen & Schäffer (1999), the Zakharov (1968) formulations for the evolution of free-surface quantities are used to obtain higer-order approximations $\Omega^2_{[M,N]}(k)$; together with an approximate solver for the Laplace equation in the fluid interior. This approximation to the Laplace equation requires the solution of several elliptic equations, containing (very) high-order spatial derivatives. The use of this approximate solver makes that the model is no longer guaranteed to have a positive-definite Hamiltonian. Recent progress with respect to this method can be found in Fuhrman & Madsen (2008); they add a small amount of artificial damping for very high wave numbers to keep the numerical model stable. Note that the VBM approach always leads to (a series of) second-order elliptic equations, *i.e.* without high-order spatial derivatives. The parabolic VBM has the same linear dispersion characteristics as the Madsen & Sørensen (1992) model, see Figure 1.9. Also, the above methods use expansions of the dispersion relationship around $kh_0 = 0$, while for instance the cosh VBM (and possible extensions thereof by using more shape functions) can be tuned at an arbitrary wave number.

Another approach is the Green–Naghdi (1976) theory, which uses a polynomial description of flow quantities over the vertical. The flow may be rotational, and the continuity equation is satisfied everywhere in the fluid. This contrasts with the VBM whose flow approximations violate the continuity equation – but do conserve depth-integrated mass.[9] On the other hand, the solutions of the Green–Naghdi method

[9] The latter is due to the fact that an arbitrary constant can be added to the used velocity potential $\varphi(\boldsymbol{x}, t)$, without changing the flow. By Noether's theorem, this results in depth-integrated mass conservation (Benjamin & Olver, 1982).

are rotational, also when starting the flow from rest (Shields & Webster, 1988); while the VBM has exact irrotationality due to the velocity potential formulation. At lowest order, the Green–Naghdi approach results in 'classical' Boussinesq equations. The Green–Naghdi equations can also be derived from a variational principle (Miles & Salmon, 1985); and the approach can also be extended to higher order (see *e.g.* Shields & Webster, 1988). In §2.4.2 a VBM power-series approach is formulated, with the resulting linear dispersion characteristics given by Eq. (2.44) and in Figure 2.2, for up to five shape functions used in the series ($M = 5$). While the Green–Naghdi approach leads to a set of coupled time-evolution equations for all components in the power series (Shields & Webster, 1988), the VBM only has two evolution equations, one for $\zeta(\boldsymbol{x},t)$ and one for $\varphi(\boldsymbol{x},t)$; as well as a set of M elliptic equations for the parameter fields $\psi_m(\boldsymbol{x},t)$ $(m = 1, 2, \cdots, M)$. The non-linear performance of the power-series VBM has not been tested yet by use of a numerical model.

Other approaches to obtain Boussinesq-like models with improved frequency dispersion are *e.g.*: Nadaoka *et al.* (1997), using a series of hyperbolic-cosine shape functions; Lynett & Liu (2004*a*,*b*) (see also Lynett, 2006), using a layered Boussinesq approach; and Stelling & van Kester (2001) who utilise a layered non-hydrostatic shallow-water approach (see also Zijlema & Stelling, 2008, for recent developments).

Hamiltonian dynamics are used by Craig & Groves (1994) and Craig *et al.* (2005), starting from Craig & Sulem (1993), in order to obtain Boussinesq-type equations – as well as KdV-type and Kadomtsev–Petviashvilii (KP) type – with improved frequency dispersion. The Hamiltonians in these models are not positive definite.

A non-linear extension of the Eckart–Berkhoff mild-slope equation is made by Radder & Dingemans (1985) – from a canonical formulation and a positive-definite Hamiltonian. They show that the mild-slope equation always has the wrong sign in its approximation to the dispersion curvature $\partial_k^2\Omega$, a primary parameter in the description of wave group dynamics in deeper water by *e.g.* NLS-like equations, see Figure 1.9. As a result, non-linear extensions of the Eckart–Berkhoff mild-slope equation are of limited use.

The search for Boussinesq-like equations with positive-definite Hamiltonian is started by Broer (1974, 1975). See Radder (1999) and Dingemans (1997, §5.6), for reviews on the subject. The approach is to construct positive-definite approximations to the kinetic energy – valid for fairly long waves and weak non-linearity. These models have linear dispersion characteristics corresponding with those of the 'classical' Boussinesq equations, see Figure 1.9. Later, Mooiman (1991*a*,*b*), Mooiman & Verboom (1992), van der Veen & Wubs (1995), continue this development, and construct numerical Boussinesq models with improved frequency dispersion and positive Hamiltonian for wave propagation over 2DH bathymetry. At the start of my research, see §1.3.1 for my motivation, the first model that comes up by the use of the present approach is the parabolic VBM, Eqs. (2.11), with similar dispersion characteristics as Mooiman & Verboom (1992) and Madsen & Sørensen (1992). By trying to tune in at a certain characteristic wave number $\kappa(\boldsymbol{x})$ at each location $\boldsymbol{x}$, the cosh VBM results, §2.4.1. Note that all presented VBM models, due to the structure $\Phi(\boldsymbol{x},z,t) = \varphi(\boldsymbol{x},t) + \sum f_m(z)\,\psi_m(\boldsymbol{x},t)$, Eq. (2.4), have – besides depth-integrated mass conservation –

always the correct shallow water limit $\Omega(k) \to k\sqrt{gh_0}$, as $kh_0 \to 0$ for long waves. Further improvements with respect to frequency dispersion are possible by the use of additional shape function, *e.g.* as in the power-series approach of §2.4.2.

1.5 Outline

The following chapters contain reprints of papers on the variational modelling of Boussinesq-type waves. The only changes made are in creating a uniform lay-out, as well as using the same bibliographic referencing system everywhere, *i.e.* using the authors names and year of publication.

Chapter 2 contains the derivation of the variational model for Boussinesq-type waves, as well as a description of its linear characteristics with respect to frequency dispersion and wave shoaling. Further, examples are given on the application of the parabolic VBM for three different cases of one-dimensional wave propagation:

1. non-linear periodic waves over a flat bed (for which highly-accurate solutions to the full potential flow model are known; Rienecker & Fenton, 1981),
2. periodic waves over an underwater bar (Dingemans, 1997, §5.9), for which measurement data from detailed laboratory measurements are available (Luth *et al.*, 1994),
3. the propagation and deformation of a confined wave group over a slope into shallower water – and the associated release of long waves – verified using the accurate numerical solution by a finite-element method for the full non-linear potential-flow problem (van Groesen & Westhuis, 2002).

Another case of confined wave groups propagating and transforming over an underwater bar, also releasing free long waves, is presented in Appendix A. These long waves are of direct practical importance, since they can induce strong motions of moored ships (enhanced by harbour resonances, or very soft-springed moorings). Correlations between the short-wave energy fluctuations and the long wave motion may also induce cross-shore sediment transport in the coastal zone (van Rijn, 2009; Battjes, 1988; Battjes *et al.*, 2004).

In Chapter 3, the refraction and diffraction of non-linear periodic waves – propagating in two horizontal dimensions – by an underwater elliptical shoal is computed, using the parabolic VBM. The results of this are compared with those of a laboratory experiment (Berkhoff *et al.*, 1982).

The linear reflection characteristics, of both the parabolic and cosh VBM, are studied in Chapter 4. Wave reflection is often a topic on which many wave models do not perform well; but it is also of less importance in several coastal engineering applications. While the parabolic and cosh VBM, in the full formulation ('steep-slope' variant), perform very well regarding linear wave reflection, they perform not so well when the quasi-homogeneous approximation ('mild-slope' variants) is used. A method to remedy this is proposed, and shown to work well.

Finally, in Chapter 5, conclusions are drawn and recommendations are made.

1.6 References

Agnon, Y., Madsen, P. A. & Schäffer, H. A. 1999 A new approach to high-order Boussinesq models. *J. Fluid Mech.* **399**, 319–333.

Batchelor, G. K. 1967 *An introduction to fluid dynamics*. Cambridge Univ. Press. Xviii+615 pp.

Bateman, H. 1929 Notes on a differential equation which occurs in the two-dimensional motion of a compressible fluid and the associated variational problems. *Proc. R. Soc. London A* **125** (799), 598–618.

Battjes, J. A. 1988 Surf-zone dynamics. *Ann. Rev. Fluid Mech.* **20**, 257–291.

Battjes, J. A., Bakkenes, H. J., Janssen, T. T. & van Dongeren, A. R. 2004 Shoaling of subharmonic gravity waves. *J. Geophys. Res.* **109** (C2), C02009. 15 pp.

Benjamin, T. B. 1967 Instability of periodic wave trains in nonlinear periodic dispersive systems. *Proc. R. Soc. London A* **299** (1456), 59–75. Proc. of "A Discussion on Nonlinear Theory of Wave Propagation in Dispersive Systems" (June 13, 1967).

Benjamin, T. B., Bona, J. L. & Mahony, J. J. 1972 Model equations for long waves in nonlinear dispersive systems. *Phil. Trans. R. Soc. London A* **272** (1220), 47–78.

Benjamin, T. B. & Olver, P. J. 1982 Hamiltonian structure, symmetries and conservation laws for water waves. *J. Fluid Mech.* **125**, 137–185.

Berkhoff, J. C. W. 1972 Computation of combined refraction–diffraction. In *Proc. 13^{th} Int. Conf. Coastal Eng.,* Vancouver, pp. 796–81. ASCE.

Berkhoff, J. C. W. 1976 *Mathematical models for simple harmonic linear water waves – wave diffraction and refraction*. PhD Thesis, Delft Univ. Technology, Delft, The Netherlands. 112 pp. Also: Delft Hydraulics Publ. 163.

Berkhoff, J. C. W., Booij, N. & Radder, A. C. 1982 Verification of numerical wave propagation models for simple harmonic linear water waves. *Coastal Eng.* **6** (3), 255–279.

Booij, N. 1983 A note on the accuracy of the mild-slope equation. *Coastal Eng.* **7** (3), 191–203.

Borsboom, M., Doorn, N., Groeneweg, J. & van Gent, M. 2001 Near-shore wave simulations with a Boussinesq-type model including breaking. In *Proc. 4^{th} Int. Conf. on Coastal Dyn.,* Lund, Sweden (ed. H. Hanson & M. Larson), pp. 759–768. ASCE.

Broer, L. J. F. 1974 On the Hamiltonian theory of surface waves. *Appl. Sci. Res.* **29**, 430–446.

Broer, L. J. F. 1975 Approximate equations for long wave equations. *Appl. Sci. Res.* **31** (5), 377–395.

Broer, L. J. F., van Groesen, E. W. C. & Timmers, J. M. W. 1976 Stable model equations for long water waves. *Appl. Sci. Res.* **32** (6), 619–636.

Chamberlain, P. G. & Porter, D. 1995 The modified mild-slope equation. *J. Fluid Mech.* **291**, 393–407.

Chen, Y. & Liu, P. L.-F. 1995 Modified Boussinesq equations and associated parabolic models for water wave propagation. *J. Fluid Mech.* **288**, 351–381.

Clamond, D. & Grue, J. 2001 A fast method for fully nonlinear water wave

computations. *J. Fluid Mech.* **447**, 337–355.

Cotter, C. & Bokhove, O. 2010 Variational water-wave model with accurate dispersion and vertical vorticity. *J. Eng. Math.* 22 pp., in press.

Craig, W. & Groves, M. D. 1994 Hamiltonian long-wave approximations to the water-wave problem. *Wave Motion* **19** (4), 367–389.

Craig, W., Guyenne, P., Nicholls, D. P. & Sulem, C. 2005 Hamiltonian long-wave expansions for water waves over a rough bottom. *Proc. Roy. Soc. A* **461** (2055), 839–873.

Craig, W. & Sulem, C. 1993 Numerical simulation of gravity waves. *J. Comput. Mech.* **108** (1), 73–83.

Dingemans, M. W. 1985 Surface wave propagation over an uneven bottom; evaluation of two-dimensional horizontal wave propagation models. *Tech. Rep.*. Delft Hydraulics, Delft, The Netherlands. W301 part 5, 117 pp. & 70 figures.

Dingemans, M. W. 1997 *Water wave propagation over uneven bottoms*, *Adv. Ser. on Ocean Eng.*, vol. 13. World Scientific, Singapore. 2 Parts, 967 pp.

Dingemans, M. W. & Klopman, G. 2009 Effects of normalisation and mild-slope approximation on wave reflection by bathymetry in a Hamiltonian wave model. In *Proc. 24th Int. Workshop on Water Waves and Floating Bodies,* Zelenogorsk, Russia, April 2009.

Dommermuth, D. G. & Yue, D. K. P. 1987 A high-order spectral method for the study of nonlinear gravity waves. *J. Fluid Mech.* **184**, 267–288.

Dysthe, K. B. 1979 Note on a modification to the nonlinear Schrödinger equation for application to deep water waves. *Proc. R. Soc. London A* **369**, 105–114.

Eckart, C. 1952 The propagation of gravity waves from deep to shallow water. In *Gravity waves*, pp. 165–173. National Bureau of Standards, Washington. Circular 521.

Fructus, D., Clamond, D., Grue, J. & Kristiansen, Ø. 2005*a* Efficient numerical model for three-dimensional gravity waves simulations. Part I: Periodic domains. *J. Comput. Phys.* **205** (2), 665–685.

Fructus, D. & Grue, J. 2007 An explicit method for the nonlinear interaction between water waves and variable and moving bottom topography. *J. Comput. Phys.* **222** (2), 720–739.

Fructus, D., Kharif, C., Francius, M., Kristiansen, Ø., Clamond, D. & Grue, J. 2005*b* Dynamics of crescent water wave patterns. *J. Fluid Mech.* **537**, 155–186.

Fuhrman, D. R. & Madsen, P. A. 2008 Simulation of nonlinear wave run-up with a high-order Boussinesq model. *Coastal Eng.* **55** (2), 139–154.

Green, A. E. & Naghdi, P. M. 1976 A derivation of equations for wave propagation in water of variable depth. *J. Fluid Mech.* **78** (2), 237–246.

van Groesen, E. & Andonowati 2007 Variational derivation of KdV-type models for surface water waves. *Phys. Lett. A* **366** (3), 195–201.

van Groesen, E., Andonowati, She Liam, L. & Lakhturov, I. 2010 Accurate modelling of uni-directional surface waves. *J. Comput. Appl. Math.* Article in press.

van Groesen, E. & de Jager, E. M. 1994 *Mathematical structures in continuous dynamical systems: Poisson systems and complete integrability with applications from fluid dynamics*, *Studies in mathematical physics*, vol. 6. North-Holland, Am-

sterdam. Xiv+617 pp.

van Groesen, E. & Westhuis, J. H. 2002 Modelling and simulation of surface water waves. *Math. Comput. Sim.* **59** (4), 341–360.

van Groesen, E. W. C. 1978 *Variational methods in mathematical physics*. PhD Thesis, Technische Hogeschool Eindhoven, Eindhoven, The Netherlands. 216 pp.

Guyenne, P. & Nicholls, D. P. 2007 A high-order spectral method for nonlinear water waves over moving bottom topography. *SIAM J. Sci. Comput.* **30** (1), 81–101.

Hayes, W. D. 1970*a* Conservation of action and modal wave action. *Proc. R. Soc. London A* **330** (1541), 187–208.

Hayes, W. D. 1973 Group velocity and nonlinear dispersive wave propagation. *Proc. R. Soc. London A* **332** (1589), 199–221.

Janssen, T. T., Herbers, T. H. C. & Battjes, J. A. 2006 Generalized evolution equations for nonlinear surface gravity waves over two-dimensional topography. *J. Fluid Mech.* **552**, 393–418.

Klopman, G. & Dingemans, M. W. 2010 Reflection in variational models for linear water waves. *Wave Motion* Accepted for publication.

Klopman, G., Dingemans, M. W. & van Groesen, E. 2005 A variational model for fully non-linear water waves of Boussinesq type. In *Proc. 20th Int. Workshop on Water Waves and Floating Bodies,* Longyearbyen, Spitsbergen, Norway, May 2005.

Klopman, G., Dingemans, M. W. & van Groesen, E. 2007 The propagation of wave groups over bathymetry using a variational Boussinesq model. In *Proc. 22th Int. Workshop on Water Waves and Floating Bodies,* Plitvice, Croatia, April 2007.

Klopman, G., van Groesen, E. & Dingemans, M. W. 2010 A variational approach to Boussinesq modelling of fully non-linear water waves. *J. Fluid Mech.* Accepted for publication.

Lakhturov, I. & van Groesen, E. 2010 Optimized Variational Boussinesq Modelling for broad-band waves over flat bottom. *Submitted for publication* .

Lighthill, M. J. 1978 *Waves in fluids*. Cambridge Univ. Press. 504 pp.

Longuet-Higgins, M. S. & Fenton, J. D. 1974 On the mass, momentum, energy and circulation of a solitary wave. II. *Proc. R. Soc. London A* **340** (1623), 471–493.

Luke, J. C. 1967 A variational principle for a fluid with a free surface. *J. Fluid Mech.* **27** (2), 395–397.

Luth, H. R., Klopman, G. & Kitou, N. 1994 Project 13G: Kinematics of waves breaking partially on an offshore bar. LDV measurements for waves with and without a net onshore current. *Tech. Rep.* H1573. Delft Hydraulics, Delft, The Netherlands. 40 pp.

Lynett, P. J. 2006 Nearshore wave modeling with high-order Boussinesq-type equations. *J. Waterway, Port, Coastal and Ocean Eng.* **132** (5), 348–357.

Lynett, P. J. & Liu, P. L.-F. 2004*a* a two-layer approach to wave modelling. *Proc. R. Soc. A* **460** (2049), 2637–2669.

Lynett, P. J. & Liu, P. L.-F. 2004*b* linear analysis of the multi-layer model. *Coastal Eng.* **51** (5–6), 439–454.

Madsen, P. A., Murray, R. & Sørensen, O. R. 1991 A new form of the Boussinesq equations with improved linear dispersion characteristics. *Coastal Eng.*

15 (4), 371–388.

Madsen, P. A. & Schäffer, H. A. 1999 A review of Boussinesq-type equations for gravity waves. In *Adv. Coastal Ocean Eng.* (ed. P. L.-F. Liu), , vol. 5, pp. 1–95. World Scientific.

Madsen, P. A. & Sørensen, O. R. 1992 A new form of the Boussinesq equations with improved linear dispersion characteristics. Part 2. A slowly-varying bathymetry. *Coastal Eng.* **18** (3–4), 183–204.

Milder, D. M. 1977 A note on: 'On Hamilton's principle for surface waves'. *J. Fluid Mech.* **83** (1), 159–161.

Milder, D. M. 1990 The effect of truncation on surface-wave Hamiltonians. *J. Fluid Mech.* **216**, 249–262.

Miles, J. W. 1977 On Hamilton's principle for surface waves. *J. Fluid Mech.* **83** (1), 153–158.

Miles, J. W. & Salmon, R. 1985 Weakly dispersive nonlinear gravity waves. *J. Fluid Mech.* **157**, 519–531.

Mooiman, J. 1991*a* Boussinesq equations based on a positive definite Hamiltonian. *Tech. Rep.* Z294. Delft Hydraulics, Delft, The Netherlands. 78 pp.

Mooiman, J. 1991*b* Comparison between measurements and a Boussinesq model for wave deformation by a shoal. *Tech. Rep.* Z294, Part 2. Delft Hydraulics, Delft, The Netherlands. 25 pp.

Mooiman, J. & Verboom, G. K. 1992 A new Boussinesq model based on a positive definite Hamiltonian. In *Int. Conf. on Comput. Meth. in Water Resources IX* (ed. T. F. Russel, R. E. Ewing, C. A. Brebbia, W. G. Gray & G. F. Pinder), , vol. 2, pp. 513–527. Comput. Mech. Publ.

Nadaoka, K., Beji, S. & Nakagawa, Y. 1997 A fully-dispersive weakly nonlinear model for water waves. *Proc. R. Soc. London A* **453** (1957), 303–318.

Otta, A. K., Dingemans, M. W. & Radder, A. C. 1996 A Hamiltonian model for nonlinear water waves and its applications. In *Proc.* 25^{th} *Int. Conf. Coastal Eng.,* Orlando, , vol. 1, pp. 1156–1167. ASCE, New York, U.S.A.

Peregrine, D. H. 1972 Equations for water waves and the approximation behind them. In *Waves on beaches and resulting sediment transport* (ed. R. E. Meyer), pp. 95–122. Academic Press.

Porter, R. & Porter, D. 2006 Approximations to the scattering of water waves by steep topography. *J. Fluid Mech.* **562**, 279–302.

Radder, A. C. 1999 Hamiltonian dynamics of water waves. In *Adv. in Coastal and Ocean Eng.* (ed. P. L.-F. Liu), , vol. 4, pp. 21–59. World Scientific, Singapore.

Radder, A. C. & Dingemans, M. W. 1985 Canonical equations for almost periodic, weakly nonlinear gravity waves. *Wave Motion* **7** (5), 473–485.

Rienecker, M. M. & Fenton, J. D. 1981 A Fourier approximation method for steady water waves. *J. Fluid Mech.* **104**, 119–137.

van Rijn, L. C. 2009 Prediction of dune erosion due to storms. *Coastal Eng.* **56** (4), 441–457.

Salmon, R. 1988*a* Hamiltonian fluid dynamics. *Ann. Rev. Fluid Mech.* **20**, 225–256.

She Liam, L. & van Groesen, E. 2010 Variational derivation of improved KP-type of equations. *Phys. Lett. A* **374** (3), 411–415.

Shepherd, T. G. 1990 Symmetries, conservation laws, and Hamiltonian structure in geophysical fluid dynamics. *Adv. Geophys.* **32**, 287–338.

Shields, J. J. & Webster, W. C. 1988 On direct methods in water-wave theory. *J. Fluid Mech.* **197**, 171–199.

Stelling, G. S. & van Kester, J. 2001 Efficient non hydrostatic free surface models. In *Estuarine and Coastal Modeling 2001,* Proc. 7th Int. Conf., St. Petersburg, Florida (ed. M. L. Spaulding), pp. 709–724. ASCE.

Tanaka, M. 1986 The stability of solitary waves. *Phys. Fluids* **29** (3), 650–655.

Trulsen, K. 2007 Weakly nonlinear sea surface waves – Freak waves and deterministic forecasting. In *Geometric modelling, numerical simulation, and optimization. Applied Mathematics at SINTEF.* Part II (ed. G. Hasle, K.-A. Lie & E. Quak), pp. 191–209. Springer.

Trulsen, K., Kliakhandler, I., Dysthe, K. B. & Velarde, M. G. 2000 On weakly nonlinear modulation of waves on deep water. *Phys. Fluids* **12** (10), 2432–2437.

van der Veen, W. A. & Wubs, F. W. 1995 A Hamiltonian approach to fairly low and fairly long gravity waves. *J. Eng. Math.* **29** (4), 329–345.

Watson, K. M. & West, B. J. 1975 A transport-equation description of nonlinear ocean surface wave interactions. *J. Fluid Mech.* **70** (4), 815–826.

West, B. J., Brueckner, K. A., Janda, R. S., Milder, D. M. & Milton, R. L. 1987 A new numerical method for surface hydrodynamics. *J. Geophys. Res.* **92** (C11), 11803–11824.

Whitham, G. B. 1967*b* Variational methods and applications to water waves. *Proc. R. Soc. London A* **299** (1456), 6–25. Proc. of "A Discussion on Nonlinear Theory of Wave Propagation in Dispersive Systems" (June 13, 1967).

Whitham, G. B. 1974 *Linear and nonlinear waves*. Wiley–Interscience.

Williams, J. M. 1981 Limiting gravity waves in water of finite depth. *Phil. Trans. R. Soc. London A* **302** (1466), 139–188.

Witting, J. M. 1984 A unified model for the evolution of nonlinear water waves. *J. Comput. Phys.* **56** (4), 203–236.

Zakharov, V. E. 1968 Stability of periodic waves of finite amplitude on the surface of a deep fluid. *J. Appl. Mech. and Techn. Phys.* **9** (2), 190–194. Originally in: *Zhurnal Prildadnoi Mekhaniki i Tekhnicheskoi Fiziki* **9**(2), pp. 86–94, 1968.

Zijlema, M. & Stelling, G. S. 2008 Efficient computation of surf zone waves using the nonlinear shallow water equations with non-hydrostatic pressure. *Coastal Eng.* **55** (10), 780–790.

Chapter 2

A variational approach to Boussinesq modelling of fully non-linear water waves[1]

Abstract

In this paper we present a new method to derive from a variational principle Boussinesq-type equations, for nonlinear surface water-waves propagating over bathymetry. The vertical structure of the flow, required in the Hamiltonian, is approximated by a (series of) vertical shape functions associated with unknown parameter(s). It is not necessary to make approximations with respect to the non-linearity of the waves. The resulting approximate Hamiltonian is positive definite, contributing to the good dynamical behaviour of the resulting equations. The resulting flow equations consist of temporal evolution equations for the surface elevation and potential, as well as a (set of) elliptic equations for some auxiliary parameter(s). All equations only contain low-order spatial derivatives and no mixed time-space derivatives. Since one of the parameters, the surface potential, can be associated with a uniform shape function, the resulting equations are very well suited for wave-current interacting flows.

The variational method is applied to two simple models, one with a parabolic vertical shape function and the other with a hyperbolic-cosine vertical structure. For both, as well as the general series model, the flow equations are derived. Linear dispersion and shoaling are studied using the average Lagrangian. The model with a parabolic vertical shape function has improved frequency dispersion, as compared to classical Boussinesq models. The model with a hyperbolic-cosine vertical structure can be made to have exact phase and group velocity, as well as shoaling, for a certain frequency.

For the model with a parabolic vertical structure, numerical computations are made with a one-dimensional pseudo-spectral code. These show the non-linear capabilities for periodic waves over a horizontal bed and an underwater bar. Further some long-distance computations for soliton wave groups over bathymetry are presented.

[1]In press, accepted for publication:
Klopman, G., van Groesen, E. & Dingemans, M. W. 2010 A variational approach to Boussinesq modelling of fully non-linear water waves. *J. Fluid Mech.*

2.1 Introduction

The discovery of the Hamilton theory for surface water waves, independently made by Zakharov (1968), Broer (1974) and Miles (1977) (see also Milder, 1977), was associated with the search for approximate Hamiltonian models containing as much as possible of the essential characteristics of the exact theory. While Zakharov (1968) focussed especially on deep water waves, Broer (1974, 1975) and Miles (1977) also paid attention to relatively long waves of Boussinesq type.

Positive-definiteness of the Hamiltonian is one of the important properties of the Hamiltonian, since it attributes to the good dynamical behaviour of the resulting equations. Non-positivity of the approximate Hamiltonian may lead to instabilities, see *e.g.* Milder (1990), Broer (1974) and Katopodes & Dingemans (1989).

Dingemans (1997, §5.6) describes several methods for constructing Boussinesq-type models with positive-definite Hamiltonian, but these methods are quite tedious and have certain ambiguities regarding the order of certain operators, see also Broer (1974, 1975); Broer, van Groesen & Timmers (1976). The described models are weakly non-linear.

Further, there is the demand for improved frequency dispersion and non-linear characteristics in Boussinesq models, as compared to the classical ones. As a result several improved Boussinesq-type models have been developed, starting with Madsen *et al.* (1991), Madsen & Sørensen (1992) using methods of Witting (1984). Another step was made with the introduction of a high-order non-linear Boussinesq-type model in Agnon *et al.* (1999) (see also Madsen *et al.*, 2003; Fuhrman & Bingham, 2004), which uses the free-surface boundary conditions as found from Hamilton theory. However, the additional approximations to relate the free-surface quantities to those at another fixed level destroy the positive definiteness of the Hamiltonian. The same is true for other high order methods, *e.g.* Dommermuth & Yue (1987) and West *et al.* (1987).

Lynett & Liu (2004*a*,*b*) derive a (non-Hamiltonian) Boussinesq-type of model in which they use a multi-layer approach in the vertical. In each layer they use a parabolic vertical structure for the horizontal velocity, and a linear one for the vertical velocity. By adding layers, the frequency-dispersion characteristics can be improved (Lynett & Liu, 2004*b*; Hsiao *et al.*, 2005).

A fully non-linear and positive-definite Hamiltonian model for waves over bathymetry has been devised by Radder (1992), which however is of quite complicated form especially when constructing numerical solutions (Otta *et al.*, 1996). See Radder (1999) for a review of Hamiltonian models for water waves.

Here, we will present a variational method to derive Boussinesq models for water waves over bathymetry (for shortness, we will speak of variational Boussinesq models). The present method is relatively easy, leads to a positive-definite Hamiltonian and can be fully non-linear if desired. Besides the general form we also give some simple examples for three different vertical velocity-potential structures: parabolic, hyperbolic cosine and by a power series. We restrict ourselves to mildly-sloping bathymetry, to simplify the resulting equations, but this is not essential to the

method. The advantage of the present variational Boussinesq model is, that no higher-order spatial and/or mixed spatial-temporal derivatives appear. But, this is at the cost of the requirement to solve one or more additional linear elliptic equations in the horizontal plane.

First, we will outline the methodology of our method in §2.2. Then, in §2.3, we will apply this to a simple parabolic shape function. Thereafter we will present the general case of a series of vertical shape functions and associated parameters in §2.4. Also two more examples of the method will be given, one with a cosh (hyperbolic-cosine) vertical shape function, and another with a power-series representation of the vertical structure. Some linear characteristics, *e.g.* frequency dispersion and shoaling by depth changes, will be studied in §2.5. For this we will use the average Lagrangian technique of Whitham (1974), and apply it also to the three model examples. Finally, in §2.6, we will present numerical simulations using the parabolic vertical-structure model, in order to study the applicability and non-linear characteristics of the model. Periodic waves and confined wave groups will be computed, both when propagating over a horizontal bed, as well as over bathymetry.

2.2 Variational principle and modelling

We start from the variational principle for irrotational surface water waves on an incompressible inviscid homogeneous fluid, in the form as given by Miles (1977). With $\phi(\mathbf{x}, z, t)$ the velocity potential, $\zeta(\mathbf{x}, t)$ the free-surface elevation and $\varphi(\mathbf{x}, t) \equiv \phi(\mathbf{x}, \zeta(\mathbf{x}, t), t)$ the velocity potential at the free surface, we have:

$$0 = \delta\mathscr{L} = \delta \iiint L \, \mathrm{d}\mathbf{x} \, \mathrm{d}t \quad \text{with} \tag{2.1a}$$

$$L = \varphi \, \partial_t \zeta - H \quad \text{and} \quad H = \int_{-h_0}^{\zeta} \frac{1}{2} \left[(\boldsymbol{\nabla}\phi)^2 + (\partial_z \phi)^2 \right] \mathrm{d}z + \frac{1}{2} g \, \zeta^2. \tag{2.1b}$$

Here $\mathscr{L}(\zeta, \varphi)$ is the Lagrangian, $L(\zeta, \varphi; \mathbf{x}, t)$ is the associated Lagrangian density per unit of horizontal area and time and $H(\zeta, \varphi; \mathbf{x}, t)$ is the Hamiltonian density, *i.e.* the sum of the kinetic and potential energy densities per unit area. The horizontal and vertical coordinates are $\mathbf{x} = (x_1, x_2)^T$ and z respectively, and t is the time coordinate. The irrotational fluid flow is described by a velocity potential $\phi(\mathbf{x}, z, t)$, with the horizontal and vertical flow velocities given by $\boldsymbol{\nabla}\phi$ and $\partial_z\phi$ respectively, where $\boldsymbol{\nabla} \equiv (\partial_{x_1}, \partial_{x_2})^T$ is the horizontal gradient operator. With $(\boldsymbol{\nabla}\phi)^2$ is meant the inner product $(\boldsymbol{\nabla}\phi) \cdot (\boldsymbol{\nabla}\phi)$. The fluid domain is bounded below by the sea bed at $z = -h_0(\mathbf{x})$ and above by a free surface at $z = \zeta(\mathbf{x}, t)$. Further g is the acceleration by gravity, the fluid mass density is taken to be constant and equal to one.

As shown by Miles (1977), the above Lagrangian variational principle is equivalent to the Hamiltonian approach. The Hamiltonian $\mathscr{H}(\zeta, \varphi; t)$ itself is the spatial integral of (2.1b):

$$\mathscr{H} = \iint H \, \mathrm{d}\mathbf{x}. \tag{2.2}$$

The flow dynamics are completely described by ζ and φ, provided that in the fluid interior the Laplace equation is satisfied, as well as the kinematic boundary condition at the sea bed (Zakharov, 1968; Broer, 1974; Miles, 1977; Milder, 1977).

While the above equations are exact and give all the equations necessary for the description of the flow, they are in general not solvable in closed form. Therefore, for practical applications approximations have to be made. We directly model the horizontal and vertical velocities, $\boldsymbol{\nabla}\phi$ and $\partial_z\phi$, in the Hamiltonian density H, equation (2.1b), and apply this in the variational principle (2.1a). In doing so, several characteristics of the exact Hamiltonian system can be transferred into the approximate flow equations. By Noether's theorem, symmetries in the variational principle translate into conservation laws (see *e.g.* Benjamin, 1984; Benjamin & Olver, 1982; Brizard, 2005). Among these are conservation of energy and mass; this is due to the independence of the Hamiltonian on time translations and on the choice of the zero level of the velocity potential. In general, the Hamiltonian is not constant under changes of the horizontal position $\mathbf{x}$, since the still water depth h_0 is a function of $\mathbf{x}$. So, apart from the special case when h_0 is a constant, horizontal momentum will not be conserved. But conservation of mass and energy can easily be maintained in approximate models (as well as horizontal momentum for the case of h_0 constant). Another property of the Hamiltonian density (2.1b) is that it is positive definite.

For shortness of notation, the summation convention is used throughout this paper, *i.e.* a repeated index indicates summation is used:

$$\alpha_m\,\beta_m \;\equiv\; \sum_{m=1}^{M} \alpha_m\,\beta_m. \tag{2.3}$$

Repeated roman indices indicate summation from 1 to M.

Since we are interested in large horizontal domains with the surface waves propagating horizontally, we choose to approximate the potential ϕ in the fluid interior by a vertical structure:

$$\phi(\mathbf{x},z,t) \;=\; \varphi(\mathbf{x},t) \;+\; f_m(z;h_0,\zeta,\kappa_m)\;\psi_m(\mathbf{x},t), \qquad \text{with} \tag{2.4a}$$

$$f_m \;=\; 0 \quad \text{at } z=\zeta(\mathbf{x},t) \qquad \text{for } m=1,2\cdots M. \tag{2.4b}$$

Here $f_m(z;h_0,\zeta,\kappa_m)$ are the prescribed vertical shape functions associated with the parameters $\psi_m(\mathbf{x},t)$ for $m=1,2\cdots M$, with M the (small) number of shape functions used. Further, the $\kappa_m(\mathbf{x})$ are optional shape parameters, which may eventually be specified (*e.g.* an expected curvature of the velocity profile based on knowledge of the incoming wave field). Note that we assume $\kappa_m(\mathbf{x})$ to be known and fixed *a priori*.

The requirement (2.4b) is essential: the shape functions f_m have to be zero at the free surface. It guarantees that only two evolution equations with simple time derivatives $\partial_t\zeta$ and $\partial_t\varphi$ will appear, when taking the variations with respect to the surface potential φ and elevation ζ of the term $\varphi\;\partial_t\zeta$ in the Lagrangian (2.1) [2].

[2] Whitham (1967*b*), in deriving Boussinesq-type equations using a Lagrangian variational approach, also remarks that the flow equations become simpler in terms of the surface potential.

Note, that in the approximation (2.4a), the first term $\varphi(\mathbf{x},t)$ can be thought of as being associated with a uniform shape function, *i.e.* equal to one for all z. This means that the model will always include a description well suitable for interactions between short waves and long waves or currents. As a result, we have the following Hamiltonian description in terms of the canonical variables ζ and φ:

$$\partial_t\zeta \;=\; +\,\frac{\delta\mathscr{H}}{\delta\varphi} \qquad \text{and} \qquad \partial_t\varphi \;=\; -\,\frac{\delta\mathscr{H}}{\delta\zeta} \tag{2.5a}$$

under the requirement that

$$\frac{\delta\mathscr{H}}{\delta\psi_m} \;=\; 0 \qquad \text{for } m=1,2\cdots M, \tag{2.5b}$$

where $\delta\mathscr{H}/\delta\zeta$, $\delta\mathscr{H}/\delta\varphi$ and $\delta\mathscr{H}/\delta\psi_m$ denote the variational derivatives of $\mathscr{H}(\zeta,\varphi,\psi_m)$ with respect to ζ, φ and ψ_m respectively.

Using (2.4a), we have the following expressions for the flow velocities:

$$\begin{aligned}\boldsymbol{\nabla}\phi =\;& \boldsymbol{\nabla}\varphi \;+\; f_m\,\boldsymbol{\nabla}\psi_m \;+\; (\partial_\zeta f_m)\,\psi_m\,\boldsymbol{\nabla}\zeta \\ &+\; (\partial_{h_0} f_m)\,\psi_m\,\boldsymbol{\nabla}h_0 \;+\; (\partial_{\kappa_m} f_m)\,\psi_m\,\boldsymbol{\nabla}\kappa_m \qquad \text{and} \qquad (2.6a)\\ \partial_z\phi =\;& (\partial_z f_m)\,\psi_m \qquad \text{for } m=1,2\cdots M. \qquad (2.6b)\end{aligned}$$

Since our interest is in waves propagating in the coastal zone, where bed slopes are typically small, we restrict ourselves to mildly sloping beds. The bed slopes $\boldsymbol{\nabla}h_0$ and parameter derivatives $\boldsymbol{\nabla}\kappa_m$ then are neglected when approximating the horizontal and vertical flow velocities, $\boldsymbol{\nabla}\phi$ and $\partial_z\phi$, in the Hamiltonian density H. If the mild-slope assumption is not imposed, additional terms appear in the (still positive-definite) Hamiltonian density H and in the resulting flow equations. These extra terms are of importance for wave reflections and in case of rather steep slopes (Dingemans & Klopman, 2009).

Using the mild slope approximation, equations (2.6) simplify to:

$$\begin{aligned}\boldsymbol{\nabla}\phi \approx\;& \boldsymbol{\nabla}\varphi \;+\; f_m\,\boldsymbol{\nabla}\psi_m \;+\; (\partial_\zeta f_m)\,\psi_m\,\boldsymbol{\nabla}\zeta \qquad \text{and} \qquad (2.7a)\\ \partial_z\phi =\;& (\partial_z f_m)\,\psi_m \qquad \text{for } m=1,2\cdots M. \qquad (2.7b)\end{aligned}$$

When applied in (2.1b), a positive-definite Hamiltonian density $H(\zeta,\varphi,\psi_m;\mathbf{x},t)$ will be the result. Furthermore, the cross space z is integrated out, and the resulting system is only a function of the propagation space $\mathbf{x}$ and time t. Since, in our approximation, the highest spatial derivatives in the Hamiltonian density H are (quadratics of) first derivatives, the highest derivatives in the potential flow equations (2.5) will be second-order spatial derivatives. No mixed time-space derivatives appear. As we will see later, (2.5b) is, for given ζ and φ, a set of coupled linear second-order elliptic equations in the additional functions ψ_m, $m=1,2\cdots M$.

While the above equations (2.5) are in terms of the surface potential φ, it is also possible to express them in terms of the surface-potential gradient $\mathbf{u}\equiv\boldsymbol{\nabla}\varphi$. Note that $\mathbf{u}$ is not equal to the horizontal flow velocity $\boldsymbol{\nabla}\phi$ at the free surface, *i.e.* $\mathbf{u}=$

$[\boldsymbol{\nabla}\phi]_{z=\zeta} + [\partial_z\phi]_{z=\zeta}\boldsymbol{\nabla}\zeta$. After replacing $\boldsymbol{\nabla}\varphi$ with $\mathbf{u} = (u_1, u_2)^T$ in the Hamiltonian $\mathscr{H}$, we get the following Hamiltonian system:

$$\partial_t\zeta \;=\; -\mathrm{div}\,\frac{\delta\mathscr{H}}{\delta\mathbf{u}} \qquad \text{and} \qquad \partial_t\mathbf{u} \;=\; -\boldsymbol{\nabla}\,\frac{\delta\mathscr{H}}{\delta\zeta}, \tag{2.8}$$

under the additional requirement that each $\delta\mathscr{H}/\delta\psi_m = 0$ for all $m = 1, 2\cdots M$. As for all Boussinesq models, the Laplace equation is no longer satisfied exactly in the fluid interior. So while the flow is still irrotational, the fluid is no longer exactly incompressible. However, as can be seen from the equation for $\partial_t\zeta$ in (2.8), we still have depth-integrated mass-conservation (also in the velocity-potential formulation). Notice that an extension to flow with vorticity can easily be carried out using Shepherd (1990, equation (4.45)).

As a practical and simple application of the above approach, we will next consider the example of a single parabolic shape function ($M = 1$), which we will call hereafter the parabolic structure model. Next, we will continue with the more general case of several shape functions ($M > 1$). Finally, we discuss the case of a hyperbolic-cosine shape function (to be called the cosh or hyperbolic-cosine structure model in the remainder).

2.3 Parabolic structure model

Boussinesq (1872), for the case of a horizontal bottom, expressed the velocity potential ϕ as a series in the z-direction around the bed level $z = -h_0$. Due to the impermeability of the bed, the vertical velocity $\partial_z\phi$ will be zero at the bed level $z = -h_0$. Then, to lowest order, the first deviation from a depth-uniform potential will be a parabolic contribution, in terms of the distance $z + h_0$ to the bed. Therefore, as a simple vertical structure model, we take $M = 1$ in equation (2.4a) and a parabolic shape function $f^{(p)}(z;\zeta,h_0)$:

$$f^{(p)}(z;\zeta,h_0) \;=\; \frac{1}{2}\,(\,z \;-\; \zeta\,)\;\frac{2\,h_0 \;+\; z \;+\; \zeta}{h_0 \;+\; \zeta}, \tag{2.9}$$

satisfying $\partial_z f^{(p)} = 0$ at the bed $z = -h_0$ and $f^{(p)} = 0$ at the free surface $z = \zeta$. Further $f^{(p)}$ has been scaled in such a way that the associated parameter $\psi^{(p)}(\mathbf{x},t)$ equals the vertical velocity $\partial_z\phi$ at the free surface. It is assumed that the above parabolic structure model is also a good approximation for the vertical flow structure in case of mild bottom slopes.

For shortness of notation, we introduce the total water depth $h(\mathbf{x},t) \equiv h_0(\mathbf{x}) + \zeta(\mathbf{x},t)$. The Hamiltonian density $H^{(p)}(\zeta,\varphi,\psi^{(p)};\mathbf{x},t)$ becomes, for the parabolic shape function (2.9) – after vertical integration using equations (2.7) and (2.1b):

$$\begin{aligned} H^{(p)} \;=\; & \frac{1}{2}\,h\,\left(\boldsymbol{\nabla}\varphi \;-\; \frac{2}{3}\,\psi^{(p)}\,\boldsymbol{\nabla}\zeta \;-\; \frac{1}{3}\,h\,\boldsymbol{\nabla}\psi^{(p)}\right)^2 \\ & +\; \frac{1}{90}\,h\,\left(\psi\,\boldsymbol{\nabla}\zeta \;-\; h\,\boldsymbol{\nabla}\psi^{(p)}\right)^2 \;+\; \frac{1}{6}\,h\,\left(\psi^{(p)}\right)^2 \;+\; \frac{1}{2}\,g\,\zeta^2, \end{aligned} \tag{2.10}$$

which indeed is positive definite, since the water depth h is always positive. Note that the Hamiltonian density is fully non-linear: no approximations have been made apart from the form and number of the shape functions, and the mild-slope approximation. The latter is only for convenience and is not essential to the method.

Taking the variations of the Hamiltonian $\mathscr{H} = \iint H \, \mathrm{d}\mathbf{x}$, the flow equations (2.5) become, after some re-arrangements:

$$\partial_t \zeta + \boldsymbol{\nabla} \cdot \left(h \, \mathbf{U}^{(p)} \right) \, = \, 0, \tag{2.11a}$$

$$\begin{aligned} \partial_t \varphi + \frac{1}{2} \left(\mathbf{U}^{(p)} \right)^2 - \frac{1}{45} \left(\psi^{(p)} \, \boldsymbol{\nabla}\zeta \, + \, h \, \boldsymbol{\nabla}\psi^{(p)} \right)^2 + \frac{1}{6} \left(1 + \frac{1}{5} (\boldsymbol{\nabla}\zeta)^2 \right) \left(\psi^{(p)} \right)^2 + \\ + \, \boldsymbol{\nabla} \cdot \left[h \, \left(\frac{2}{3} \boldsymbol{\nabla}\varphi \, - \, \frac{7}{15} \psi^{(p)} \, \boldsymbol{\nabla}\zeta \, - \, \frac{1}{5} h \, \boldsymbol{\nabla}\psi^{(p)} \right) \psi^{(p)} \right] + \, g \, \zeta \, = 0, \end{aligned} \tag{2.11b}$$

$$\begin{aligned} h \, \psi^{(p)} \left(\frac{1}{3} \, + \, \frac{7}{15} (\boldsymbol{\nabla}\zeta)^2 \right) \, - \, \left(\frac{2}{3} h \, \boldsymbol{\nabla}\varphi \, - \, \frac{1}{5} h^2 \, \boldsymbol{\nabla}\psi^{(p)} \right) \cdot \boldsymbol{\nabla}\zeta + \\ + \boldsymbol{\nabla} \cdot \left(\frac{1}{3} h^2 \, \boldsymbol{\nabla}\varphi \, - \, \frac{1}{5} h^2 \, \psi^{(p)} \, \boldsymbol{\nabla}\zeta \, - \, \frac{2}{15} h^3 \, \boldsymbol{\nabla}\psi^{(p)} \right) \, = \, 0, \end{aligned} \tag{2.11c}$$

where $\mathbf{U}^{(p)}(\mathbf{x}, t)$ is the depth-averaged velocity:

$$\mathbf{U}^{(p)} \, = \, \boldsymbol{\nabla}\varphi \, - \, \frac{2}{3} \psi^{(p)} \, \boldsymbol{\nabla}\zeta \, - \, \frac{1}{3} h \, \boldsymbol{\nabla}\psi^{(p)}. \tag{2.12}$$

For one spatial dimension, these equations are equal to those derived in Klopman *et al.* (2005). So equations (2.11a,b) are the mass-conservation equation for the time evolution of ζ and a Bernouilli-like equation for the surface potential φ. Further, we have to solve a linear elliptic equation (2.11c) in terms of $\psi^{(p)}$, for given ζ and φ.

Later, in §2.6, we will give the results of some numerical simulations using equations (2.11) in one spatial dimension. The linear characteristics of the parabolic structure model, *i.e.* linear dispersion and shoaling, will be derived in §2.5.

2.4 General series model

Now we treat the general case of a vertical velocity-potential structure, as given in equation (2.4). By carefully choosing a small number M of shape functions $f_m(z; h_0, \zeta, \kappa_m)$, $m = 1 \cdots M$, one aims at getting a good approximation to the exact vertical flow structure. Using equation (2.7) in (2.5), we find for $H(\zeta, \varphi, \psi_m; \mathbf{x}, t)$:

$$\begin{aligned} H = \frac{1}{2} \, (\, h_0 \, + \, \zeta \,) \, (\, \boldsymbol{\nabla}\varphi \,)^2 \, + \\ + \, \frac{1}{2} F_{mn} \, (\, \boldsymbol{\nabla}\psi_m \,) \cdot (\, \boldsymbol{\nabla}\psi_n \,) \, + \, \frac{1}{2} G_{mn} \, \psi_m \, \psi_n \, (\, \boldsymbol{\nabla}\zeta \,)^2 \, + \, \frac{1}{2} K_{mn} \, \psi_m \, \psi_n \, + \\ + \, P_m \, (\, \boldsymbol{\nabla}\psi_m \,) \cdot (\, \boldsymbol{\nabla}\varphi \,) \, + \, Q_m \, \psi_m \, (\, \boldsymbol{\nabla}\varphi \,) \cdot (\, \boldsymbol{\nabla}\zeta \,) \, + \, R_{mn} \, \psi_n (\, \boldsymbol{\nabla}\psi_m \,) \cdot (\, \boldsymbol{\nabla}\zeta \,) \, + \\ + \, \frac{1}{2} \, g \, \zeta^2, \end{aligned} \tag{2.13}$$

where the integrals herein are defined by:

$$F_{mn}(\zeta,h_0;\kappa_m,\kappa_n) = \int_{-h_0}^{\zeta} f_m\, f_n \,\mathrm{d}z \qquad = F_{nm}, \tag{2.14a}$$

$$G_{mn}(\zeta,h_0;\kappa_m,\kappa_n) = \int_{-h_0}^{\zeta} (\,\partial_\zeta f_m\,)\,(\,\partial_\zeta f_n\,)\,\mathrm{d}z = G_{nm}, \tag{2.14b}$$

$$K_{mn}(\zeta,h_0;\kappa_m,\kappa_n) = \int_{-h_0}^{\zeta} (\,\partial_z f_m\,)\,(\,\partial_z f_n\,)\,\mathrm{d}z = K_{nm}, \tag{2.14c}$$

$$P_m(\zeta,h_0;\kappa_m) = \int_{-h_0}^{\zeta} f_m \,\mathrm{d}z, \tag{2.14d}$$

$$Q_m(\zeta,h_0;\kappa_m) = \int_{-h_0}^{\zeta} (\,\partial_\zeta f_m\,)\,\mathrm{d}z \qquad \text{and} \tag{2.14e}$$

$$R_{mn}(\zeta,h_0;\kappa_m,\kappa_n) = \int_{-h_0}^{\zeta} f_m\,(\,\partial_\zeta f_n\,)\,\mathrm{d}z. \tag{2.14f}$$

Taking the variations of $\mathscr{H}$, as required by the Hamiltonian system (2.5), and keeping in mind that the coefficients as given in (2.14) also depend on $\zeta(\mathbf{x},t)$, gives the following flow equations:

$$\partial_t\zeta + \boldsymbol{\nabla}\cdot\Big[\,(h_0+\zeta)\,\boldsymbol{\nabla}\varphi \;+\; P_m\,\boldsymbol{\nabla}\psi_m \;+\; Q_m\,\psi_m\,\boldsymbol{\nabla}\zeta\,\Big] \;=\; 0, \tag{2.15a}$$

$$\partial_t\varphi + \frac{1}{2}\,(\boldsymbol{\nabla}\varphi)^2 \;+\; g\,\zeta \;+\; \mathcal{R} \;=\; 0 \tag{2.15b}$$

and

$$\begin{aligned}\Big[\;G_{lm}\,(\boldsymbol{\nabla}\zeta)^2 \;+\; K_{lm}\,\Big]\,\psi_m \;+\; Q_l\,(\boldsymbol{\nabla}\varphi)\cdot(\boldsymbol{\nabla}\zeta) \;+\; R_{ml}\,(\boldsymbol{\nabla}\psi_m)\cdot(\boldsymbol{\nabla}\zeta) \;+\\ -\;\boldsymbol{\nabla}\cdot\Big(\,F_{lm}\,\boldsymbol{\nabla}\psi_m \;+\; P_l\,\boldsymbol{\nabla}\varphi \;+\; R_{lm}\,\psi_m\,\boldsymbol{\nabla}\zeta\,\Big) \;=\; 0, \quad \text{for } l=1\cdots M,\end{aligned} \tag{2.15c}$$

where the non-hydrostatic term $\mathcal{R}(\mathbf{x},t)$ is given by:

$$\begin{aligned}\mathcal{R} = \;&\frac{1}{2}\,F'_{mn}\,(\boldsymbol{\nabla}\psi_m)\cdot(\boldsymbol{\nabla}\psi_n) \;+\; \frac{1}{2}\,\Big[\,G'_{mn}\,(\boldsymbol{\nabla}\zeta)^2 \;+\; K'_{mn}\,\Big]\,\psi_m\,\psi_n \;+\\ &+\;\Big[\,P'_m\,\boldsymbol{\nabla}\psi_m \;+\; Q'_m\,\psi_m\,\boldsymbol{\nabla}\zeta\,\Big]\cdot\boldsymbol{\nabla}\varphi \;+\; R'_{mn}\,(\boldsymbol{\nabla}\zeta)\cdot(\boldsymbol{\nabla}\psi_m)\,\psi_n \;+\\ &-\;\boldsymbol{\nabla}\cdot\Big[\,G_{mn}\,\psi_m\,\psi_n\,\boldsymbol{\nabla}\zeta \;+\; Q_m\,\psi_m\,\boldsymbol{\nabla}\varphi \;+\; R_{mn}\,(\boldsymbol{\nabla}\psi_m)\,\psi_n\,\Big].\end{aligned} \tag{2.16}$$

Here a prime denotes variation with respect to $\zeta(x,t)$, *e.g.* $K'_{mn} \equiv \delta K_{mn}/\delta\zeta$. Observe that, as a result of $f_m = 0$ at $z = \zeta(x,t)$, we have:

$$F'_{mn} \;=\; R_{mn} \;+\; R_{nm} \qquad \text{and} \qquad P'_m \;=\; Q_m. \tag{2.17}$$

As before, for the parabolic structure model, we have a mass conservation equation (2.15a), a Bernoulli equation (2.15b) and a series of second-order elliptic equations (2.15c), linear in ψ_m. The highest derivatives are second-order spatial derivatives. For numerical applications, the solution of the elliptic equations requires that they are well conditioned, *i.e.* that the l-th elliptic equation is independent of the n-th equation, for $l \neq n$. Therefore these shape functions f_m have to be sufficiently independent of each other. This may pose restrictions on the choice of the shape functions f_m, as well as the maximum number of shape functions M. See *e.g.* Dommermuth & Yue (1987), where the computations only converged for a small number of shape functions.

Fortunately, in general, only a small number of well-chosen shape functions is sufficient to get good approximate models. Often, using only one shape function, *i.e.* $M = 1$, may already give good results. In the remainder, we will treat a few examples. Besides the parabolic structure model, with shape function $f^{(p)}(z;\zeta,h_0)$ and presented in §2.3, we will discuss two other examples: a cosh (hyperbolic-cosine) structure model and a power-series structure model.

2.4.1 Hyperbolic-cosine structure model

First, one possibility is to exploit the well-known hyperbolic-cosine vertical structure as found in the full linear wave theory:

$$f^{(c)}(z;\zeta,h_0,\kappa) \;=\; \cosh\,\kappa\,(\,h_0\;+\;z\,)\;-\;\cosh\,\kappa\,(\,h_0\;+\;\zeta\,)\,, \tag{2.18}$$

where $\kappa(\mathbf{x})$ is an additional parameter, which can be chosen for instance on the basis of the carrier-wave angular frequency ω_0 of incoming waves and the local water depth $h_0(\mathbf{x})$, using the linear dispersion relationship.

The vertical integrals (2.14), as well as their ζ-derivatives, as valid for the cosh and power-series structure model are given in Appendix 2.A. Then the associated Hamiltonian density $H^{(c)}(\zeta,\varphi,\psi^{(c)};\mathbf{x},t)$, using equation (2.13), becomes after some manipulations:

$$\begin{aligned} H^{(c)} = \;& \frac{1}{2}\,h\,\Big(\,\boldsymbol{\nabla}\varphi\;-\;\mathcal{D}\,\boldsymbol{\nabla}\psi^{(c)}\;-\;\kappa\,\mathcal{S}\,\psi^{(c)}\,\boldsymbol{\nabla}\zeta\,\Big)^2\;+ \\ & +\;\frac{1}{4}\,\frac{1}{\kappa}\,\Big(\,\kappa\,h\;+\;\mathcal{S}\,\mathcal{C}\;-\;2\,\frac{\mathcal{S}^2}{\kappa\,h}\,\Big)\,\Big(\,\boldsymbol{\nabla}\psi^{(c)}\Big)^2\;+ \\ & +\;\frac{1}{4}\,\kappa\,\Big(\,\mathcal{S}\,\mathcal{C}\;-\;\kappa\,h\,\Big)\,\Big(\psi^{(c)}\Big)^2\;+\;\frac{1}{2}\,g\,\zeta^2. \end{aligned} \tag{2.19}$$

with

$$\mathcal{D}\;\equiv\;\cosh\,(\kappa\,h)\;-\;\frac{\sinh\,(\kappa\,h)}{\kappa\,h},\quad \mathcal{S}\;\equiv\;\sinh\,(\kappa\,h)\quad\text{and}\quad \mathcal{C}\;\equiv\;\cosh\,(\kappa\,h). \tag{2.20}$$

The Hamiltonian density $H^{(c)}$ is indeed positive definite, since the coefficients in front of $(\boldsymbol{\nabla}\psi)^2$ and $(\psi^{(c)})^2$, in the second and third term on the right hand side, are

always positive for $\kappa > 0$ and $h > 0$. When the integrals from equation (2.56) are applied to equation (2.15), we get after some algebraic manipulations:

$$\partial_t \zeta + \boldsymbol{\nabla} \cdot \left(h\, \mathbf{U}^{(c)} \right) \;=\; 0, \tag{2.21a}$$

$$\begin{aligned}
\partial_t \varphi + \; & \frac{1}{2} \left(\mathbf{U}^{(c)} \right)^2 \; + \; \frac{1}{2} \kappa^2 \, \mathcal{S}^2 \left(\psi^{(c)} \right)^2 \; + \; \frac{1}{2} \, \mathcal{D}^2 \left(\boldsymbol{\nabla} \psi^{(c)} \right)^2 \; + \\
& - \; \kappa \, h \, \mathbf{U}^{(c)} \; \cdot \left[\left(\mathcal{S} \; - \; \frac{\mathcal{D}}{\kappa \, h} \right) \boldsymbol{\nabla} \psi^{(c)} \; + \; \kappa \, \mathcal{C} \; \psi^{(c)} \, \boldsymbol{\nabla} \zeta \right] \; + \\
& + \; \boldsymbol{\nabla} \cdot \left(\kappa \, h \, \mathcal{S} \; \mathbf{U}^{(c)} \; \psi^{(c)} \right) \; + \; g \; \zeta \; = \; 0,
\end{aligned} \tag{2.21b}$$

$$\begin{aligned}
-\kappa \, h \, \mathcal{S} \; & \left(\boldsymbol{\nabla} \varphi \; - \; \mathcal{D} \; \boldsymbol{\nabla} \psi^{(c)} \; - \; \kappa \, \mathcal{S} \; \psi^{(c)} \; \boldsymbol{\nabla} \zeta \right) \; \cdot \; \boldsymbol{\nabla} \zeta \; + \; \frac{1}{2} \kappa \left(\mathcal{S} \, \mathcal{C} \; - \; \kappa \, h \right) \psi^{(c)} \; + \\
& + \; \boldsymbol{\nabla} \cdot \left[h \, \mathcal{D} \left(\boldsymbol{\nabla} \varphi \; - \; \kappa \, \mathcal{S} \; \psi^{(c)} \; \boldsymbol{\nabla} \zeta \right) \; + \right. \\
& \qquad \left. + \; \frac{1}{\kappa} \left(\frac{\mathcal{S}^2}{\kappa \, h} \; - \; \mathcal{D}^2 \, \kappa \, h \; - \; \frac{1}{2} \kappa \, h \; - \; \frac{1}{2} \mathcal{S} \, \mathcal{C} \right) \boldsymbol{\nabla} \psi^{(c)} \right] \; = \; 0,
\end{aligned} \tag{2.21c}$$

where $\mathbf{U}^{(c)}(\mathbf{x}, t)$ is the depth-averaged velocity:

$$\mathbf{U}^{(c)} \; \equiv \; \boldsymbol{\nabla} \varphi \; - \mathcal{D} \; \boldsymbol{\nabla} \psi^{(c)} \; - \; \kappa \; \mathcal{S} \; \psi^{(c)} \; \boldsymbol{\nabla} \zeta. \tag{2.22}$$

We did not use $\mathbf{U}^{(c)}$ in the equation (2.21c), since this is basically an elliptic equation in terms of $\psi^{(c)}$ and $\mathbf{U}^{(c)}$ depends on $\psi^{(c)}$.

2.4.2 Power-series structure model

Second, in the power-series structure model, we use for the vertical shape functions a power-series expansion around the free surface $z = \zeta(x, t)$. So:

$$f_m^{(s)} \; = \; (z - \zeta(\mathbf{x}, t))^m, \qquad \text{with } m = 1 \cdots M. \tag{2.23}$$

This can be seen as a generalisation of the parabolic structure model. Through the choice of the expansion around the free surface, the still water depth h_0 is not present in the shape functions. For this particular choice, the terms on the second line of equation (2.6a) disappear. So, equation (2.7a) is exact. The bottom-slope terms in the flow equations now appear through the variations of the Hamiltonian. Because no explicit approximation in the bottom-slope terms have been made, we have not made a mild-slope assumption in this case. The integrals, required in the Hamiltonian density (2.1b) and in the flow equations (2.15), are given by equation (2.58).

We do not yet know the maximum value of M for which the shape functions $f_m^{(s)}$ are sufficiently independent of each other, in order that the numerical approximation to the flow equations will result in a well-conditioned set of equations. Convergence may be improved by using orthogonal Chebychev polynomials instead of the simple power series resulting from (2.23).

Some linear characteristics of the variational Boussinesq model, *i.e.* the linear dispersion characteristics and the linear shoaling behaviour, will be derived in the next section. They will be applied to the three given examples with parabolic, cosh and power-series shape functions.

2.5 Linear wave characteristics from the average Lagrangian

2.5.1 Average Lagrangian for linear waves

The linear frequency dispersion and shoaling of the variational Boussinesq model is studied. Since we have a variational model, we apply the average Lagrangian technique (see *e.g.* Whitham, 1974, §11.7 and Chapter 14) to the one-dimensional linearised wave equations. This leads, due to the invariance with respect to wave phase, to a wave action equation (Hayes, 1970*a*,*b*, 1973; Whitham, 1974). For time-periodic waves, the invariance of the wave action flux provides the shoaling characteristics. The present analysis method is easier to apply than the direct manipulations of Boussinesq equations by a WKBJ approach (Madsen & Sørensen, 1992; Dingemans, 1997, §5.5.8 and §5.5.9; Ludwig, 1970). Furthermore, the variational approach gives a direct representation of the *global* (integral) effects of shoaling from one location to another, using the invariance of the action flux. Previous WKBJ approaches give *local* changes, associated, in our case, with the spatial derivative of the wave action flux. Chen & Liu (1995) integrate the local shoaling characteristics to obtain the global shoaling behaviour. It is not clear *a priori* that the integration of the local shoaling behaviour gives a conservation law for the energy flux in many Boussinesq models. In our case the conservation of wave action is guaranteed, because we start with a variational model.

For a linear problem with one spatial dimension x, the Lagrangian will be a second-degree polynomial in terms of ζ, φ, ψ and their derivatives. So, for the linear wave problem the Lagrangian and Hamiltonian densities, L_0 and H_0 respectively, become by use and reduction of equations (2.1) and (2.13):

$$L_0 = \varphi\,\partial_t\zeta \;-\; H_0, \tag{2.24a}$$

$$H_0 = \frac{1}{2}\,h_{\circ}\,(\partial_x\varphi)^2 \;+\; \frac{1}{2}\,\overline{F}_{mn}\,(\partial_x\psi_m)\,(\partial_x\psi_n) \;+\; \frac{1}{2}\,\overline{K}_{mn}\,\psi_m\,\psi_n + \\ +\; \overline{P}_m\,(\partial_x\psi_m)\,(\partial_x\varphi) \;+\; \frac{1}{2}\,g\,\zeta^2, \tag{2.24b}$$

with $\overline{(\cdot)}$ denoting evaluation of the quantity at $\zeta = 0$. By taking variations of

$$\mathscr{L}_0(\zeta,\varphi,\psi_m) \equiv \iint L_0(\zeta,\varphi,\psi_m;x,t)\;\mathrm{d}x\,\mathrm{d}t \tag{2.25}$$

with respect to $\varphi(x,t)$, $\zeta(x,t)$ and $\psi_l(x,t)$, we get from $\delta\mathscr{L}_0 = 0$:

$$\partial_t\zeta \;+\; \partial_x\left(\, h_{_0}\;\partial_x\varphi \;+\; \overline{P}_m\,\partial_x\psi_m \,\right) = 0, \tag{2.26a}$$

$$\partial_t\varphi \;+\; g\;\zeta = 0 \qquad \text{and} \tag{2.26b}$$

$$\overline{K}_{lm}\;\psi_m \;-\; \partial_x\left(\, \overline{F}_{lm}\,\partial_x\psi_m \;+\; \overline{P}_l\,\partial_x\varphi \,\right) = 0, \qquad \text{for } l = 1, 2\cdots M. \tag{2.26c}$$

We use the average Lagrangian technique of Whitham (1974) to study the linear dispersion and shoaling characteristics of the equations.

Assuming slowly modulated waves, we use the following approximation for $\zeta(x,t)$, $\varphi(x,t)$ and $\psi_m(x,t)$:

$$\zeta(x,t) = a(\mu x,\mu t)\;\cos\theta(x,t), \qquad \varphi(x,t) = b(\mu x,\mu t)\;\sin\theta(x,t) \quad \text{and} \tag{2.27a}$$

$$\psi_m(x,t) = c_m(\mu x,\mu t)\;\sin\theta(x,t), \quad \text{for } m = 1, 2\cdots M, \tag{2.27b}$$

in agreement with the solution of equation (2.26) for progressive harmonic waves over a horizontal bed. Here, $\mu \ll 1$ is a small modulation parameter and $\theta(x,t)$ is the wave phase. Neglecting derivatives of the amplitudes $a(\mu x,\mu t)$, $b(\mu x,\mu t)$ and $c(\mu x,\mu t)$, since they are $\mathcal{O}(\mu)$ compared to the leading-order terms, we have:

$$\partial_t\zeta \;\approx\; \omega\;a\;\sin\theta, \quad \partial_x\varphi \;\approx\; k\;b\;\cos\theta \quad \text{and} \quad \partial_x\psi_m \;\approx\; k\;c_m\;\cos\theta, \tag{2.28}$$

with the angular wave frequency $\omega(x,t)$ and wave number $k(x,t)$ *defined* as

$$\omega \;\equiv\; -\,\partial_t\theta \qquad \text{and} \qquad k \;\equiv\; +\,\partial_x\theta. \tag{2.29}$$

The linear approximations (2.27) and (2.28) are used in (2.24) to compute the Lagrangian density $L_0(a,b,c_m,\theta;x,t)$. Next, Whitham (1974) introduces the average Lagrangian density $\langle L_0\rangle\,(a,b,c_m,\theta;x,t)$ as:

$$\langle L_0\rangle \;=\; \frac{1}{2\pi}\int_0^{2\pi} L_0\;\mathrm{d}\theta. \tag{2.30}$$

For slowly-varying wave fields with negligible reflection, this can be assumed to give a good description. In our case, we get for the average Lagrangian density $\langle L_0\rangle$ and (positive definite) average Hamiltonian density $\langle H_0\rangle$:

$$\langle L_0\rangle \;=\; \frac{1}{2}\,\omega\,a\,b \;-\; \langle H_0\rangle\,, \qquad \text{with} \tag{2.31a}$$

$$\langle H_0\rangle \;=\; \frac{1}{4}\,k^2\,h_{_0}\,b^2 \;+\; \frac{1}{4}\left(\overline{F}_{mn}\,k^2 \;+\; \overline{K}_{mn}\right)\,c_m\,c_n \;+\; \frac{1}{2}\,\overline{P}_m\,k^2\,b\,c_m \;+\; \frac{1}{4}\,g\,a^2. \tag{2.31b}$$

Using the variations of $\langle\mathscr{L}_0\rangle\,(a,b,c_m) = \iint\,\langle L_0\rangle\;\mathrm{d}x\,\mathrm{d}t$ with respect to $a(\mu x,\mu t)$ and $c_l(\mu x,\mu t)$, we get:

$$b \;=\; \frac{g}{\omega}\;a \qquad \text{and} \qquad \left(\,\overline{K}_{lm} \;+\; k^2\;\overline{F}_{lm}\,\right)\;c_m \;=\; -\,\frac{g}{\omega}\;k^2\;\overline{P}_l\;a, \tag{2.32}$$

for $l = 1, 2 \cdots M$. The last equation can be written in matrix form as:

$$\left(\overline{\mathsf{K}} \, + \, k^2 \, \overline{\mathsf{F}} \right) \, \mathbf{c} \; = \; - \, \frac{g}{\omega} \, k^2 \, \overline{\mathbf{p}} \, a. \tag{2.33}$$

Because of the positive-definite Hamiltonian $\langle \mathscr{H}_0 \rangle \, (a, b) = \int \langle H_0 \rangle \, \mathrm{d}x$, this matrix equation is invertible. With $\overline{\mathsf{W}}$ denoting the inverse of the matrix in front of $\mathbf{c}$, we can write

$$\mathbf{c} \; = \; - \, \frac{g}{\omega} \, k^2 \, \overline{\mathsf{W}} \, \overline{\mathbf{p}} \, a \qquad\qquad \text{where} \qquad \overline{\mathsf{W}} \; \equiv \; \left(\overline{\mathsf{K}} \, + \, k^2 \, \overline{\mathsf{F}} \right)^{-1}. \tag{2.34a}$$

Or, in component form:

$$c_m \; = \; - \, \frac{g}{\omega} \, k^2 \, \overline{W}_{mn} \, \overline{P}_n \, a, \qquad\qquad \text{for} \qquad m \; = \; 1, 2 \cdots M. \tag{2.34b}$$

Note from equation (2.33) that $\overline{W}_{mn}$ will be a rational function in terms of k^2. Applying these to the average Lagrangian density $\langle L_0 \rangle$, b and c_m can be eliminated from $\langle L_0 \rangle$, and we get after some algebraic manipulations:

$$\langle L_0 \rangle \; = \; \frac{1}{4} \, \left\{ 1 \, - \, (\, k \, h_{_0} \,)^2 \, \left[1 \, - \, (\, k \, h_{_0} \,)^2 \, \frac{\overline{W}_{mn} \, \overline{P}_m \, \overline{P}_n}{h_{_0}^3} \right] \frac{g}{\omega^2 \, h_{_0}} \right\} \, g \, a^2. \tag{2.35}$$

This will be used consecutively to find the linear dispersion and shoaling characteristics.

2.5.2 Linear dispersion

As is well known (*e.g.* Hayes, 1970*a*,*b*, 1973; Whitham, 1974, §11.7), for linear waves the average Lagrangian density $\langle L_0 \rangle$ has the form:

$$\langle L_0 \rangle \; = \; D(\omega, k) \, a^2, \tag{2.36}$$

with $D(\omega, k)$ the dispersion relationship. So variation with respect to $a(\mu x, \mu t)$ directly gives the linear dispersion relation $D(\omega, k) = 0$. In our case, we have from the terms between brackets in (2.35) being equal to zero:

$$\omega = \Omega(k, h_{_0}) \qquad \text{with} \qquad \frac{\Omega^2 \, h_{_0}}{g} \; \equiv \; (\, k \, h_{_0} \,)^2 \, \left[1 \, - \, (\, k \, h_{_0} \,)^2 \, \frac{\overline{W}_{mn} \, \overline{P}_m \, \overline{P}_n}{h_{_0}^3} \right]. \tag{2.37}$$

Furher, we introduce the phase speed $C \equiv \Omega(k)/k$, for which we find:

$$\frac{C^2}{g \, h_{_0}} \; = \; \left[1 \, - \, (\, k \, h_{_0} \,)^2 \, \frac{\overline{W}_{mn} \, \overline{P}_m \, \overline{P}_n}{h_{_0}^3} \right]. \tag{2.38}$$

For example, consider the parabolic structure model, which has $M = 1$, so, using the integrals in Appendix 2.A evaluated at $\zeta = 0$:

$$\overline{F}^{(p)} \; = \; \frac{2}{15} \, h_{_0}^3, \qquad \overline{K}^{(p)} \; = \; \frac{1}{3} \, h_{_0} \qquad \text{and} \qquad \overline{P}^{(p)} \; = \; - \, \frac{1}{3} \, h_{_0}^2. \tag{2.39}$$

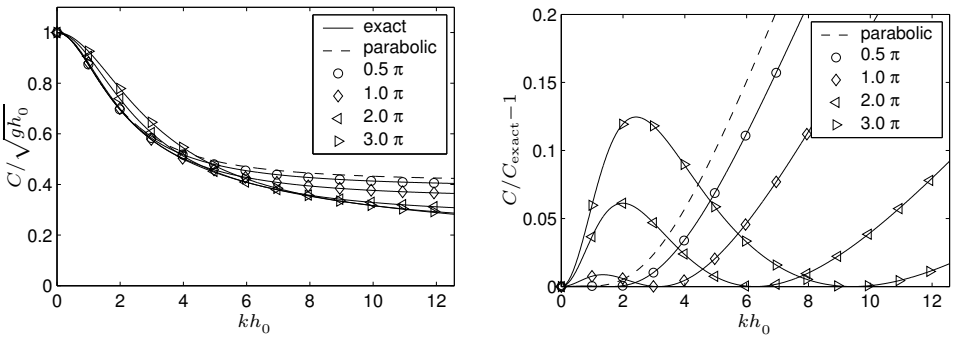

Figure 2.1: Linear dispersion characteristics of the parabolic and cosh structure model as a function of kh_0. (a) Phase speed $C/\sqrt{g\,h_0}$ (with $C \equiv \Omega/k$) in the cosh structure model (solid lines with markers) *vs* the exact linear phase speed (solid line, lowest curve) and the parabolic structure model (dashed line). (b) Relative error $C/C_{\rm exact} - 1$ (on a linear scale) in the phase speed of the cosh structure model (solid lines) and the parabolic structure model (black dashed line). The markers are for different values of κh_0: $\frac{1}{2}\pi$ (–○–), π (–◇–), 2π (–◁–) and 3π (–▷–).

From equations (2.33), (2.34) and (2.37) we find for the linear dispersion relationship:

$$\frac{\left(C^{(p)}\right)^2}{g\,h_0} \;=\; \frac{1 \;+\; \dfrac{1}{15}\,k^2\,h_0^2}{1 \;+\; \dfrac{2}{5}\,k^2\,h_0^2}. \tag{2.40}$$

This is the same dispersion relation as for the Boussinesq equations with improved linear dispersion of Madsen *et al.* (1991, equation (15) for the case $B = 1/15$). The linear dispersion characteristics, as compared with the exact result for the full linear theory:

$$\frac{C^2_{\rm exact}}{g\,h_0} \;=\; \frac{\tanh\,k\,h_0}{k\,h_0}, \tag{2.41}$$

are shown in Figure 2.1, up to $kh_0 = 4\pi$ (which corresponds to a water depth of twice the wave length, *i.e.* deep water). Up to $kh_0 = \pi$ the relative error in the phase speed is less than 3%.

In our second example, the cosh structure model, we have from equations (2.18) and (2.56) for the required integrals:

$$\overline{F}^{(c)} \;=\; -\frac{3}{2}\,\frac{1}{\kappa}\,\overline{\mathcal{S}}\,\overline{\mathcal{C}} + \frac{1}{2}\,h_0 + h_0\,\overline{\mathcal{C}}^2, \qquad \overline{K}^{(c)} \;=\; \frac{1}{2}\,\kappa\,\overline{\mathcal{S}}\,\overline{\mathcal{C}} - \frac{1}{2}\,\kappa^2\,h_0, \qquad \overline{P}^{(c)} \;=\; -h_0\,\overline{\mathcal{D}}, \tag{2.42}$$

with $\overline{\mathcal{D}} \equiv \cosh(\kappa\,h_0) \;-\; \dfrac{\sinh(\kappa\,h_0)}{\kappa\,h_0}$, $\overline{\mathcal{S}} \equiv \sinh(\kappa\,h_0)$ and $\overline{\mathcal{C}} \equiv \cosh(\kappa\,h_0)$.
Using these in equation (2.33), (2.34) and (2.37) we find:

$$\frac{\left(C^{(c)}\right)^2}{g\,h_0} \;=\; \frac{\left(\dfrac{\overline{\mathcal{S}}\,\overline{\mathcal{C}}}{\kappa\,h_0} \;-\; 1\right)\left(1 \;-\; \dfrac{k^2}{\kappa^2}\right) \;+\; 2\,\dfrac{k^2}{\kappa^2}\,\dfrac{\overline{\mathcal{S}}}{\kappa\,h_0}\,\overline{\mathcal{D}}}{\left(\dfrac{\overline{\mathcal{S}}\,\overline{\mathcal{C}}}{\kappa\,h_0} \;-\; 1\right)\left(1 \;-\; \dfrac{k^2}{\kappa^2}\right) \;+\; 2\,\dfrac{k^2}{\kappa^2}\,\overline{\mathcal{C}}\,\overline{\mathcal{D}}}. \tag{2.43}$$

As can be seen from this approximate dispersion relation, we regain the exact value of the linear dispersion relation at $k = \kappa$. Also the group velocity $V = \partial_k \Omega$ is exact at $k = \kappa$, *i.e.* $\partial_k \Omega^{(c)}(\kappa) = \partial_k \Omega_{\text{exact}}(\kappa)$. The linear dispersion characteristics and associated errors (as compared to the full linear theory) for the cosh structure model are shown in figure 2.1. The fact that the dispersion errors are small both near $kh_0 = \kappa h_0$ and near $kh_0 = 0$ is advantageous for the study of narrow-banded non-linear wave groups, where besides the carrier waves with wave numbers approximately equal to k_0, there are also sub-harmonics present with wave numbers near zero. This is also a desirable feature when studying the interaction between (very) long waves and shorter waves. Further note that $\kappa(x)$ can be a spatially varying parameter, and may be chosen differently at different locations to best facilitate the local conditions, *i.e.* local still water-depth h_0 and carrier wave number k_0.

Next, we consider the power-series structure model (2.23). Here, for $M > 1$, we have to solve equation (2.33) using the integrals as given in equation (2.58). For some small values of M we have done this (using the MAPLE symbolic algebraic manipulator), and as a result we obtained the following dispersion characteristics, with $q \equiv kh_0$:

$$\frac{\left(C_1^{(s)}\right)^2}{g\,h_0} = \frac{1+\frac{1}{12}q^2}{1+\frac{1}{3}q^2}, \tag{2.44a}$$

$$\frac{\left(C_2^{(s)}\right)^2}{g\,h_0} = \frac{1+\frac{1}{10}q^2+\frac{1}{720}q^4}{1+\frac{13}{30}q^2+\frac{1}{80}q^4}, \tag{2.44b}$$

$$\frac{\left(C_3^{(s)}\right)^2}{g\,h_0} = \frac{1+\frac{13}{105}q^2+\frac{1}{420}q^4+\frac{1}{100800}q^6}{1+\frac{16}{35}q^2+\frac{3}{140}q^4+\frac{1}{6300}q^6}, \tag{2.44c}$$

$$\frac{\left(C_4^{(s)}\right)^2}{g\,h_0} = \frac{1+\frac{17}{126}q^2+\frac{11}{3024}q^4+\frac{1}{42336}q^6+\frac{1}{25401600}q^8}{1+\frac{59}{126}q^2+\frac{19}{720}q^4+\frac{5}{14112}q^6+\frac{1}{1016064}q^8}, \tag{2.44d}$$

$$\frac{\left(C_5^{(s)}\right)^2}{g\,h_0} = \frac{1+\frac{14}{99}q^2+\frac{373}{83160}q^4+\frac{1}{22680}q^6+\frac{1}{7983360}q^8+\frac{1}{10059033600}q^{10}}{1+\frac{47}{99}q^2+\frac{163}{5544}q^4+\frac{16}{31185}q^6+\frac{67}{23950080}q^8+\frac{1}{279417600}q^{10}}. \tag{2.44e}$$

Here $C_M^{(s)}(k, h_0)$ is the phase speed for the case with M terms in the power-series expansion. A comparison for the phase speed and the relative error therein is made in Figure 2.2, as a function of the relative depth kh_0. As can be seen, for $M = 2$ the relative error $\varepsilon \equiv C_M^{(s)}/C_{\text{exact}} - 1$ is less than 0.01 for $kh_0 < 2.77$, *i.e.* for almost the whole range of shallow to deep water waves (considering $kh_0 > \pi$ as deep water). For $M = 3$ and $M = 5$ the range where $\varepsilon < 0.01$ has extended to $kh_0 < 5.53$ and $kh_0 < 14.07$ respectively.

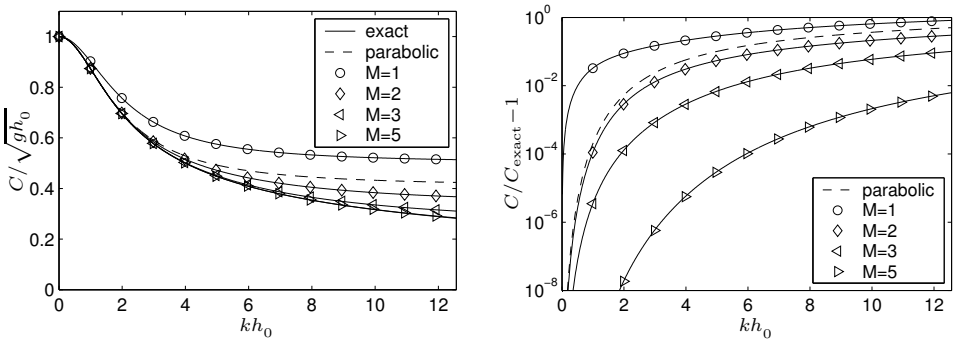

Figure 2.2: Linear dispersion characteristics of the power-series structure model as a function of kh_0. (a) Phase speed $C_M^{(s)}/\sqrt{g\,h_0}$ (with $C_M^{(s)} \equiv \Omega_M^{(s)}/k$) in the power-series structure model (solid lines with markers) *vs* the exact linear phase speed (solid line, lowest curve) and the parabolic structure model (dashed line). (b) Relative error $C_M^{(s)}/C_{\mathrm{exact}} - 1$ (on a linear scale) in the phase speed of the cosh structure model (solid lines with markers) and the parabolic structure model (dashed line). The markers for different values of M are: $M = 1$ (–○–), $M = 2$ (–◇–), $M = 3$ (–◁–) and $M = 5$ (–▷–).

Concerning the accuracy of these phase velocities, we notice that these approximations are not the same as the Padé approximations to the exact linear phase velocity squared C^2_{exact}, see (2.41). For $M = 3$ the result is about the same as for the $[4,4]$ Padé approximation, whereas it is not as accurate as the $[6,6]$ Padé (which has the same powers of q in the numerator and denominator). For $M = 4$ the accuracy is in between those of the $[4,4]$ and $[6,6]$ Padé approximations.

2.5.3 Linear shoaling

The linear shoaling characteristics are studied using the wave action equation, resulting from the variation of the average Lagrangian $\langle \mathscr{L}_0 \rangle \equiv \iint \langle L_0 \rangle \,\mathrm{d}x\,\mathrm{d}t$ with respect to the wave phase $\theta(x,t)$. Using equation (2.37), we can write the average Lagrangian density $\langle L_0 \rangle$, equation (2.35), as:

$$\langle L_0 \rangle \;=\; \left(1 \;-\; \frac{\Omega^2(k,h_0)}{\omega^2}\right) \;\frac{1}{2}\; g\; a^2. \tag{2.45}$$

Note that through the phase averaging, the phase $\theta(x,t)$ itself no longer appears in the average Lagrangian density $\langle L_0 \rangle\,(a,k,\omega;x,t)$, equation (2.35), but only its derivatives $\omega \equiv -\partial_t\theta$ and $k \equiv +\partial_x\theta$. Consequently, the result is a conservation equation (Whitham, 1974; Hayes, 1970*a*,*b*, 1973):

$$\partial_t \mathscr{A} \;+\; \partial_x \mathscr{B} \;=\; 0, \tag{2.46}$$

with, using equation (2.45),

$$\mathscr{A} \;\equiv\; +\frac{\partial\,\langle L_0 \rangle}{\partial \omega} \;=\; \frac{\frac{1}{2}\,g\,a^2}{\omega} \qquad \text{and} \qquad \mathscr{B} \;\equiv\; -\frac{\partial\,\langle L_0 \rangle}{\partial k} \;=\; V\;\frac{\frac{1}{2}\,g\,a^2}{\omega}. \tag{2.47}$$

Here $\mathscr{A}(x,t)$ is the wave action, $\mathscr{B}(x,t)$ is the wave action flux. Further, $V(x,t) \equiv \partial\mathscr{B}/\partial\mathscr{A} = \mathscr{B}/\mathscr{A} = \partial_k\Omega$ is the group velocity (Hayes, 1973), which depends on the dispersion characteristics of the specific variational Boussinesq model under consideration.

Now, when studying the linear shoaling behaviour for the variational Boussinesq model, we consider time-harmonic waves: *i.e.* the wave amplitude $a(x,t)$ is constant in time and the angular frequency ω is a constant. Hence $\partial_t\mathscr{A} = 0$, and equation (2.46) becomes

$$\partial_x \left(V\, \mathscr{A} \right) \;=\; 0. \tag{2.48}$$

As a result, we have that

$$\sqrt{V}\; a \;=\; \text{constant} \tag{2.49}$$

when going from one depth $h_0(x)$ to another. So, when the wave has an amplitude $a_1 \equiv a(x_1)$ at location x_1, the wave amplitude at x_2 will be $a_2 = \sqrt{V_1/V_2}\; a_1$, when V_1 and V_2 the group velocity at x_1 and x_2, respectively.

As an example, we consider the parabolic structure model, with linear frequency dispersion given by equation (2.40). Consequently, the group velocity $V^{(p)} \equiv \partial_k\Omega^{(p)}$ for this model is:

$$V^{(p)} \;=\; \frac{\Omega}{k} \left[1 \;-\; \frac{\frac{1}{3}\, k^2\, h_0^2}{\left(1 \;+\; \frac{1}{15}\, k^2\, h_0^2 \right) \left(1 \;+\; \frac{2}{5}\, k^2\, h_0^2 \right)} \right]. \tag{2.50}$$

Note that in the shallow-water limit $kh_0 \to 0$ we have $V^{(p)} \to \sqrt{gh_0}$. And for the deep-water case $kh_0 \to \infty$ we have that $V^{(p)} \to \sqrt{gh_0/6}$.

This can be compared with the full linear theory, where we have for the group velocity V_{exact} (see *e.g.* Dingemans, 1997, equation (2.29)):

$$V_{\text{exact}} \;=\; \frac{1}{2}\, \frac{\Omega_{\text{exact}}}{k} \left(1 \;+\; k\, h_0\, \frac{1 \;-\; \tanh^2\, k\, h_0}{\tanh\, k\, h_0} \right), \tag{2.51}$$

which has the shallow water limit $V_{\text{exact}} \,/\, \sqrt{gh_0} \to 1$ for $kh_0 \to 0$ and the deep-water limit $V_{\text{exact}} \,/\, \sqrt{g/k} \to \frac{1}{2}$ for $kh_0 \to \infty$ (and keeping k fixed).

Considering again the parabolic structure model, the integral shoaling behaviour according to equation (2.49), and associated errors as compared with full linear theory, have been depicted in Figure 2.3. As can be seen, the agreement between the approximate model and the full linear theory result is quite good. For instance, for periodic waves propagating from a location with $kh_0 = \pi$ to a very shallow location ($kh_0 \to 0$), the relative error in the wave amplitude a at the shallow-water location is less than 10%. And when starting at $kh_0 = \frac{1}{2}\pi$, the shallow water wave-amplitude is less than 1% in error with the full linear theory result.

A different approach to the study of linear wave shoaling, without demanding energy or action conservation, has been used by *e.g.* Madsen & Sørensen (1992) (and

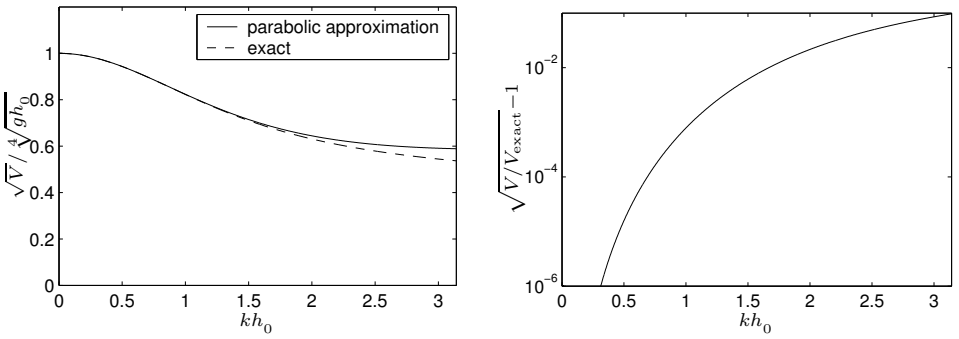

(a) **(b)**

Figure 2.3: Linear shoaling behaviour of the parabolic structure model as a function of kh_0. (a) Square-root of the relative group velocity $(V/\sqrt{gh_0})^{\frac{1}{2}}$, for the parabolic structure model (solid line) and according to the exact linear shoaling factor $(V_{\text{exact}}/\sqrt{gh_0})^{\frac{1}{2}}$ (dashed line). (b) Relative error $\sqrt{V/V_{\text{exact}}}-1$ on a semi-logarithmic scale.

Dingemans, 1997, §5.5). They use a WKBJ method directly on the wave evolution equations themselves, ending up with a description of the *local* shoaling behaviour, *i.e.* how $a'(x)/a(x)$ depends on $h_0'(x)/h_0(x)$, with $(\cdot)'$ denoting x-derivatives. Our result is the same as for the Madsen & Sørensen (1992) model, see Dingemans (1997, equation (5.190)). This result has also been obtained by a local analysis using the method of Ludwig (1970), see also Dingemans (1997, p. 569), on the flow equations (2.26) themselves. Which is not surprising, since Bretherton (1968) has shown the correspondence between the conservation of wave action and the WKBJ approach for linear systems arising from a variational principle.

With regard to the cosh structure model, we can remark that since the group velocity is exact for $k = \kappa$, we can have exact linear shoaling for mono-chromatic waves with frequency ω_0, provided κ is chosen according to the local depth and the linear dispersion relation $\omega_0^2 = g\kappa \tanh \kappa h_0$. For the power-series structure model, the shoaling coefficient behaves in a similar fashion as for the parabolic structure model: the relative error in $\sqrt{V}$ is larger than the error in the phase speed C, but of the same order (typically two to five times as large). The analytical expressions for the group speed become quite lengthy for the cosh structure model and for the power-series structure model with $M \geq 3$, and will not be presented here.

2.6 Numerical simulations for the parabolic structure model

2.6.1 Numerical method

The parabolic structure model (2.11) in one spatial-dimension is used to study the applicability and non-linear behaviour of the variational Boussinesq model numerically. Instead of the surface potential $\varphi(x,t)$, we work with its gradient $u(x,t) \equiv \partial_x \varphi$. So, the equations to be solved are, taking the x-derivative of equation (2.11b):

$$\partial_t \zeta + \partial_x \left(h\, U^{(p)} \right) \;=\; 0, \tag{2.52a}$$

$$\begin{aligned} \partial_t u + \; \partial_x \Bigg\{ & \frac{1}{2} \left(U^{(p)} \right)^2 \;+\; g\,\zeta \;-\; \frac{1}{45} \left(\psi^{(p)}\, \partial_x \zeta \;+\; h\, \partial_x \psi^{(p)} \right)^2 \;+ \\ & +\; \frac{1}{6} \left(1 + \frac{1}{5} \left(\partial_x \zeta \right)^2 \right) \left(\psi^{(p)} \right)^2 \;+ \\ & +\; \partial_x \left[h \left(\frac{2}{3}\, u \;-\; \frac{7}{15}\, \psi^{(p)}\, \partial_x \zeta \;-\; \frac{1}{5}\, h\, \partial_x \psi^{(p)} \right) \psi^{(p)} \right] \Bigg\} \;= 0, \end{aligned} \tag{2.52b}$$

$$\begin{aligned} h\, \psi^{(p)} \left(\frac{1}{3} \;+\; \frac{7}{15} \left(\partial_x \zeta \right)^2 \right) \;-\; \left(\frac{2}{3}\, h\, u \;-\; \frac{1}{5}\, h^2\, \partial_x \psi^{(p)} \right) \partial_x \zeta \;+ \\ + \partial_x \left(\frac{1}{3}\, h^2\, u \;-\; \frac{1}{5}\, h^2\, \psi^{(p)}\, \partial_x \zeta \;-\; \frac{2}{15}\, h^3\, \partial_x \psi^{(p)} \right) \;=\; 0, \end{aligned} \tag{2.52c}$$

with the depth-averaged velocity

$$U^{(p)} \;=\; u \;-\; \frac{2}{3}\, \psi^{(p)}\, \partial_x \zeta \;-\; \frac{1}{3}\, h\, \partial_x \psi^{(p)}. \tag{2.53}$$

Note that the equations solved in the numerical model are dimensional.

We use the method of lines for the numerical solution of this set of partial differential equations: first the equations are discretised in space, and then the resulting sets of ordinary differential equations for the temporal evolution are marched in time. For the spatial discretisation, a pseudo-spectral method is used on a periodic spatial domain. The flow quantities ζ, u and $\psi^{(p)}$, as well as the still water depth h_0, are discretised on a uniform grid of N intervals and step size Δx: $\zeta_{,j}$, $u_{,j}$, $\psi^{(p)}_{,j}$ and $h_{0,j}$ denote the respective quantities at a location $x = j\,\Delta x$. Spatial derivatives of a quantity are computed in the Fourier wave-number domain, using the Fast Fourier Transform (FFT) to switch back and forth between the spatial and the wave-number domain.

As a result, equations (2.52a,b) become a set of N first-order ordinary differential equations for the time evolution of $\zeta_{,j}$ and $\varphi_{,j}$, $j = 1 \cdots N$. These are marched in time using a variable step-size Runge-Kutta time integrator ('ode45' in MATLAB).

Furthermore, we have to solve the linear system of equations resulting from equation (2.52c) for $\psi^{(p)}_{,j}$, $j = 1 \cdots N$, for given $\zeta_{,j}$ and $\varphi_{,j}$ at each time level. This is

done by using a conjugate-gradient (CG) method, 'bicgstab' in MATLAB. Due to the use of Fourier series for determining derivatives, the associated system matrix is fully populated and evaluating the system of equations directly by matrix-vector multiplication will involve N^2 operations. Fortunately, at each stage in the CG method, not the system matrix, but only the vector of residuals for each of the equations is needed. This can efficiently be determined by use of the FFT, resulting in $N \log N$ operations, which is much less than N^2. The solution of the previous stage in the time-stepping procedure is used as an initial estimate for the solution $\psi_{,j}^{(p)}$, $j = 1 \cdots N$.

The CG method is accelerated by using as a pre-conditioner the LU decomposition of a second-order central finite-difference approximation to equation (2.52c). As a result, only a few iterations (typically 2 to 7) are necessary to let the CG process converge to a relative residual norm of 10^{-7}. The overall computing time of the above described pseudo-spectral method is proportional to $N \log N$, *i.e.* almost proportional to N for large N.

Because the equations are non-linear, the discretization may result in aliasing errors. The equations involve at most quartic operations on combinations of flow quantities (and depth h_0). If the flow quantities contain only energy for wave numbers below $k_{\max}$, the quartic operations will result in a transfer of energy to higher wave numbers, up to $4\,k_{\max}$. However, if this post-operation wave number is larger than the Nyquist wave number $k_N = \pi/\Delta x$, it will by aliasing fold back to the lower frequency $k_N - (4\,k_{\max} - k_N)$. To prevent the contamination by aliasing of results for wave numbers below $k_{\max}$, we have to demand:

$$k_{\max} \;\leq\; k_N \;-\; 4\,k_{\max}, \qquad \text{which amounts to} \qquad k_{\max} \;\leq\; \frac{2}{5}\,k_N. \tag{2.54}$$

So, the time derivatives of $\zeta_{,j}$ and $\varphi_{,j}$, $j = 1 \cdots N$, are spatially low-pass filtered to prevent aliasing by energy content in the wave number range above $2\pi/(5\Delta x)$.

No artificial damping or smoothing have been been used, apart from the small numerical damping inherent to the Runge-Kutta time integration used. The numerical model was found to be very robust, to which we think the positive-definiteness of the Hamiltonian density has contributed significantly.

Next we will present several examples computed with the pseudo-spectral implementation of the parabolic structure model. First, periodic waves are considered, both over a horizontal bed and propagating over an underwater bar. Thereafter, the propagation of confined wave groups over a horizontal bed and a slope will be presented.

2.6.2 Periodic waves

Periodic waves over a horizontal bed

First, some test cases for periodic waves over a horizontal bed have been computed. As initial condition, we use accurate solutions according to fully non-linear potential

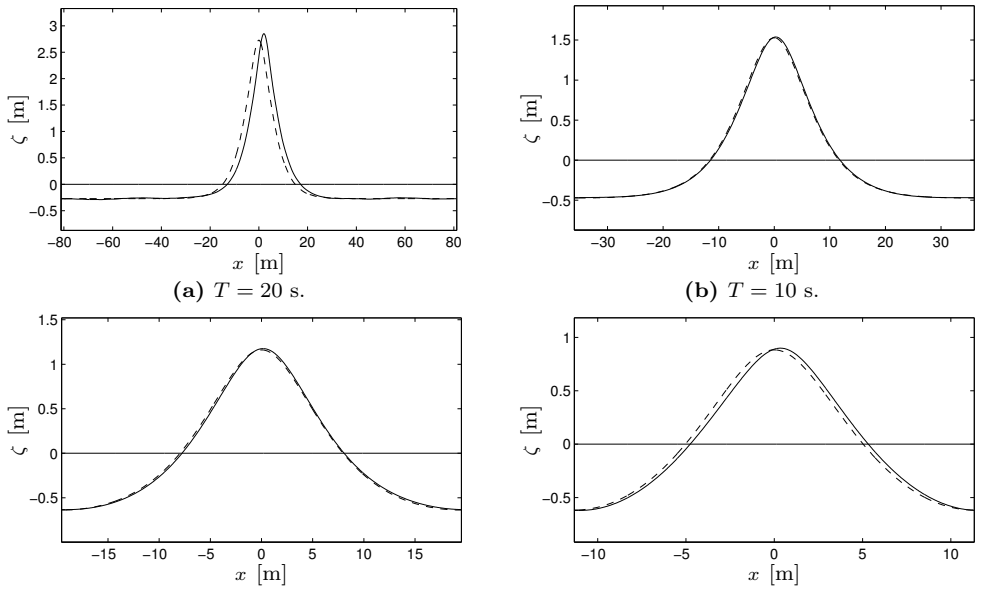

(a) $T = 20$ s. **(b)** $T = 10$ s. **(c)** $T = 6$ s. **(d)** $T = 4$ s.

Figure 2.4: Snapshots of the free-surface elevation after 5 wave periods: the parabolic structure variational model (solid line) and the Rienecker and Fenton solution (dashed line).

theory for periodic waves, computed with the method of Rienecker & Fenton (1981). In all cases we use a constant water depth $h_0 = 5$ m and $g = 9.81$ m/s^2. We consider the four wave conditions as given in table 2.1. The length of the periodic computational domain is equal to the wave length.

The computed free-surface elevations after a simulation time of five wave periods are presented in Figure 2.4. As can be seen, the model performs quite well. The phase speed of the non-linear waves computed with the parabolic structure model is somewhat larger than the exact wave speed, in agreement with what has been found in the analysis of linear waves, see Figure 2.1. As an indication of the accuracy of the numerical method, we give the changes in the spatial-averaged values of the Hamiltonian and depth-integrated horizontal momentum, for the case of $T = 6$ s. The spatial-averaged Hamiltonian, *i.e.* sum of kinetic and potential energy per unit

T [s]	H [m]	kh_0	H/h_0
20[a]	3.0	0.1935	0.60
10	2.0	0.4367	0.40
6	1.8	0.8042	0.36
4	1.5	1.3872	0.30

[a]For the case $T = 20$ s and $H = 3.0$ m we have used 200 points per wave length, instead of the 100 points per wave length we have used in all other cases.

Table 2.1: Conditions for periodic waves over a horizontal bed.

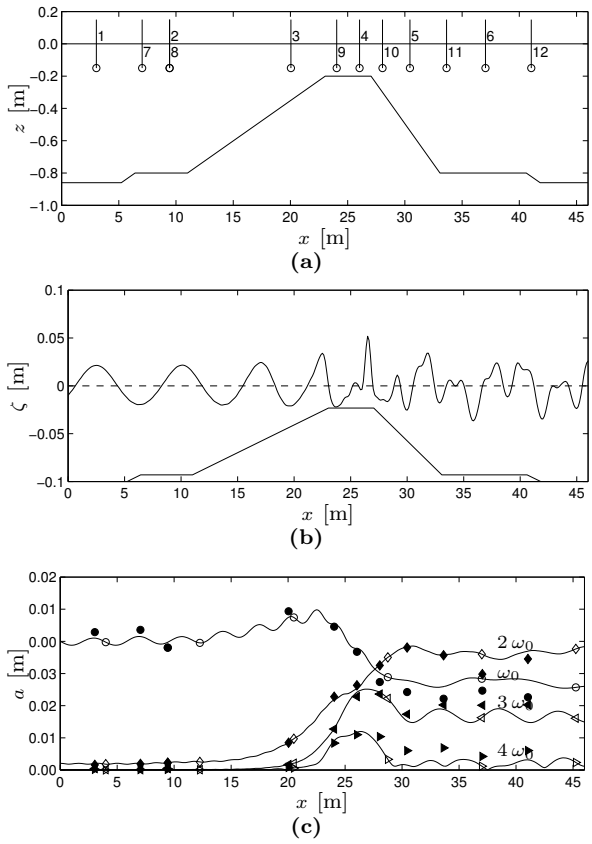

Figure 2.5: Periodic waves over a bar, test case A. (a) Experimental setup, showing bottom topography and measurement locations 1 to 12. (b) Snapshot of the computed free-surface elevation at $t = 60$ s, and bottom topography (on a different, vertical distorted scale). (c) Amplitudes of surface elevation harmonics as a function of x, for the computation (open symbols and drawn lines) and measurements (filled symbols), at the carrier-wave frequency ω_0 ($\circ$), and super-harmonic frequencies $2\,\omega_0$ ($\diamond$), $3\,\omega_0$ ($\triangleleft$) and $4\,\omega_0$ ($\triangleright$).

length, is initially equal to 3.684 m^2, and reduces by $-2.1 \cdot 10^{-7}$ and $-3.7 \cdot 10^{-5}$ m^2 after respectively 5 and 1000 wave periods. The spatial-averaged horizontal momentum is initially equal to $-2.1 \cdot 10^{-8}$ m^2/s (instead of zero, its exact value), and becomes $-3.3 \cdot 10^{-8}$ and $-5.7 \cdot 10^{-6}$ m^2/s after 5 and 1000 wave periods respectively. These errors are mainly due to the errors in the CG solver for the elliptic equation and the numerical damping in the time-integration method. The spatial averages of the free-surface elevation ζ and potential gradient u are conserved to within machine accuracy.

Periodic waves over an underwater bar

As a second test case, we consider periodic waves propagating over an underwater bar (Dingemans, 1997, §5.9), for which measurements from a laboratory experiment

are available (with the same experimental setup as in Luth *et al.*, 1994). The experimental setup is shown in figure 2.5(a), with the waves traveling from left to right. We will consider test case A, with waves of period $T = 2.857$ s and amplitude $a = 0.020$ m. The still water depth in front of the bar is 0.80m, and on top of the bar 0.20 m. The front bed slope of the bar is 1/20, the 0.20 m depth region extends over 4.0 m and the back slope of the bar is 1/10. For further details we refer to Dingemans (1997) and Luth *et al.* (1994).

A snapshot of the computed free-surface elevation is shown in Figure 2.5(b). As the waves waves propagate up the front slope, they increase in amplitude and are non-linearly distorted. The generated super-harmonics travel further as free waves after the shallow part of the bar. This generates a complex pattern of different frequency components traveling at different phase speeds after the bar. The amplitudes of free-surface harmonics at the carrier-wave frequency ω_0, as well as the amplitudes of the first three super-harmonics, are shown in Figure 2.5(c). As can be seen, the computed amplitudes compare quite well with the measured ones. Notice that the oscillations in the amplitude of the principal harmonic are due to (linear) reflections due to the bar bathymetry.

Since the parabolic structure model has the same linear dispersion characteristics as the model of Madsen *et al.* (1991), the results for the present parabolic structure model are very similar, see Dingemans (1997, figure 5.30–5.34). The phase speed of the free super-harmonics after the bar, in relative deep water, is over-estimated. This results in phase errors between the components, especially at furthest measuring locations 6 and 12. Models with better linear dispersion characteristics are known to perform better in this region, see *e.g.* Dingemans (1994, 1997, §5.9.3) and Lynett & Liu (2004*a*). In the present approach, this may be achieved by using for instance the cosh structure model with well-chosen x-variations of the parameter κ (see Figure 2.1), or the general series model with $M \geq 3$ (see Figure 2.2).

2.6.3 Confined wave groups

When wave groups propagate over variable bathymetry, one has besides the distortion of the wave group (Djordjević & Redekopp, 1978*b*; Turpin, Benmoussa & Mei, 1983) also the effect of the generation of free long waves (Mei & Benmoussa, 1984; Liu, 1989). These long waves are of interest for coastal morphology and the forcing of moored floating structures and ships. Here, we will study the capabilities of the variational Boussinesq model with parabolic vertical structure in predicting wave group deformation and long wave generation. This will be done using confined wave groups, with a sech (hyperbolic-secans) envelope of the carrier waves.

First, we will look into the propagation of a confined wave group over a horizontal bed, and look into its deformation as it propagates and the emission of spurious waves due to imperfect initial conditions. Second, the propagation of this wave group over a slope into a shallower constant-depth region will be computed, and compared with the results of van Groesen & Westhuis (2002).

The initial water depth in all computations is $h_0 = 12$ m, the carrier wave frequency

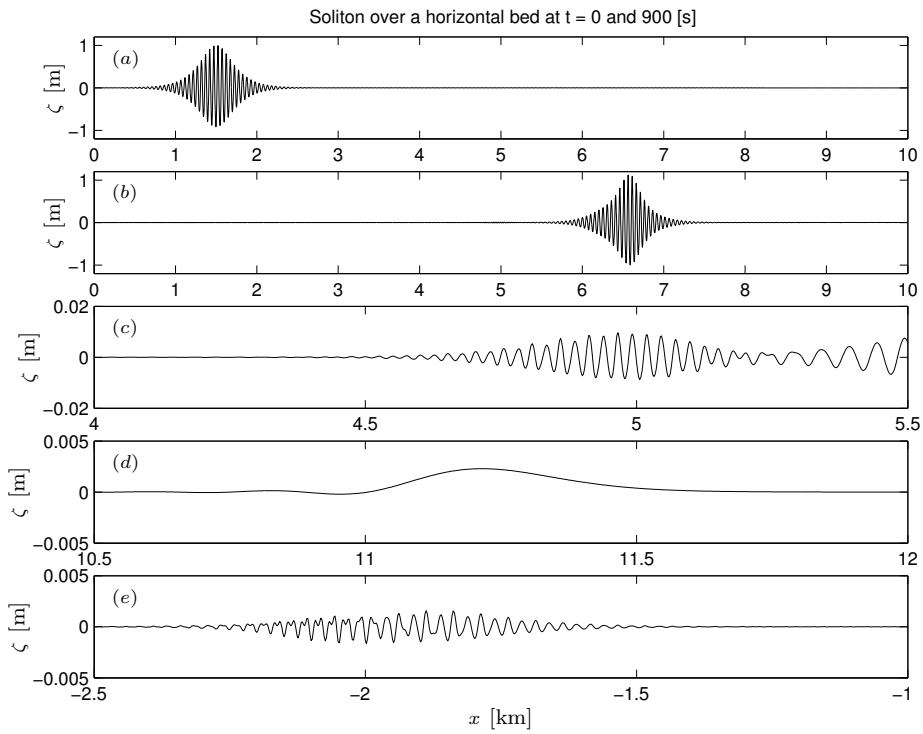

Figure 2.6: Surface elevation for a confined wave group over a horizontal bed and scattered spurious waves. (a) Wave group at $t = 0$ s, (b) wave group at $t = 900$ s, (c) detail of slow right-traveling short-wave tail at $t = 900$ s, (d) detail of fast right-traveling long wave at $t = 900$ s, (e) detail of slow left-traveling short-wave group at $t = 900$ s.

of the confined wave group is $\omega_0 = \pi/3$ rad/s, the carrier wave amplitude in the center of the group is $a_0 = 1.0$ m and the gravitational acceleration is $g = 9.81$ m/s^2. The spatial step was taken equal to 2 m in all subsequent computations, *i.e.* about 25 points per wave length. With the maximum wave number restricted by equation (2.54), this means that up to the fifth spatial harmonic can be represented on this grid.

The initial conditions for the free-surface elevation $\zeta(x,t)$ and potential-gradient $u(x,t)$, including second-order sub- and super-harmonics, as well as second-order modulation effects on $u(x,t)$, were computed from the formulations as given in Dingemans & Otta (2001), equations (39)–(45), (101)–(103)[3]. These correspond with the hyperbolic-secans solution of the non-linear Schrödinger (NLS) equation, as derived by a multiple-scales perturbation-series approach from the full non-linear potential flow problem. A NLS equation derived from the parabolic structure model will have slightly different values of the coefficients and the second-order sub- and super-harmonics.

[3] Note there is a small typographical error in equation (44) of Dingemans & Otta (2001): the second transformation should be $\kappa_2^\phi = (\omega^2/g^2)\kappa_2^\zeta$.

Confined wave group over a horizontal bed

Given the initial conditions for ζ and u as specified above, the flow evolution equations are computed for 900 s, *i.e.* 150 carrier wave periods. The results are shown in Figure 2.6. As can be seen, the wave group envelope does not deform much, after traveling for about 100 carrier-wave lengths and five wave-group lengths. The wave envelope has become a bit narrower and peaked, and a bit asymmetrical horizontally around its center.

Further some spurious waves are shed, by the deviation of the parabolic structure model from the fully non-linear potential-flow equations, as well as from the approximations underlying the NLS equation. In Figure 2.6(c) a spurious wave group with wave numbers $2\,k_0$ twice the carrier-wave number k_0 is seen, of amplitude 0.01 m, *i.e.* about one percent of the carrier-wave amplitude $a_0 = 1.0$ m. These spurious waves travel slower than the carrier waves. In Figure 2.6(d) a near-solitary long wave of about 2.5 mm height has traveled about twice the distance of the carrier wave group. Finally, in Figure 2.6(e) a group of left-traveling spurious waves with wave numbers near $2\,k_0$ and higher can be found, of amplitudes less than 2 mm.

Confined wave group on a slope

Next, we will consider the same confined wave group encountering an underwater slope. Significant depth changes will start at shorter distances from the initial wave group location, than the group travel distance discussed above. Therefore, we may consider the discussed initial wave conditions an adequate approximation to the 'exact' soliton-envelope wave-group solution to the parabolic structure model (if it exists).

The confined wave group will now propagate from a region with its initial and constant water depth $h_0 = 12$ m, via a 0.012 slope of 500 m horizontal extend, into another region of constant and shallower depth, $h_0 = 6$ m. We will compare our results with those of van Groesen & Westhuis (2002, see also Westhuis, 2001), who use a finite element method to solve the fully non-linear problem of surface waves on a potential flow. Van Groesen & Westhuis (2002) use a different method to initialise the confined wave group. This, in itself, will create some differences between their and our results.

Notice that in the deeper part we have for the carrier waves a relative depth $k_0 h_0 = 1.49$, and in the shallow part $k_0 h_0 = 0.92$. At $kh = 1.36$ the non-linearity coefficient in the NLS equation changes sign, see *e.g.* Benjamin & Feir (1967). So, for the NLS equation, we go from the focussing regime for $kh > 1.36$ in the deeper part, where the hyperbolic-secans soliton solution exists, to the defocussing regime with $kh < 1.36$.

Two snapshots of the free surface elevation at $t = 0$ and $t = 900$ s, as computed with the parabolic structure model, are given in Figure 2.7. Clearly the deformation of the wave group, as well as the generation of a free long wave, can be seen. In order to compare with van Groesen & Westhuis (2002), some details are given in Figure 2.8 at $t = 900$ s. Note the appearance of the longer waves in the front of the deforming

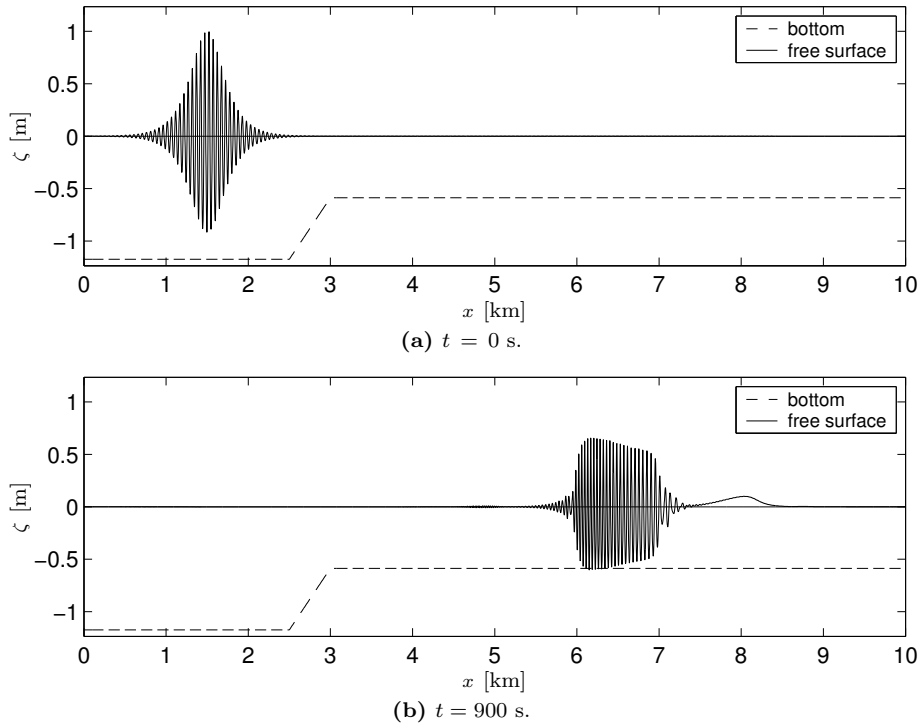

Figure 2.7: Wave group propagating over a slope: surface elevation $\zeta(x,t)$ (solid line) as a function of x. (a) $t = 0$ s, and (b) $t = 900$ s. The dashed line is the bottom elevation (not on scale).

wave group and the shorter waves in its tail. There is quite good agreement, both in the evolution of the carrier-wave amplitude (top Figure) as well as in the generated free long wave (bottom figure). However, there are phase differences between the two models, which we are addressing now. In Figure 2.8 the phase difference is small near the front of the wave group at $x = 7$ km, and the phase difference is about half a wave length in error near $x = 6$ km. With a carrier wave length of about 41 m this is a localisation error of approximately 20 m over a wave group length of ≈ 25 waves, and after propagating over more than a hundred carrier wave lengths.

Analysis showed us that the observed phase differences cannot be explained by either the phase-speed error introduced by the model approximation or the one from the numerical method. We conclude that the difference is due to the difference in the initial conditions used in our model compared to those used by Westhuis (2001), see Figure 2.9. As can be observed, differences appear at the front of the wave group ($x > 1500$ m). In this region, the wave amplitudes used by Westhuis (2001) are smaller than the theoretical ones.

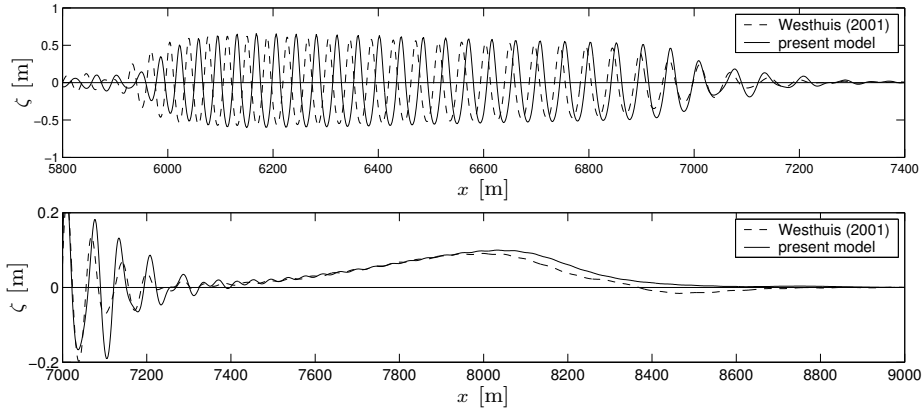

Figure 2.8: Wave group propagating over a slope: details of the surface elevation $\zeta(x,t)$ as a function of x at $t = 900$ s. Present parabolic structure model (solid line) and the model of van Groesen & Westhuis (2002) (dashed line).

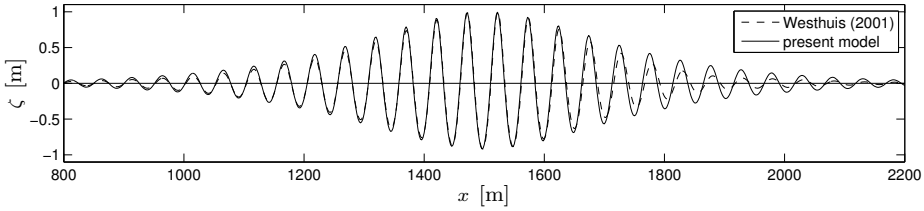

Figure 2.9: Wave group propagating over a slope: intial condition of the surface elevation $\zeta(x,t)$ as a function of x at $t = 0$ s. Present parabolic structure model (solid line) and the model of van Groesen & Westhuis (2002) (dashed line).

2.7 Conclusions

Variational Boussinesq models with positive-definite Hamiltonian density, *i.e.* energy densities per unit of horizontal area, are presented. The models are derived by approximating the horizontal and vertical velocities in the kinetic energy, using a series expansion with a small-number of vertical shape functions for the velocity (potential).

It is essential that the first shape function equals to one at the free surface and all other shape functions are zero at the free surface. This ensures that only two time-evolution equations appear in terms of the canonical variables, *viz.* the surface elevation $\zeta(\mathbf{x},t)$ and the free-surface potential $\varphi(\mathbf{x},t)$ in case of a velocity potential model, see equations (2.15a–b). The additional parameters $\psi_m(\mathbf{x},t)$ are solved by a (series of) second-order elliptic equations, linear in $\psi_m(\mathbf{x},t)$, see equation (2.15c). All equations contain only low-order partial derivatives: first-order time derivatives, second-order spatial derivatives for the Hamiltonian models written in the surface potential and third-order spatial derivatives for the models written in terms of velocities. No mixed space-time derivatives appear. The cost is, as compared to classical

Boussinesq models, that we have to solve (a series of) additional elliptic equations in the flow parameters $\psi_m(\mathbf{x}, t)$ associated with the introduced shape function(s).

The variational Boussinesq models thus derived have a positive-definite Hamiltonian, which is important for a good dynamical behaviour of the model. Further several symmetries of the 'exact' Hamiltonian for water waves are also transferred to the variational Boussinesq models. This results in associated conservation laws, among others depth-integrated mass conservation and energy conservation (for a horizontal bed also momentum conservation). Apart from the approximations to the vertical velocity structure (which may include a, non-essential, mild-slope approximation), no further approximations are made. The resulting models are therefore fully non-linear, *i.e.* without approximations regarding the wave amplitude.

As examples, we have derived vertical flow structure models with one parabolic shape function, one hyperbolic-cosine shape function and a polynomial power-series expansion with several parameters. The linear characteristics of these models are studied, using the average Lagrangian. The resulting linear frequency-dispersion relationships are all well behaved, *i.e.* no real-valued poles in the resulting rational functions in terms of the wave number k. This is a result of the positive-definite Hamiltonian. Also, wave action conservation can be used to show the integral effect of linear shoaling from one location with a certain depth (and group velocity) to another.

To study the non-linear characteristics, we present numerical simulations for the parabolic structure model in one horizontal dimension, using a pseudo-spectral method. We only worked out numerical results for the parabolic structure model, because it is the simplest of the models considered. We expect that the cosh structure model and the power-series structure model (with $M > 2$) are able to give more accurate results. For practical purposes, we recommend to use the cosh structure model, since it provides a good balance between accuracy on arbitrary depth and numerical efforts. However, this is a point of further study. Recently, it has been shown by Dingemans & Klopman (2009) that reflection properties are much improved by a different normalisation of the structure functions. Further properties are still under investigation.

Using the parabolic structure model, the propagation and deformation of periodic waves and confined wave groups have been computed, both over a horizontal bed and then over bathymetry. Comparison with other numerical methods, solving the fully non-linear potential-flow problem, as well as with measurements, show the capacities of the model. Besides, no numerical instabilities have been encountered, despite the absence of dissipation in the numerical model – apart from the small dissipation in the Runge-Kutta time integration. This may be attributed to the positive-definiteness of the Hamiltonian density.

Appendix 2.A Vertical integrals for the parabolic, cosh and power-series structure model

For the parabolic vertical structure of the flow, as given by (2.9), the integrals (2.14) and their ζ-derivatives become, using as before $h \equiv h_0 + \zeta$ and dropping the indices (since $M = 1$):

$$F^{(p)} = \frac{2}{15}\,h^3, \quad F'^{(p)} = \frac{2}{5}\,h^2, \quad G^{(p)} = \frac{7}{15}\,h, \quad G'^{(p)} = \frac{7}{15}, \tag{2.55a}$$

$$K^{(p)} = \frac{1}{3}\,h, \quad K'^{(p)} = \frac{1}{3}, \quad P^{(p)} = -\frac{1}{3}\,h^2, \quad P'^{(p)} = -\frac{2}{3}\,h, \tag{2.55b}$$

$$Q^{(p)} = -\frac{2}{3}\,h, \quad Q'^{(p)} = -\frac{2}{3}, \quad R^{(p)} = \frac{1}{5}\,h^2, \quad R'^{(p)} = \frac{2}{5}\,h. \tag{2.55c}$$

In the hyperbolic-cosine assumption for the vertical flow structure, as given in equation (2.18), the integrals from equation (2.14) become:

$$F^{(c)} = -\frac{3}{2}\,\frac{1}{\kappa}\,\mathcal{S}\,\mathcal{C} + \frac{1}{2}\,h + h\,\mathcal{C}^2, \quad F'^{(c)} = 2\,\kappa\,h\,\mathcal{S}\,\mathcal{D}, \tag{2.56a}$$

$$G^{(c)} = \kappa^2\,h\,\mathcal{S}^2, \quad G'^{(c)} = \kappa^2\,\mathcal{S}\left[2\,\kappa\,h\,\mathcal{C} + \mathcal{S}\right], \tag{2.56b}$$

$$K^{(c)} = \frac{1}{2}\,\kappa\,\mathcal{S}\,\mathcal{C} - \frac{1}{2}\,\kappa^2\,h, \quad K'^{(c)} = \kappa^2\,\mathcal{S}^2, \tag{2.56c}$$

$$P^{(c)} = -h\,\mathcal{D}, \quad P'^{(c)} = -\kappa\,h\,\mathcal{S}, \tag{2.56d}$$

$$Q^{(c)} = -\kappa\,h\,\mathcal{S}, \quad Q'^{(c)} = -\kappa^2\,h\,\mathcal{C} - \kappa\,\mathcal{S}, \tag{2.56e}$$

$$R^{(c)} = \kappa\,h\,\mathcal{S}\,\mathcal{D} \quad \text{and} \quad R'^{(c)} = \kappa^2\,h\left[\mathcal{C}^2 + \mathcal{S}^2\right] - \kappa\,\mathcal{S}\,\mathcal{C}, \tag{2.56f}$$

with

$$\mathcal{D} \equiv \cosh(\kappa\,h) - \frac{\sinh(\kappa\,h)}{\kappa\,h}, \quad \mathcal{S} \equiv \sinh(\kappa\,h) \quad \text{and} \quad \mathcal{C} \equiv \cosh(\kappa\,h). \tag{2.57}$$

For the power-series flow structure, as given in equation (2.23), the integrals and their derivatives become:

$$F^{(s)}_{mn} = (-1)^{m+n}\,\frac{h^{m+n+1}}{m+n+1}, \quad F'^{(s)}_{mn} = (-1)^{m+n}\,h^{m+n}, \tag{2.58a}$$

$$G^{(s)}_{mn} = (-1)^{m+n}\,m\,n\,\frac{h^{m+n-1}}{m+n-1}, \quad G'^{(s)}_{mn} = (-1)^{m+n}\,m\,n\,h^{m+n-2}, \tag{2.58b}$$

$$K^{(s)}_{mn} = G^{(s)}_{mn}, \quad K'^{(s)}_{mn} = G'^{(s)}_{mn}, \tag{2.58c}$$

$$P^{(s)}_{m} = (-1)^{m}\,\frac{h^{m+1}}{m+1}, \quad P'^{(s)}_{m} = (-1)^{m}\,h^{m}, \tag{2.58d}$$

$$Q^{(s)}_{m} = (-1)^{m-1}\,h^{m}, \quad Q'^{(s)}_{m} = (-1)^{m-1}\,m\,h^{m-1}, \tag{2.58e}$$

$$R^{(s)}_{mn} = (-1)^{m+n-1}\,n\,\frac{h^{m+n}}{m+n} \quad \text{and} \quad R'^{(s)}_{mn} = (-1)^{m+n-1}\,n\,h^{m+n-1}. \tag{2.58f}$$

2.8 References

Agnon, Y., Madsen, P. A. & Schäffer, H. A. 1999 A new approach to high-order Boussinesq models. *J. Fluid Mech.* **399**, 319–333.

Benjamin, T. B. 1984 Impulse, flow force and variational principles. *IMA J. Appl. Math.* **32** (1–3), 3–68. With errata in the preamble of the same issue.

Benjamin, T. B. & Feir, J. E. 1967 The disintegration of wave trains on deep water, Part 1. Theory. *J. Fluid Mech.* **27** (3), 417–430.

Benjamin, T. B. & Olver, P. J. 1982 Hamiltonian structure, symmetries and conservation laws for water waves. *J. Fluid Mech.* **125**, 137–185.

Boussinesq, J. 1872 Théorie des ondes et des remous qui se propagent le long d'un canal rectangulaire horizontal, en communiquant au liquide contenu dans ce canal des vitesses sensiblement pareilles de la surface au fond. *J. de Mathématique Pures et Appliquées,* Deuxième Série **17**, 55–108.

Bretherton, F. P. 1968 Propagation in slowly varying waveguides. *Proc. R. Soc. London A* **302** (1471), 555–576.

Brizard, A. J. 2005 Noether methods for fluids and plasmas. *J. Plasma Phys.* **71** (2), 225–236.

Broer, L. J. F. 1974 On the Hamiltonian theory of surface waves. *Appl. Sci. Res.* **29**, 430–446.

Broer, L. J. F. 1975 Approximate equations for long wave equations. *Appl. Sci. Res.* **31** (5), 377–395.

Broer, L. J. F., van Groesen, E. W. C. & Timmers, J. M. W. 1976 Stable model equations for long water waves. *Appl. Sci. Res.* **32** (6), 619–636.

Chen, Y. & Liu, P. L.-F. 1995 Modified Boussinesq equations and associated parabolic models for water wave propagation. *J. Fluid Mech.* **288**, 351–381.

Dingemans, M. W. 1994 *Comparison of computations with Boussinesq-like models and laboratory measurements*. Delft Hydraulics. MAST-G8M note, H1684, 32 pp.

Dingemans, M. W. 1997 *Water wave propagation over uneven bottoms*, *Adv. Ser. on Ocean Eng.*, vol. 13. World Scientific, Singapore. 2 Parts, 967 pp.

Dingemans, M. W. & Klopman, G. 2009 Effects of normalisation and mild-slope approximation on wave reflection by bathymetry in a Hamiltonian wave model. In *Proc. 24th Int. Workshop on Water Waves and Floating Bodies,* Zelenogorsk, Russia, April 2009.

Dingemans, M. W. & Otta, A. K. 2001 Nonlinear modulation of water waves. In *Adv. in Coastal and Ocean Eng.* (ed. P. L.-F. Liu), , vol. 7, pp. 1–76. World Scientific, Singapore.

Djordjević, V. D. & Redekopp, L. G. 1978*b* On the development of packets of surface gravity waves moving over an uneven bottom. *J. Appl. Math. Phys. (ZAMP)* **29**, 950–962.

Dommermuth, D. G. & Yue, D. K. P. 1987 A high-order spectral method for the study of nonlinear gravity waves. *J. Fluid Mech.* **184**, 267–288.

Fuhrman, D. R. & Bingham, H. B. 2004 Numerical solutions of fully non-linear and highly dispersive Boussinesq equations in two horizontal dimensions. *Int. J. Num. Meth. Fluids* **44** (3), 231–255.

van Groesen, E. & Westhuis, J. H. 2002 Modelling and simulation of surface water waves. *Math. Comput. Sim.* **59** (4), 341–360.

Hayes, W. D. 1970*a* Conservation of action and modal wave action. *Proc. R. Soc. London A* **330** (1541), 187–208.

Hayes, W. D. 1970*b* Kinematic wave theory. *Proc. R. Soc. London A* **330** (1541), 209–226.

Hayes, W. D. 1973 Group velocity and nonlinear dispersive wave propagation. *Proc. R. Soc. London A* **332** (1589), 199–221.

Hsiao, S.-C., Lynett, P., Hwung, H.-H. & Liu, P. L.-F. 2005 Numerical simulations of nonlinear short waves using a multilayer model. *J. Eng. Mech.* **131** (3), 231–243.

Katopodes, N. D. & Dingemans, M. W. 1989 Hamiltonian approach to surface wave models. In *Comput. Mod. and Exp. Meth. in Hydraulics (HYDROCOMP '89),* Dubrovnik, Yugoslavia (ed. Č. Maksimovič & M. Radojkovič), pp. 137–147. Elsevier.

Klopman, G., Dingemans, M. W. & van Groesen, E. 2005 A variational model for fully non-linear water waves of Boussinesq type. In *Proc. 20th Int. Workshop on Water Waves and Floating Bodies,* Longyearbyen, Spitsbergen, Norway, May 2005.

Liu, P. L.-F. 1989 A note on long waves induced by short-wave groups over a shelf. *J. Fluid Mech.* **205**, 163–170.

Ludwig, D. 1970 Modified W.K.B. method for coupled ionospheric equations. *J. Atmosph. Terr. Phys.* **32** (6), 991–998.

Luth, H. R., Klopman, G. & Kitou, N. 1994 Project 13G: Kinematics of waves breaking partially on an offshore bar. LDV measurements for waves with and without a net onshore current. *Tech. Rep.* H1573. Delft Hydraulics, Delft, The Netherlands. 40 pp.

Lynett, P. J. & Liu, P. L.-F. 2004*a* a two-layer approach to wave modelling. *Proc. R. Soc. A* **460** (2049), 2637–2669.

Lynett, P. J. & Liu, P. L.-F. 2004*b* linear analysis of the multi-layer model. *Coastal Eng.* **51** (5–6), 439–454.

Madsen, P. A., Bingham, H. B. & Schäffer, H. A. 2003 Boussinesq-type formulations for fully nonlinear and extremely dispersive water waves: derivation and analysis. *Proc. R. Soc. London A* **459**, 1075–1104.

Madsen, P. A., Murray, R. & Sørensen, O. R. 1991 A new form of the Boussinesq equations with improved linear dispersion characteristics. *Coastal Eng.* **15** (4), 371–388.

Madsen, P. A. & Sørensen, O. R. 1992 A new form of the Boussinesq equations with improved linear dispersion characteristics. Part 2. A slowly-varying bathymetry. *Coastal Eng.* **18** (3–4), 183–204.

Mei, C. C. & Benmoussa, C. 1984 Long waves induced by short-wave groups over an uneven bottom. *J. Fluid Mech.* **139**, 219–235.

Milder, D. M. 1977 A note on: 'On Hamilton's principle for surface waves'. *J. Fluid Mech.* **83** (1), 159–161.

Milder, D. M. 1990 The effect of truncation on surface-wave Hamiltonians. *J. Fluid Mech.* **216**, 249–262.

Miles, J. W. 1977 On Hamilton's principle for surface waves. *J. Fluid Mech.* **83** (1), 153–158.

Otta, A. K., Dingemans, M. W. & Radder, A. C. 1996 A Hamiltonian model

for nonlinear water waves and its applications. In *Proc.* 25^{th} *Int. Conf. Coastal Eng.,* Orlando, , vol. 1, pp. 1156–1167. ASCE, New York, U.S.A.

Radder, A. C. 1992 An explicit Hamiltonian formulation of surface waves in water of finite depth. *J. Fluid Mech.* **237**, 435–455.

Radder, A. C. 1999 Hamiltonian dynamics of water waves. In *Adv. in Coastal and Ocean Eng.* (ed. P. L.-F. Liu), , vol. 4, pp. 21–59. World Scientific, Singapore.

Rienecker, M. M. & Fenton, J. D. 1981 A Fourier approximation method for steady water waves. *J. Fluid Mech.* **104**, 119–137.

Shepherd, T. G. 1990 Symmetries, conservation laws, and Hamiltonian structure in geophysical fluid dynamics. *Adv. Geophys.* **32**, 287–338.

Turpin, F.-M., Benmoussa, C. & Mei, C. C. 1983 Effects of slowly varying depth and current on the evolution of a Stokes wavepacket. *J. Fluid Mech.* **132**, 1–23.

West, B. J., Brueckner, K. A., Janda, R. S., Milder, D. M. & Milton, R. L. 1987 A new numerical method for surface hydrodynamics. *J. Geophys. Res.* **92** (C11), 11803–11824.

Westhuis, J.-H. 2001 *The numerical simulation of nonlinear waves in a hydrodynamic model test basin*. PhD Thesis, University of Twente, Enschede, The Netherlands.

Whitham, G. B. 1967*b* Variational methods and applications to water waves. *Proc. R. Soc. London A* **299** (1456), 6–25. Proc. of "A Discussion on Nonlinear Theory of Wave Propagation in Dispersive Systems" (June 13, 1967).

Whitham, G. B. 1974 *Linear and nonlinear waves*. Wiley–Interscience.

Witting, J. M. 1984 A unified model for the evolution of nonlinear water waves. *J. Comput. Phys.* **56** (4), 203–236.

Zakharov, V. E. 1968 Stability of periodic waves of finite amplitude on the surface of a deep fluid. *J. Appl. Mech. and Techn. Phys.* **9** (2), 190–194. Originally in: *Zhurnal Prildadnoi Mekhaniki i Tekhnicheskoi Fiziki* **9**(2), pp. 86–94, 1968.

Chapter 3

Two-dimensional wave propagation over bathymetry[1]

3.1 Introduction

Surface water waves propagating into shallow water are affected by the changes in the sea bed. Often, Boussinesq-type wave models are used to take these finite-depth effects into account. In Klopman *et al.* (2005), a variational method has been used to derive fully non-linear Boussinesq-type models from the full three-dimensional Hamiltonian structure. The canonical structure, as well as the positive definiteness of the Hamiltonian are preserved by this approach. In our view and experience, the positive definiteness of the resulting Hamiltonian ensures the good dynamical behaviour of the resulting equations.

In Klopman *et al.* (2005), the variational model has been derived for one horizontal dimension, and numerical examples have been presented for waves propagating over a horizontal bed. Here, we will extend the model to two horizontal dimensions. The model will be applied to the computation of waves propagating over an elliptic shoal on a slope (Berkhoff *et al.*, 1982). This test case is known to be affected by wave shoaling, refraction, diffraction and non-linearity (Kirby & Dalrymple, 1984; Dingemans *et al.*, 1984).

3.2 Hamiltonian model for waves propagating in two horizontal dimensions

The Hamiltonian theory for surface water waves on an incompressible fluid with an irrotational flow was independently discovered by Zakharov (1968), Broer (1974) and Miles (1977). Consider a fluid layer bounded below by the sea bed at $z = -h_0(\boldsymbol{x})$ and above by the free surface $z = \zeta(\boldsymbol{x}, t)$, where $\boldsymbol{x} = (x, y)^T$ are the horizontal coordinates, z is the vertical coordinate and t is the time. The irrotational flow of

[1]Published as:
Klopman, G., Dingemans, M. W. & van Groesen, E. 2007 The propagation of wave groups over bathymetry using a variational Boussinesq model. In *Proc. 22th Int. Workshop on Water Waves and Floating Bodies,* Plitvice, Croatia, April 2007.

the homogeneous fluid of unit mass density is described with a velocity potential $\phi(\boldsymbol{x}, z, t)$, *i.e.* $\boldsymbol{\nabla}\phi = (\partial_x\phi, \partial_y\phi)^T$ are the horizontal flow velocity components and $\partial_z\phi$ is the vertical velocity component. The potential at the free surface is denoted as $\varphi(\boldsymbol{x}, t) \equiv \phi(\boldsymbol{x}, \zeta(\boldsymbol{x}, t), t)$. Then ζ and φ are canonical variables, and the Hamiltonian description of the flow is given by:

$$\partial_t\zeta \;=\; +\frac{\delta\mathscr{H}}{\delta\varphi} \qquad \text{and} \qquad \partial_t\varphi \;=\; -\frac{\delta\mathscr{H}}{\delta\zeta}, \tag{3.1}$$

provided the flow in the fluid interior satisfies the Laplace equation, the bottom boundary condition at $z = -h(\boldsymbol{x})$ and the free-surface condition $\phi = \varphi(\boldsymbol{x}, t)$ at $z = \zeta(\boldsymbol{x}, t)$. The Hamiltonian $\mathscr{H}(\zeta, \varphi)$ is equal to the sum of the kinetic and potential energy of the fluid:

$$\mathscr{H} \;=\; \iint \left\{ \int_{-h_0(\boldsymbol{x})}^{\zeta(\boldsymbol{x},t)} \frac{1}{2} \left[\mid \boldsymbol{\nabla}\phi \mid^2 \;+\; (\,\partial_z\phi\,)^2 \right] \mathrm{d}z \;+\; \frac{1}{2}\,g\,\zeta^2 \right\} \mathrm{d}\boldsymbol{x}, \tag{3.2}$$

where g is the value of the gravitational acceleration, with gravity acting in the negative z-direction.

Now, in order to be able to derive a model only in the horizontal coordinates $\boldsymbol{x}$ and time t, we assume a vertical structure of the flow:

$$\phi(\boldsymbol{x}, z, t) \;=\; \varphi(\boldsymbol{x}, t) \;+\; f(z; h_0, \zeta)\,\psi(\boldsymbol{x}, t), \tag{3.3}$$

assuming $f(z; h_0, \zeta)$ to be given. To preserve the canonical structure, and to arrive at time-evolution equations for only ζ and ϕ, it is essential to require that $f = 0$ at the free surface $z = \zeta(\boldsymbol{x}, t)$. In accordance with the classical Boussinesq model, with a parabolic shape for the vertical flow structure and $\partial_z f = 0$ at the sea bed, we choose:

$$f(z; h_0, \zeta) \;=\; \frac{1}{2}\,(z - \zeta)\,\left(1 \;+\; \frac{h_0 \,+\, z}{h_0 \,+\, \zeta}\right), \tag{3.4}$$

which is expected to be a good approximation for mildly-sloping sea beds and intermediate to shallow water depths. In this case, the function $f(z; h_0, \zeta)$ has been normalized, in order to have $\psi(\boldsymbol{x}, t)$ equal to the vertical velocity at the free surface. Note that also other forms of $f(z; h_0, \zeta)$ may be taken, as well as a series of vertical shape functions (each equal to zero at the free surface).

We use the approximation (3.3) to compute the velocities needed in the Hamiltonian (3.2), and use a mild-slope assumption by neglecting the sea bed slopes in the velocities (but not in the functional derivatives of $\mathscr{H}$). Then the Hamiltonian $\mathscr{H}(\zeta, \varphi; \psi)$ for the Boussinesq model becomes:

$$\begin{aligned} \mathscr{H} = \iint \Bigg\{ & \frac{1}{2}\,(\,h_0 \,+\, \zeta\,) \left| \boldsymbol{\nabla}\varphi \;-\; \frac{2}{3}\,\psi\,\boldsymbol{\nabla}\zeta \;-\; \frac{1}{3}\,(\,h_0 \,+\, \zeta\,)\,\boldsymbol{\nabla}\psi \right|^2 \\ & + \frac{1}{90}\,(\,h_0 \,+\, \zeta\,) \left| \psi\,\boldsymbol{\nabla}\zeta \;-\; (\,h_0 \,+\, \zeta\,)\,\boldsymbol{\nabla}\psi \right|^2 \;+\; \frac{1}{6}\,(\,h_0 \,+\, \zeta\,)\,\psi^2 \;+\; \frac{1}{2}\,g\,\zeta^2 \Bigg\}\,\mathrm{d}\boldsymbol{x}, \end{aligned} \tag{3.5}$$

which is indeed seen to be positive definite.

Next, we introduce the horizontal gradient of the velocity potential, $\boldsymbol{u} \equiv \boldsymbol{\nabla}\varphi$ and the instantaneous total depth $h(\boldsymbol{x},t) \equiv h_0(\boldsymbol{x})+\zeta(\boldsymbol{x},t)$. Note that $\boldsymbol{u}(\boldsymbol{x},t)$ is different from the horizontal velocity components $\boldsymbol{\nabla}\phi$ at the free surface, since $\varphi(\boldsymbol{x},t)$ is not at a fixed level but at the moving free surface. Then, from Eq. (3.1) and from $\delta\mathscr{H}/\delta\psi = 0$, we get after taking the gradient of the equation for $\varphi(\boldsymbol{x},t)$:

$$\partial_t \zeta + \boldsymbol{\nabla}\cdot(h\,\boldsymbol{U}) = 0, \tag{3.6a}$$

$$\partial_t \boldsymbol{u} + \boldsymbol{\nabla}\left\{\frac{1}{2}|\boldsymbol{U}|^2 - \frac{1}{45}\left|\psi\,\boldsymbol{\nabla}\zeta + h\,\boldsymbol{\nabla}\psi\right|^2 + \frac{1}{6}\left(1+\frac{1}{5}|\boldsymbol{\nabla}\zeta|^2\right)\psi^2 + \right.$$
$$\left. + \boldsymbol{\nabla}\cdot\left[h\left(\frac{2}{3}\boldsymbol{u} - \frac{7}{15}\psi\,\boldsymbol{\nabla}\zeta - \frac{1}{5}h\,\boldsymbol{\nabla}\psi\right)\psi\right] + g\,\zeta\right\} = 0, \tag{3.6b}$$

$$h\,\psi\left(\frac{1}{3} + \frac{7}{15}|\boldsymbol{\nabla}\zeta|^2\right) - \left(\frac{2}{3}h\,\boldsymbol{u} - \frac{1}{5}h^2\,\boldsymbol{\nabla}\psi\right)\cdot\boldsymbol{\nabla}\zeta +$$
$$+\boldsymbol{\nabla}\cdot\left(\frac{1}{3}h^2\,\boldsymbol{u} - \frac{1}{5}h^2\,\psi\,\boldsymbol{\nabla}\zeta - \frac{2}{15}h^3\,\boldsymbol{\nabla}\psi\right) = 0, \tag{3.6c}$$

where

$$\boldsymbol{U}(\boldsymbol{x},t) = \boldsymbol{u} - \frac{2}{3}\psi\,\boldsymbol{\nabla}\zeta - \frac{1}{3}h\,\boldsymbol{\nabla}\psi \tag{3.7}$$

is the depth-averaged velocity. For one horizontal spatial dimension, the above set of equations is equal to the one derived in Klopman *et al.* (2005). Note that the third equation in (3.6) is an elliptic equation for ψ, and also that it is a linear equation in terms of ψ.

3.3 Waves over an elliptic shoal on a uniform slope

The laboratory setup for the elliptic shoal test (Berkhoff *et al.*, 1982) is shown in Figure 3.1, also showing the measurement sections. The deeper part of the wave basin has a constant depth of 0.45 m. The elliptic shoal is placed on a 1/50 sloping bottom, with the depth contours on the slope making an angle of 20^o with the x-axis. The centre of the shoal is located at a distance (perpendicular to the depth contours) of 5.84 m from the toe of the slope, and the shoal thickness d is given by:

$$d = -0.3 + 0.5\sqrt{1 + \left(\frac{x'}{5}\right)^2 + \left(\frac{y'}{3.75}\right)^2}, \tag{3.8}$$

with all distances in m. The incoming periodic waves are propagating in the negative y-direction and have a wave period of 1.00 s and wave amplitude of 23.2 mm, with wave amplitude defined as half the wave height. Wave amplitudes have been measured in a large number of points on a 0.25 by 0.25 m grid (Dingemans, 1997, Section 4.7.2, Note 4.2).

For our computations we use a pseudo-spectral code to solve the set (3.6), similar to the one used in Klopman *et al.* (2005), but now extended to two horizontal dimensions. The resulting set of ordinary differential equations for ζ and $\boldsymbol{u}$ in the

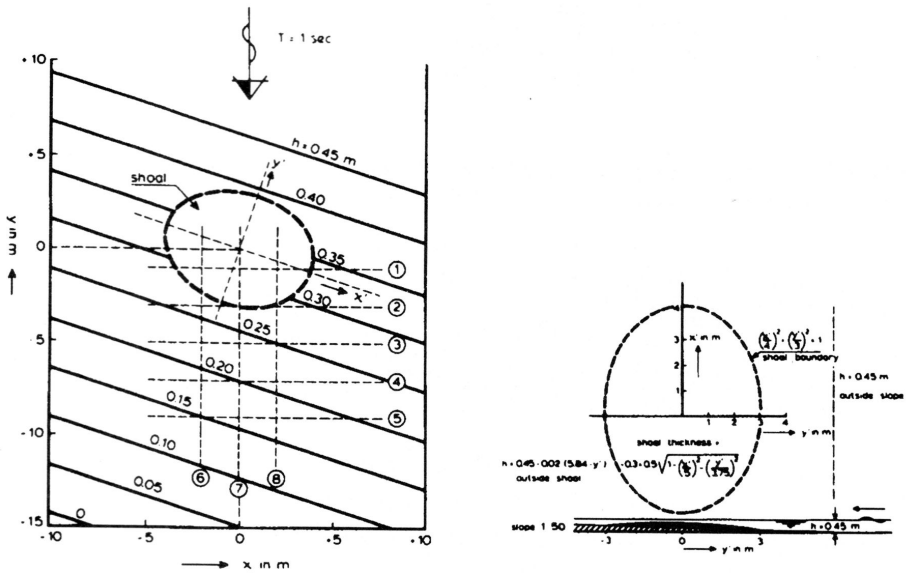

Figure 3.1: Setup of the elliptic shoal test case.

grid points is solved with a high-order ODE solver with variable step size (MATLAB function 'ode113'). At the start of each time step, ψ is determined for given ζ and φ, by solving the elliptic equation (3.6a) for ψ with a pre-conditioned conjugate-gradient method (MATLAB function 'bicgstab'). On average, about 2 to 4 iterations are necessary to lower the residual in the ψ-equations to a relative error of 10^{-5}. Computation time is about twice the time needed by the pseudo-spectral model for solving the shallow-water equations. The computations have been performed on a spatial grid of 240 by 360 grid points with 0.125 m spacing, and for a duration of 25 wave periods.

Figures 3.2 and 3.3 give a comparison between the computations and the measurements. Figure 3.3b clearly shows the diffraction pattern, as well as the wave focussing by refraction. The two most discriminating sections, 5 and 6, show quite good agreement between the measurements and the computations, comparable to the results of other wave models (Mooiman, 1991*b*; Kirby & Dalrymple, 1984; Dingemans *et al.*, 1984). Wave non-linearity is essential in these sections to get fair agreement with the measurements, as shown by both Dingemans *et al.* (1984) and Kirby & Dalrymple (1984).

3.4 References

Berkhoff, J. C. W., Booij, N. & Radder, A. C. 1982 Verification of numerical wave propagation models for simple harmonic linear water waves. *Coastal Eng.* **6** (3), 255–279.

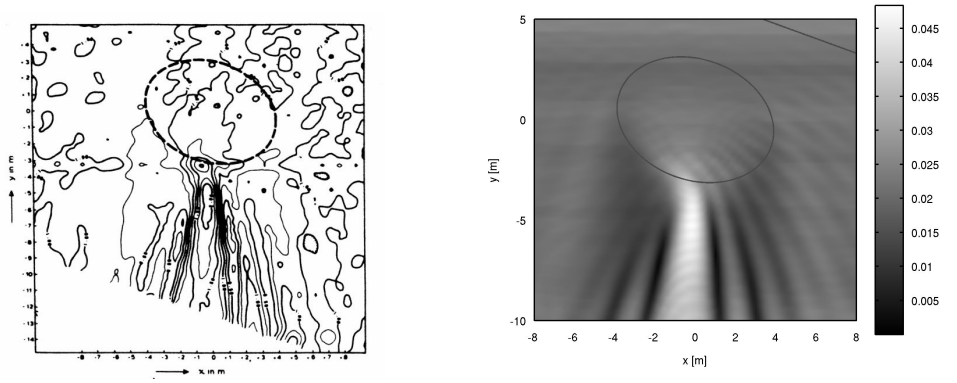

(a) Measured wave amplitude. **(b)** Computed wave amplitude.

Figure 3.2: Measured and computed wave amplitudes for the elliptic shoal test case.

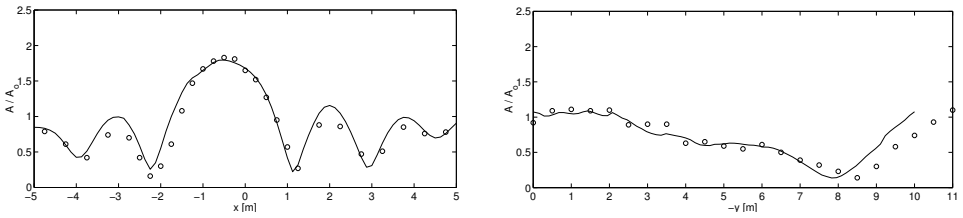

(a) Section 5: $y = -9$ m. **(b)** Section 6: $x = -2$ m.

Figure 3.3: Wave amplitudes in sections 5 and 6: measurements (circles) and computation (solid line).

Broer, L. J. F. 1974 On the Hamiltonian theory of surface waves. *Appl. Sci. Res.* **29**, 430–446.

Dingemans, M. W. 1997 *Water wave propagation over uneven bottoms*, *Adv. Ser. on Ocean Eng.*, vol. 13. World Scientific, Singapore. 2 Parts, 967 pp.

Dingemans, M. W., Stive, M. J. F., Kuik, A. J., Radder, A. C. & Booij, N. 1984 Field and laboratory verification of the wave propagation model CREDIZ. In *Proc. 19th Int. Conf. Coastal Eng.,* Houston, pp. 1178–1191. ASCE, New York, U.S.A.

Kirby, J. T. & Dalrymple, R. A. 1984 Verification of a parabolic equation for propagation of weakly-nonlinear waves. *Coastal Eng.* **8** (3), 219–232.

Klopman, G., Dingemans, M. W. & van Groesen, E. 2005 A variational model for fully non-linear water waves of Boussinesq type. In *Proc. 20th Int. Workshop on Water Waves and Floating Bodies,* Longyearbyen, Spitsbergen, Norway, May 2005.

Miles, J. W. 1977 On Hamilton's principle for surface waves. *J. Fluid Mech.* **83** (1), 153–158.

Mooiman, J. 1991*b* Comparison between measurements and a Boussinesq model for wave deformation by a shoal. *Tech. Rep.* Z294, Part 2. Delft Hydraulics, Delft, The Netherlands. 25 pp.

Zakharov, V. E. 1968 Stability of periodic waves of finite amplitude on the surface of a deep fluid. *J. Appl. Mech. and Techn. Phys.* **9** (2), 190–194. Originally in: *Zhurnal Prildadnoi Mekhaniki i Tekhnicheskoi Fiziki* **9**(2), pp. 86–94, 1968.

Chapter 4

Reflection for linear water waves over bathymetry[1]

Abstract

The reflection characteristics are analysed for a series of Hamiltonian water-wave models. These variational models have been derived by applying a Boussinesq-like approach to the vertical flow-structure. Both parabolic and hyperbolic-cosine approximations to the vertical structure are considered. Mild-slope approximations are made for the flow velocities, by neglecting horizontal derivatives of the mean water depth in the Hamiltonian density. In all cases, a positive definite Hamiltonian is ensured, contributing to the good dynamical behaviour of the resulting flow equations.

It is found that, in general, the mild-slope approximation results in less good predictions of the reflections, as compared to the steep slope variants – *i.e.* without the mild-slope approximation – and the accurate model results of Porter & Porter (2006). However, by carefully choosing the normalisation for the mild-slope models, good reflection characteristics can be obtained while maintaining the simpler structure of the mild-slope model, as compared with the steep slope variants.

4.1 Introduction

Gravity waves on the surface of a water layer propagate in the horizontal plane. While in the third (vertical) spatial dimension a different behaviour occurs. The physical space can thus be thought of as consisting of a horizontal space, called propagation space, and a vertical one, a cross space. Our interest is in wave propagation and reflection. It is therefore advantageous to construct approximate models in which the vertical dimension – the cross space – has been eliminated. Slow variations of the bathymetry can ease the elimination of the cross space, by applying the mild-slope approximation.

An often-used approach to eliminate the cross space is by applying a Boussinesq-type approximation, where an approximate vertical flow-structure is used. Using the flow equations, the effects of the vertical flow-structure are transformed into additional terms or equations in the horizontal wave-propagation model.

[1]In press, accepted for publication:
Klopman, G. & Dingemans, M. W. 2010 Reflection in variational models for linear water waves. *Wave Motion*.

When testing the accuracy of these two-dimensional horizontal models, reflections caused by varying depths pose a strong challenge: while many models perform well for wave shoaling, refraction and diffraction, only few models obtain accurate results on wave reflection.

In case of a finite stretch with depth variations, wave re-reflections introduce an oscillatory behaviour in the size of the reflection coefficient as a function of the wave length, in combination with the length of the inhomogeneity. This is due to the possibility of resonance if the wave length matches with the distance between the points of re-reflection, see *e.g.* Kajiura (1961), Mei & Black (1969) or Dingemans (1997, §2.6.6–§2.6.8). This behaviour is confirmed by experiments, see *e.g.* Rey *et al.* (1992).

Here, we will study the reflection characteristics of Boussinesq-type models resulting from the variational approach of Klopman, van Groesen & Dingemans (2010). Notice that the Hamiltonian from which this model has been derived, is positive-definite. This results in good dynamical behaviour, also important for the numerical implementation. We use two different vertical flow structures in the variational model: a parabolic one, valid for not too large water depth ($kh < \pi$), and a hyperbolic-cosine (cosh) structure. Further, for both vertical structures, two variants are taken into consideration: firstly a simpler mild-slope variant is derived by neglecting the bottom slope terms in the Hamiltonian density, and secondly a steep-slope variant without these additional approximations is considered.

The motivation to study the effect of bottom-slope terms on reflection is in our case provided by Madsen *et al.* (2006), who note that for their model inclusion of bed slope and curvature terms is essential to obtain good results, with respect to linear reflection. Previously, in the so-called mild-slope equation, bottom-slope effects have been included (Dingemans, 1985, pp. 9–10; Dingemans, 1997, §3.1.1; Chamberlain & Porter, 1995). This results in much better reflection characteristics for the mild-slope equation. For an overview see *e.g.* Porter & Chamberlain (1997).

The linear reflection analysis is performed for a finite stretch with bottom variations in one horizontal spatial dimension. The primary test case is a shelf consisting of a straight bottom slope connecting two regions of constant, but different, depth. This case was first used by Booij (1983), and we use the accurate numerical results of Porter & Porter (2006) for this lay-out to compare our model with. However, in the Booij test case the discontinuities in the bottom slope, at the connections of the plane slope with the horizontal beds, dominate the reflection. Therefore, as a second test case, we use an infinitely smooth slope, also varying over a finite stretch, with the same maximum slope as the Booij case. As expected, the reflection coefficient of a smooth slope is much less, especially for long slopes.

One observation from these cases is the large difference between the performance of both mild-slope models, the parabolic and hyperbolic-cosine ones. While, for these cases with not-so-short waves ($kh = 0.86$ in the deep part), our expectation is that both models will perform similar – whether good or bad. The difference between the two mild-slope models is the different normalisation of the vertical flow-structure. This leads us to investigate the effect of normalisation on the reflection characteristics of mild-slope models. It is found to have a large effect, and by careful

tuning of the normalisation, mild-slope models can be constructed with excellent reflection characteristics – as good as the steep-slope models.

4.2 Positive-definite Hamiltonian description of linear water waves

The Hamiltonian structure for water waves (Zakharov, 1968; Broer, 1974; Miles, 1977), on a layer of incompressible and homogeneous fluid with an irrotational flow, is applied to long-crested linear waves propagating in the horizontal x-direction:

$$\rho\,\partial_t\zeta \;=\; +\,\frac{\delta\mathscr{H}_0}{\delta\varphi} \qquad \text{and} \qquad \rho\,\partial_t\varphi \;=\; -\,\frac{\delta\mathscr{H}_0}{\delta\zeta}, \tag{4.1}$$

where z is the vertical coordinate, the positive z-direction is upwards, while $z = \zeta(x,t)$ is the free-surface elevation as a function of x and time t. Further, ρ is the fluid mass density, taken to be a constant. The zero level of z is at the mean free surface elevation, $\bar{\zeta} = 0$. The fluid layer is bounded as $-h \le z \le \zeta$, where $h(x)$ is the still water depth which is always positive. The potential $\varphi(x,t)$ is the value of the velocity potential $\Phi(x,z,t)$ at the free surface: $\varphi(x,t) = \Phi(x,\zeta(x,t),t)$, and $\mathscr{H}_0(\zeta,\varphi)$ is the Hamiltonian of the linearised problem, *i.e.* the sum of the kinematic and potential energy in the fluid domain. In the present case, of pure waves and a linearised model, the upper limit of the vertical integral of kinetic-energy density is at the mean free-surface elevation, so the Hamiltonian $\mathscr{H}_0$ becomes:

$$\mathscr{H}_0 \;=\; \int \left\{ \int_{-h}^{0} \frac{1}{2}\,\rho \left[(\partial_x\Phi)^2 \;+\; (\partial_z\Phi)^2 \right] \mathrm{d}z \;+\; \frac{1}{2}\,\rho\, g\, \zeta^2 \right\} \mathrm{d}x, \tag{4.2}$$

with g the acceleration by gravity. The acceleration by gravity is in the negative z-direction.

The additional constraint on $\mathscr{H}_0$ is that Φ has to satisfy the Laplace equation in the fluid interior and the boundary condition at $z = -h$, *i.e.* at the bed. This corresponds with $\delta\mathscr{H}_0/\delta\Phi = 0$, with the variations $\delta\Phi$ being only non-zero in the fluid interior to obtain the Laplace equation, and with variations $\delta\Phi$ being only non-zero at $z = -h$ in order to obtain the kinematic boundary condition at the bed.

A Lagrangian formulation, equivalent to the Hamiltonian one, is given by Miles (1977):

$$\mathscr{L}_0 \;=\; \int \left[\int \rho\,\varphi\,\partial_t\zeta \,\mathrm{d}x \;-\; \mathscr{H}_0 \right] \mathrm{d}t, \tag{4.3}$$

and from considering its critical point $\delta\mathscr{L}_0 = 0$. It then follows that the variations of $\mathscr{L}_0$ with respect to ζ and Φ have to be zero, resulting in (4.1) as well as the Laplace equation in the fluid interior.

Now, approximated flow-equations, only dependent on the wave propagation direction x and time t, can be obtained by making a reasonable assumption on the

dependence of Φ on z. Then, the vertical direction z in the Hamiltonian $\mathscr{H}_0$ can be integrated out. In order to retain the Hamiltonian structure, we take the following vertical structure of the potential Φ, see Klopman, Dingemans & van Groesen (2005):

$$\Phi(x,z,t) \;=\; \varphi(x,t) \;+\; f(z;h,\kappa)\,\psi(x,t) \qquad \text{with} \qquad f(0;h,\kappa) \;=\; 0, \tag{4.4}$$

where $f(z;h,\kappa)$ is a chosen vertical structure function, dependent on the vertical coordinate z, the water depth $h(x)$ and (eventually) an additional shape parameter $\kappa(x)$. The shape function f is only dependent on x indirectly, since h and κ may be functions of x.

Essential in this approach is taking $f \;=\; 0$ at the free surface $z = \zeta(x,t)$; in the linear case – as we consider here – this means $f \;=\; 0$ at $z \;=\; 0$. This ensures that the problem maintains its canonical Hamiltonian structure (4.1). Taking $f = 0$ at the free surface $z = \zeta$ guarantees that only two evolutionary equations with simple time derivatives $\partial_t\zeta$ and $\partial_t\varphi$ will appear, when taking the variations of (4.3) with respect to the surface potential φ and elevation ζ. Note, that in the approximation (4.4) the first term $\varphi(x,t)$ can be thought as being associated with a uniform shape function, *i.e.* equal to one for all z. This means that the model will always include a description well suitable for interactions between short waves and long waves or currents.

Further, the introduced field $\psi(x,t)$, which determines the non-uniformity of the flow over the water column, has to satisfy the additional constraint:

$$\frac{\delta\mathscr{H}_0}{\delta\psi} \;=\; 0\,, \tag{4.5}$$

as a result of variation of $\mathscr{L}_0$ with respect to ψ in (4.3).

Using the approximate structure (4.4), the horizontal and vertical flow velocities, $\partial_x\Phi$ and $\partial_z\Phi$, become:

$$\partial_x\Phi \;=\; \partial_x\varphi \;+\; f\,\partial_x\psi \;+\; \psi\,\partial_x f \qquad \text{and} \tag{4.6a}$$

$$\partial_z\Phi \;=\; \psi\,\partial_z f. \tag{4.6b}$$

In the remainder, we will consider several Ansatzes for f:

$$\text{parabolic-structure model} \quad : \quad f^{(p)} = \frac{1}{2}\,\frac{(z+h)^2 - h^2}{h}, \tag{4.7a}$$

$$\text{hyperbolic-cosine (cosh) structure model} \quad : \quad f^{(c)} = \cosh\left(\kappa\,(z+h)\right) - \cosh\left(\kappa h\right), \tag{4.7b}$$

$$\text{normalised cosh-structure model} \quad : \quad f^{(cs)} = \frac{\cosh\left(\kappa\,(z+h)\right) - \cosh\left(\kappa h\right)}{\kappa\,\sinh\left(\kappa h\right)}, \tag{4.7c}$$

$$\text{optimised parabolic-structure model} \quad : \quad f^{(po)} = \frac{1}{2}\,\frac{(z+h)^2 - h^2}{h^n} \quad \text{and} \tag{4.7d}$$

$$\text{optimised cosh-structure model} \quad : \quad f^{(co)} = \frac{\cosh\left(\kappa\,(z+h)\right) - \cosh\left(\kappa h\right)}{N(\kappa h)}, \tag{4.7e}$$

with the power n, as well as the form of the normalisation $N(\kappa h)$ – optimised in some sense – being determined later on. All shape functions $f(z;\kappa,h)$ are zero at the free surface elevation $z=0$. Notice that the different shape functions have different dimensions, implying that ψ also has different dimensions for the various forms of f. And therefore the field ψ also represents a different physical quantity, depending on the chosen form of the shape function f. In all situations $f\psi$ has the same dimension as φ.

The chosen forms of the shape functions above are motivated by the knowledge that – for mono-chromatic water waves over a horizontal bed, eventually also with a z-independent uniform current – the oscillatory part of the linear-theory potential varies as $\cosh(k\,(z+h))$; with k the wave number. Clearly, to obtain $f=0$ at $z=0$, the value $\cosh(kh)$ has to be subtracted. Notice that in the potential model (4.4) the shape function f and the field $\psi(x,t)$ are only associated with the variations of Φ with z. The depth-independent term is given by $\varphi(x,t)$. In the cosh-structure models, $f^{(c)}$, $f^{(cs)}$ and $f^{(co)}$, the wave number k is replaced by $\kappa(x)$ which can be chosen according to the local water depth $h(x)$ and the waves under consideration. The only difference between the cosh-structure models considered is their normalisation, the effects of which are the subject of this paper. The parabolic-structure models $f^{(p)}$ and $f^{(po)}$ are the limiting values of the cosh structure for $\kappa h \to 0$; in that case $\kappa(x)$ becomes a multiplicative factor which is incorporated into $\psi(x,t)$. A parabolic structure is also the structure as used in so-called classical Boussinesq-type wave models, *i.e.* the first deviation of vertical structure from the depth-uniform shallow-water approximation (for a horizontal bed).

The functions $f^{(p)}(z;h)$ and $f^{(cs)}(z;\kappa,h)$ are chosen such that $\partial_z f^{(p)} = \partial_z f^{(cs)} = 1$ at $z=0$, with the result that for these models $\psi(x,t)$ equals the vertical velocity $\partial_z\Phi$ at the free surface. While for the optimised cosh-structure model (4.7e) the given normalisation is the most general form, the optimised parabolic structure (4.7d) is the most simple generalisation of Eq. (4.7a). The derivation of the form of the last two shape-functions, $f^{(po)}(z;h)$ and $f^{(co)}(z;\kappa,h)$, will be treated later when we discuss the search for mild-slope models with improved reflection characteristics in Section 4.6.

Independent of the particular choice for the function $f(z;h,\kappa)$, we can distinguish between, firstly **mild-slope** approximations, where $\partial_x f = 0$ is assumed in the horizontal velocity $\partial_x\Phi$, Eq. (4.6a). As a result there are no x-derivatives of f in the Hamiltonian $\mathscr{H}_0$. Secondly, there is the **steep-slope** case where $\partial_x f$ is fully taken into account in the flow velocities, as used in the Hamiltonian $\mathscr{H}_0$.

The velocity components are substituted into the Hamiltonian $\mathscr{H}_0$, Eq. (4.2), eventually with the mild-slope approximation where $\partial_x f$ neglected. The vertical integrations over z are performed, and the resulting approximate $\mathscr{H}_0(\zeta,\varphi;\psi)$ is always positive definite and of the form:

$$\begin{aligned}\mathscr{H}_0 \;=\; \int \rho \,\Big\{ \tfrac{1}{2}\,h\,(\partial_x\varphi)^2 \;+\; P\,(\partial_x\varphi)\,(\partial_x\psi) \;+\; X\,\psi\,(\partial_x\varphi) \;+\; Y\,\psi\,(\partial_x\psi) \\ +\; \tfrac{1}{2}\,K\,\psi^2 \;+\; \tfrac{1}{2}\,F\,(\partial_x\psi)^2 \;+\; \tfrac{1}{2}\,g\,\zeta^2 \Big\}\;\mathrm{d}x,\end{aligned} \tag{4.8}$$

where:

$$P \;=\; \int_{-h}^{0} f \,\mathrm{d}z, \qquad F \;=\; \int_{-h}^{0} f^2 \,\mathrm{d}z, \qquad X \;=\; \int_{-h}^{0} \partial_x f \,\mathrm{d}z, \tag{4.9a}$$

$$Y \;=\; \int_{-h}^{0} f\,\partial_x f \,\mathrm{d}z \qquad \text{and} \qquad K \;=\; \int_{-h}^{0} \Big[(\partial_x f)^2 \;+\; (\partial_z f)^2 \Big] \,\mathrm{d}z, \tag{4.9b}$$

which may still be (time-independent) functions of x. Note that in the mild-slope approximation X and Y, as well as the first term in the integrand of K, will be zero.

4.3 Time-harmonic linearised variational Boussinesq model

4.3.1 Time-dependent flow equations

The linearised variational Boussinesq model, for both the parabolic and cosh vertical structures, and for a varying still-water depth $h(x)$, can be derived from the Hamiltonian system (4.1) and (4.5), with the Hamiltonian (4.8). The resulting flow equations become:

$$\partial_t \zeta \;+\; \partial_x \left(h\,\partial_x \varphi \;+\; P\,\partial_x \psi \;+\; X\,\psi \right) \;=\; 0, \tag{4.10a}$$

$$\partial_t \varphi \;+\; g\,\zeta \;=\; 0 \qquad \text{and} \tag{4.10b}$$

$$K\,\psi \;-\; \partial_x \left(F\,\partial_x \psi \;+\; P\,\partial_x \varphi \;+\; Y\,\psi \right) \;+\; X\,\partial_x \varphi \;+\; Y\,\partial_x \psi \;=\; 0. \tag{4.10c}$$

The last equation can also be written as:

$$M\,\psi \;-\; \partial_x \left(F\,\partial_x \psi \;+\; P\,\partial_x \varphi \right) \;+\; X\,\partial_x \varphi \;=\; 0, \tag{4.10d}$$

with

$$M \;=\; K \;-\; \partial_x Y. \tag{4.10e}$$

For $\partial_x Y$ we have:

$$\begin{aligned} \partial_x Y \;&=\; \int_{-h}^{0} \partial_x \left(f\,\partial_x f \right) \,\mathrm{d}z \;+\; (\partial_x h) \left[f\,\partial_x f \right]_{z=-h} \\ &=\; \int_{-h}^{0} \left(\partial_x f \right)^2 \,\mathrm{d}z \;+\; \int_{-h}^{0} f\,\partial_x^2 f \,\mathrm{d}z \;+\; (\partial_x h) \left[f\,\partial_x f \right]_{z=-h}. \end{aligned} \tag{4.11}$$

So we get for M:

$$M \;=\; \int_{-h}^{0} \left(\partial_z f \right)^2 \,\mathrm{d}z \;-\; \int_{-h}^{0} f\,\partial_x^2 f \,\mathrm{d}z \;-\; (\partial_x h) \left[f\,\partial_x f \right]_{z=-h}. \tag{4.12}$$

For a smooth bed, the equations (4.10c) and (4.10d) are equivalent. However, for a *non-smooth bed* with for instance discontinuities in the bed slope, these formulations are not equivalent. The coefficients K, X and Y in the steep-slope description have discontinuities (jumps) in their values at points where the bed slope is discontinuous. Formulation (4.10) using (4.10c) is a conservative formulation which behaves correctly at slope discontinuities, also in its numerical approximation, provided an appropriate numerical method in conservation form is used: in integral form it leads directly to the correct jump conditions at the discontinuities. See Porter & Chamberlain (1997) for a discussion on jump conditions in connection with mild-slope models and slope discontinuities. However, the non-conservation form (4.10d) leads to erroneous reflections and transmissions at slope discontinuities. Therefore, equation (4.10c) is used in the remainder.

The flow equations (4.10) are associated with a positive-definite Hamiltonian $\mathscr{H}_0$, Eq. (4.8), and will form the basis for the reflection analysis below.

For a mildly-sloping bed, and a parabolic vertical flow-structure, $f^{(p)} = \frac{1}{2}\,z\,(2\,h + z)\,/\,h$, the depth integrals $F_m^{(p)}(x)$, $P_m^{(p)}(x)$, $K_m^{(p)}(x)$ and $M_m^{(p)}(x)$ are:

$$P_m^{(p)} = -\frac{1}{3}\,h^2, \qquad F_m^{(p)} = \frac{2}{15}\,h^3, \qquad X_m^{(p)} = Y_m^{(p)} = 0$$
$$\text{and} \quad K_m^{(p)} = M_m^{(p)} = \frac{1}{3}\,h, \tag{4.13}$$

where the subscript m denotes, here and in the remainder of the text, that the mild-slope approximation has been made.

For the same parabolic flow-structure, but without the mild-slope assumption, we get for the integrals (4.9):

$$\begin{aligned} &P^{(p)} = -\frac{1}{3}\,h^2, \qquad F^{(p)} = \frac{2}{15}\,h^3, \qquad X^{(p)} = -\frac{1}{6}\,h\,h', \qquad Y^{(p)} = \frac{3}{40}\,h^2\,h', \\ &K^{(p)} = \frac{1}{3}\,h + \frac{1}{20}\,h\,(h')^2 \qquad \text{and} \qquad M^{(p)} = \frac{1}{3}\,h - \frac{1}{10}\,h\,(h')^2 - \frac{3}{40}\,h^2\,h'', \end{aligned} \tag{4.14}$$

where an prime $(\cdot)'$ denotes differentiation with respect to its argument, in this case differentiation with respect to x. And for the hyperbolic-cosine shape function $f^{(c)}(z) = \cosh\left[\kappa\,(z+h)\right] - \cosh\left(\kappa\,h\right)$, with position-dependent parameter $\kappa(x)$, the depth integrals $F_m^{(c)}(x)$, $P_m^{(c)}(x)$, $K_m^{(c)}(x)$ and $M_m^{(c)}(x)$ become for the mild-slope case, *i.e.* neglecting the x-derivatives of κ and h in the flow velocities:

$$\begin{aligned} &P_m^{(c)} = \frac{1}{\kappa}\left(\mathcal{S} - \kappa\,h\,\mathcal{C}\right), \qquad F_m^{(c)} = -\frac{3}{2}\,\frac{1}{\kappa}\,\mathcal{S}\,\mathcal{C} + \frac{1}{2}\,h + h\,\mathcal{C}^2, \\ &X_m^{(c)} = Y_m^{(c)} = 0 \qquad \text{and} \qquad K_m^{(c)} = M_m^{(c)} = \frac{1}{2}\,\kappa\,\mathcal{S}\,\mathcal{C} - \frac{1}{2}\,\kappa^2\,h, \end{aligned} \tag{4.15}$$

with:

$$\mathcal{S} = \sinh\left(\kappa\,h\right) \qquad \text{and} \qquad \mathcal{C} = \cosh\left(\kappa\,h\right). \tag{4.16}$$

Including the slope and κ-gradient terms, the result is:

$$P^{(c)} = \frac{1}{\kappa}\left(\mathcal{S} - \kappa\,h\,\mathcal{C}\right), \qquad F^{(c)} = -\frac{3}{2}\,\frac{1}{\kappa}\,\mathcal{S}\,\mathcal{C} + \frac{1}{2}\,h + h\,\mathcal{C}^2, \tag{4.17a}$$

$$X^{(c)} = \left(\mathcal{C} \,-\, 1 \,-\, \kappa\, h\, \mathcal{S} \right) h' \,+\, \frac{1}{\kappa^2} \left(-\,\mathcal{S} \,+\, \kappa\, h\, \mathcal{C} \,-\, \kappa^2\, h^2\, \mathcal{S} \right) \kappa', \tag{4.17b}$$

$$Y^{(c)} = \frac{1}{2} \left[1 \,+\, 2\,\mathcal{C} \,-\, 3\,\mathcal{C}^2 \,+\, 2\,\kappa\, h\, \mathcal{S}\,\mathcal{C} \right] h' + \frac{1}{4}\,\frac{1}{\kappa^2} \left[3\,\mathcal{S}\,\mathcal{C} \,+\, 3\,\kappa\, h \left(1 \,-\, 2\,\mathcal{C}^2 \right) \,+\, 4\,\kappa^2\, h^2\, \mathcal{S}\,\mathcal{C} \right] \kappa', \tag{4.17c}$$

$$K^{(c)} = \frac{1}{2}\,\kappa\,\mathcal{S}\,\mathcal{C} \,-\, \frac{1}{2}\,\kappa^2\, h \,+\, \kappa \left[\mathcal{S} \left(2 \,-\, \frac{3}{2}\,\mathcal{C} \right) \,+\, \kappa\, h \left(\mathcal{S}^2 \,-\, \frac{1}{2} \right) \right] (h')^2 + \frac{1}{\kappa} \left[\frac{3}{2}\,\mathcal{S}^2 \,+\, \kappa\, h\, \mathcal{S} \left(2 \,-\, 3\,\mathcal{C} \right) \,+\, \kappa^2\, h^2 \left(2\,\mathcal{S}^2 \,-\, \frac{1}{2} \right) \right] \kappa'\, h' + \frac{1}{\kappa^3} \left[\frac{1}{4}\,\mathcal{S}\,\mathcal{C} \,+\, \kappa\, h \left(\frac{3}{2}\,\mathcal{S}^2 \,-\, \frac{1}{4} \right) - \frac{3}{2}\,\kappa^2\, h^2\, \mathcal{S}\,\mathcal{C} \,+\, \kappa^3\, h^3 \left(\mathcal{S}^2 \,-\, \frac{1}{6} \right) \right] (\kappa')^2 \qquad \text{and} \tag{4.17d}$$

$$M^{(c)} = \frac{1}{2}\,\kappa\,\mathcal{S}\,\mathcal{C} \,-\, \frac{1}{2}\,\kappa^2\, h \,+\, \kappa \left[\mathcal{S} \left(1 \,+\, \frac{1}{2}\,\mathcal{C} \right) \,-\, \kappa\, h \left(\frac{1}{2} + \mathcal{C}^2 \right) \right] (h')^2 + \frac{1}{\kappa} \left[\frac{3}{2}\,\mathcal{S}^2 \,+\, \kappa\, h\, \mathcal{S} \,-\, \kappa^2\, h^2 \left(\frac{1}{2} \,+\, 2\,\mathcal{C}^2 \right) \right] \kappa'\, h' + \frac{1}{\kappa^3} \left[\frac{7}{4}\,\mathcal{S}\,\mathcal{C} - \kappa\, h \left(\frac{1}{4} \,+\, \frac{3}{2}\,\mathcal{C}^2 \right) + \frac{3}{2}\,\kappa^2\, h^2\, \mathcal{S}\,\mathcal{C} - \kappa^3\, h^3 \left(\frac{1}{6} \,+\, \mathcal{C}^2 \right) \right] (\kappa')^2 + \left[1 \,-\, \mathcal{C} \,+\, \frac{3}{2}\,\mathcal{S}^2 \,-\, \kappa\, h\, \mathcal{S}\,\mathcal{C} \right] h'' + \frac{1}{\kappa^2} \left[-\frac{3}{4}\,\mathcal{S}\,\mathcal{C} \,+\, \frac{3}{4}\,\kappa\, h \left(\mathcal{S}^2 + \mathcal{C}^2 \right) \,-\, \kappa^2\, h^2\, \mathcal{S}\,\mathcal{C} \right] \kappa''. \tag{4.17e}$$

Usually κ is chosen to depend on h. Then κ depends on x since h is in general a function of x. In this paper, we will use the linear-theory dispersion relation:

$$\omega_c^2 \;=\; g\,\kappa\, \tanh\left(\kappa\, h\right), \tag{4.18}$$

with ω_c a constant and a characteristic angular frequency for the problem at hand, and chosen beforehand. The derivatives of κ with respect to x are given in Appendix 4.C.

4.3.2 Flow equations for time-harmonic motion

We consider time-harmonic motion:

$$\zeta(x,t) \;=\; \mathrm{Re}\left\{ \tilde{\zeta}(x)\, \mathrm{e}^{-i\omega t} \right\}, \tag{4.19}$$

where ω is the angular frequency and $i^2 \equiv -1$. The functions $\varphi(x,t)$ and $\psi(x,t)$ are of similar form, with complex-valued amplitudes $\tilde{\varphi}(x)$ and $\tilde{\psi}(x)$, respectively. Then

we have from (4.10) for $\tilde{\varphi}(x)$ and $\tilde{\psi}(x)$, eliminating $\tilde{\zeta}(x)$:

$$\frac{\omega^2}{g}\,\tilde{\varphi} \;+\; \left\{\, h\,\tilde{\varphi}' \;+\; P\,\tilde{\psi}' \;+\; X\,\tilde{\psi} \,\right\}' \;=\; 0, \tag{4.20a}$$

$$K\,\tilde{\psi} \;-\; \left\{\, F\,\tilde{\psi}' \;+\; P\,\tilde{\varphi}' \;+\; Y\,\tilde{\psi} \,\right\}' \;+\; X\,\tilde{\varphi}' \;+\; Y\,\tilde{\psi}' \;=\; 0, \tag{4.20b}$$

where a prime, $(\cdot)'$, denotes differentiation with respect to the argument, in this case x. The surface amplitude $\tilde{\zeta}(x)$ can be determined from:

$$\tilde{\zeta} \;=\; i\,\frac{\omega}{g}\,\tilde{\varphi}. \tag{4.20c}$$

In the remainder, we will write the complex amplitudes **without the tilde** ($\tilde{}$), for shortness.

4.4 Numerical solution method

4.4.1 Formulation as a system of first-order ODE's

We write (4.20) as a system of first-order ODE's. To start with, we introduce the auxiliary variables $q(x)$ and $r(x)$:

$$q \;=\; h\,\varphi' \;+\; P\,\psi' \;+\; X\,\psi \qquad \text{and} \qquad r \;=\; P\,\varphi' \;+\; F\,\psi' \;+\; Y\,\psi. \tag{4.21}$$

From these, we can solve for $\varphi'(x)$ and $\psi'(x)$:

$$\left(\, h\,F \;-\; P^2 \,\right)\,\varphi' \;=\; +F\,\left(\, q \;-\; X\,\psi \,\right) \;-\; P\,\left(\, r \;-\; Y\,\psi \,\right) \qquad \text{and} \tag{4.22a}$$

$$\left(\, h\,F \;-\; P^2 \,\right)\,\psi' \;=\; -P\,\left(\, q \;-\; X\,\psi \,\right) \;+\; h\,\left(\, r \;-\; Y\,\psi \,\right). \tag{4.22b}$$

The system of first-order ODE's is completed with (4.20), written in terms of $q(x)$ and $r(x)$:

$$q' \;=\; -\,\frac{\omega^2}{g}\,\varphi \qquad \text{and} \tag{4.22c}$$

$$r' \;=\; K\,\psi \;+\; X\,\varphi' \;+\; Y\,\psi'. \tag{4.22d}$$

The set (4.22) of four first-order ODE's is the set to be solved. The ODE's are solved numerically using the MATLAB function `bvp4c`.

4.4.2 Waves over a horizontal bed

Waves over a horizontal bed, of the form

$$\varphi(x) \;=\; \hat{\varphi}\,\mathrm{e}^{i\,k\,x}, \tag{4.23}$$

and similar forms for ψ, q and r, are put into Eqs. (4.22). This gives an eigenvalue problem, with the wave number k the eigenvalue. As a result, for non-trivial solutions the wave numbers k need to satisfy the dispersion relation for linearised water-wave theory :

$$\frac{\omega^2\,h}{g} \;=\; (k\,h)^2\;\frac{1\;+\;\gamma_{\rm num}\,(k\,h)^2}{1\;+\;\gamma_{\rm den}\,(k\,h)^2}, \tag{4.24}$$

with k the wave number and

$$\gamma_{\rm num} \;=\; \frac{h\,F\;-\;P^2}{h^3\,K} \qquad \text{and} \qquad \gamma_{\rm den} \;=\; \frac{F}{h^2\,K}. \tag{4.25}$$

Notice that, for the parabolic-structure model and constant depth – using integrals given by (4.13) – we regain the well-known dispersion relationship for a Boussinesq model with improved frequency dispersion:

$$\frac{\omega^2\,h}{g} \;=\; (k\,h)^2\;\frac{1\;+\;\dfrac{1}{15}\,(k\,h)^2}{1\;+\;\dfrac{2}{5}\,(k\,h)^2}. \tag{4.26}$$

The propagating wave modes, with real-valued k, have wave numbers:

$$(k\,h)^2 \;=\; \sigma\;+\;\sqrt{\sigma^2\;+\;\frac{1}{\gamma_{\rm num}}\,\frac{\omega^2\,h}{g}} \qquad \text{with} \qquad \sigma \;=\; \frac{1}{2}\,\frac{1}{\gamma_{\rm num}}\,\left(\gamma_{\rm den}\,\frac{\omega^2\,h}{g}\;-\;1\right). \tag{4.27}$$

For later use, we also determine the group velocity $V_0 \equiv \mathrm{d}\omega\,/\,\mathrm{d}k$. From (4.24) we get:

$$V_0 \;=\; \sqrt{g\,h}\;\frac{1\;+\;\gamma_{\rm num}\,(k\,h)^2\;\left(2\;+\;\gamma_{\rm den}\,(k\,h)^2\right)}{\left(1\;+\;\gamma_{\rm num}\,(k\,h)^2\right)^{1/2}\;\left(1\;+\;\gamma_{\rm den}\,(k\,h)^2\right)^{3/2}} \tag{4.28}$$

Further, by using (4.19) in (4.10), we have the following relationships between the amplitudes ζ, φ and ψ for a horizontal bed:

$$\zeta \;=\; i\,\frac{\omega}{g}\,\varphi \qquad \text{and} \qquad \psi \;=\; -\,\frac{(k\,h)^2\;P}{h^2\,K\;+\;(k\,h)^2\;F}\;\varphi. \tag{4.29}$$

4.4.3 Non-reflective boundary conditions

Non-reflective boundary conditions are applied at horizontal parts of the bed, and far enough from bed oscillations, so the evanescent modes may be considered to be negligible. The incoming waves are assumed to propagate in the positive x-direction. The in- and outflow boundaries are at $x = x_a$ and $x = x_b$ ($x_b > x_a$) with the water depth $h(x)$ varying in the region in-between.

Now φ_+ and ψ_+ are associated with the incoming wave having amplitude $\zeta_+ = A\,\exp(i\,k\,x)$, assuming that $k(x_a)$ is the positive real root of the linear-theory dispersion relation (4.24) for $h(x_a)$. So we have, using (4.29):

$$\varphi_+ \;=\; -i\,\frac{g}{\omega}\,A\,\mathrm{e}^{i\,k\,x} \qquad \text{and} \qquad \psi_+ \;=\; +\,i\,\frac{g}{\omega}\;\frac{(k\,h)^2\;P}{h^2\,K\;+\;(k\,h)^2\;F}\;A\,e^{i\,k\,x}. \tag{4.30}$$

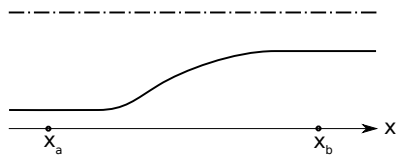

Figure 4.1: Computational domain.

At the boundaries we apply the following Sommerfeld non-reflective boundary conditions. The Sommerfeld boundary condition for time-harmonic motion results from its time-dependent form, *e.g.* $\partial_t\zeta + C_n\,\partial_n\zeta = 0$, with C_n the phase velocity at the boundary and ∂_n denoting the outward-normal derivative. As a result:

$$x = x_a: \quad \begin{cases} \varphi' + i\,k\,\varphi = \varphi'_+ + i\,k\,\varphi_+, \\ \psi' + i\,k\,\psi = \psi'_+ + i\,k\,\psi_+, \end{cases} \tag{4.31a}$$

$$x = x_b: \quad \begin{cases} \varphi' - i\,k\,\varphi = 0, \\ \psi' - i\,k\,\psi = 0, \end{cases} \tag{4.31b}$$

where for k the appropriate values for the propagating modes are to be taken at respectively $x = x_a$ and $x = x_b$, corresponding with the local values of h and κ.

4.4.4 Reflection and transmission coefficients

At the inflow boundary at $x = x_a$, we can split the potential amplitude $\varphi_1 \equiv \varphi(x_a)$ in an incoming part $\varphi_{a+} \equiv \varphi_+ \exp(-i\,k\,x_a)$ and a reflected part φ_{a-}, using (4.30):

$$\varphi_{a-} = \varphi_a - \varphi_{a+}. \tag{4.32}$$

The complex-valued reflection coefficient R is defined as:

$$R \equiv \frac{\varphi_{a-}}{\varphi_{a+}} = \frac{\varphi_a}{\varphi_+}\,\mathrm{e}^{i\,k\,x_a} - 1. \tag{4.33}$$

Note that the reflection coefficients are the same for the potential amplitude φ and the free-surface amplitude ζ, since they only differ by a constant coefficient, see (4.30).
Similarly, at the outflow boundary $x = x_b$ there are no incoming waves φ_{b-}, so there we have for the outgoing part φ_{b+} of the potential amplitude $\varphi_b \equiv \varphi(x_b)$:

$$\varphi_{b+} = \varphi_b. \tag{4.34}$$

The associated complex-valued transmission coefficient T is:

$$T \equiv \frac{\varphi_b}{\varphi_+}\,\mathrm{e}^{i\,k\,x_b}. \tag{4.35}$$

Again, the transmission coefficient for the free-surface amplitude ζ will be the same as for φ.

Now, from energy conservation, the incoming energy flux proportional to $V_a\,|A|^2$ has to be balanced by the outgoing fluxes $V_a\,|R|^2\,|A|^2$ and $V_b\,|T|^2\,|A|^2$. Here, V_a and V_b are the group velocities, as given by (4.28), at the locations $x = x_a$ and $x = x_b$ far before and after the region with bed fluctuations. So the following identity between $|R|$ and $|T|$ has to be satisfied:

$$|R|^2 \,+\, \frac{V_b}{V_a}\,|T|^2 \;=\; 1. \tag{4.36}$$

This can be used in numerical computations as a check on energy conservation.

4.5 Wave reflection by a slope

4.5.1 Introduction

A plane slope connecting two regions of constant depth, as studied by Booij (1983), is used to determine the reflection characteristics of the Hamiltonian models. For this test case, accurate numerical results for the full potential flow problem are provided in Porter & Porter (2006). The plane slope, with mean water depth

$$h(x) \;=\; \begin{cases} h_1 & \text{for } x \,<\, 0, \\ h_1 \,+\, (h_2 \,-\, h_1)\,\frac{x}{L}, & \text{for } 0 \,\leq\, x \,\leq\, L \text{ and} \\ h_2 & \text{for } x \,>\, L. \end{cases} \tag{4.37}$$

has the disadvantage that the derivatives of depth are discontinuous, introducing discontinuities in the model parameters (4.9) for the steep slope models. Therefore we also study an infinitely smooth slope, with water depth

$$h(x) \;=\; h_1 \,+\, (h_2 - h_1)\;\Upsilon\left(\frac{x - \frac{\pi}{4}L}{\frac{\pi}{2}L}\right), \quad \text{where} \tag{4.38a}$$

$$\Upsilon(s) \;=\; \begin{cases} 0 & \text{if } s \,\leq\, 0, \\ \dfrac{1}{2}\left\{1 \,+\, \tanh\left(\Xi(s)\right)\right\} & \text{if } 0 \,<\, s \,<\, 1, \quad \text{and} \\ 1 & \text{if } s \,\geq\, 0, \end{cases} \tag{4.38b}$$

$$\Xi(s) \;\equiv\; \tan\left[\pi\left(s \,-\, \frac{1}{2}\right)\right]. \tag{4.38c}$$

The smooth function Υ (see Appendix 4.B for details) is varying from zero to one over a finite interval of length $\frac{1}{2}\pi L$, and has the same maximum slope as the plane slope. The plane and smooth slopes are plotted in Figure 4.2. In Booij's test case, the non-dimensional water depths in the deep and shallow parts are $k_\infty\,h_1 \,=\, 0.6$ and $k_\infty\,h_2 \,=\, 0.2$ respectively, with $k_\infty \,\equiv\, \omega^2/g$ the deep-water wave number. The reflection coefficient $|R|$ is computed for a range of relative slope lengths $k_\infty\,L$.

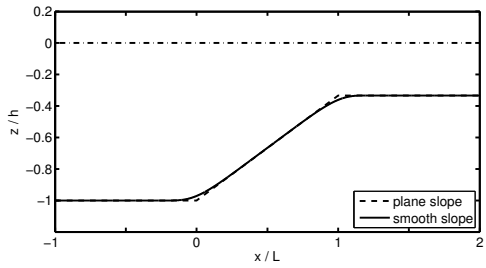

Figure 4.2: Bathymetry, for a plane slope (dashed line) and a smooth slope (solid line).

After the cases of the plane slope and smooth slope, also the effect of the normalisation of the vertical structure function $f(z;\kappa,h)$ on reflection is studied, motivated by the found differences in reflection for the parabolic and cosh-structure models in the mild-slope approximation.

One of Booij's objectives (Booij, 1983) was to assess the reflection behaviour of the classical mild-slope equation. We also compare the solutions of our Boussinesq models with the solutions of the mild-slope equations, which in time-dependent form are given by the set:

$$g\,\partial_t\zeta \,+\, \partial_x\left(C\,C_g\,\partial_x\phi\right) \,+\, \left(\kappa^2\,C\,C_g \,-\, \omega_c^2\right)\,\phi \,=\, 0 \qquad \text{and} \tag{4.39a}$$

$$\partial_t\phi \,+\, g\,\zeta \,=\, 0, \tag{4.39b}$$

see *e.g.* (Dingemans, 1997, Eq. (3.18), p. 254). Here

$$C \,\equiv\, \frac{\omega_c}{\kappa} \qquad \text{and} \qquad C_g \,\equiv\, \partial_\kappa\omega_c, \tag{4.40}$$

are parameters given as a function of ω_c and κ, which have to satisfy the linear-theory dispersion relation (4.18). Since the dispersion relation depends on the water depth h, for a given and constant ω_c the other parameters κ, C and C_g can be spatially varying.

For time-harmonic motion, using $\phi(x,t) = \mathrm{Re}\left\{\varphi(x)\,\mathrm{e}^{-i\omega t}\right\}$ and $\omega_c \,=\, \omega$, the classical mild-slope equation becomes, written as one equation for φ (which now denotes the complex-valued amplitude of the potential):

$$\left(C\,C_g\,\varphi'\right)' \,+\, \kappa^2\,C\,C_g\,\varphi \,=\, 0. \tag{4.41}$$

This will be used subsequently, for comparison with our variational models.

4.5.2 Plane slope case

First, we consider the Booij's test case (Booij, 1983) for a plane slope. In case of the mild-slope variants of the variational model, the coefficients for the parabolic-structure model are given in Eq. (4.13) and for the cosh-structure model they are

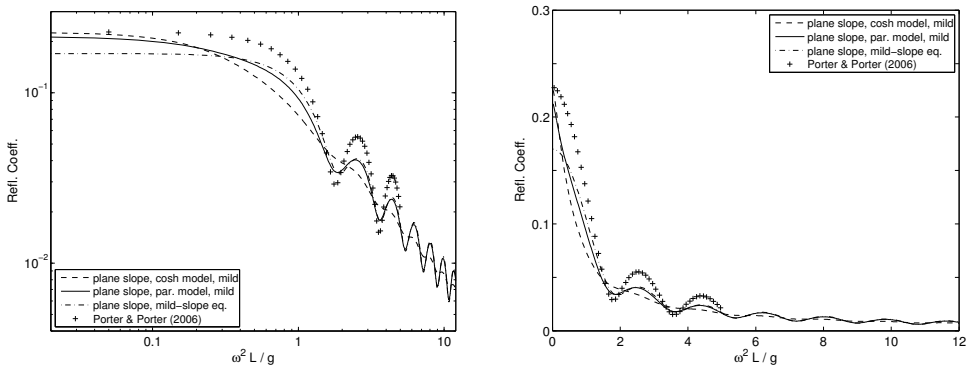

Figure 4.3: Reflection coefficients as a function of $\omega^2 L/g$ for a plane slope: mild-slope models. Solid lines: parabolic-structure model in the mild-slope approximation, model coefficients given by Eq. (4.13); dashed lines: cosh-structure model in the mild-slope approximation, model coefficients given by Eq. (4.15); dash-dot lines: mild-slope equation (4.41); +: Porter & Porter (2006).

given in Eq. (4.15). The results are presented in Figure 4.3, as well as those for the classical mild-slope equation (4.41), and the numerical results of Porter & Porter (2006). The left Figure gives the reflection coefficient $|R|$ as a function of the dimensionless slope length $\omega^2 L/g$ on a double-logarithmic scale. The right Figure shows the same on a linear scale, emphasising the true value of differences between models, as well as the repetitive structure of the oscillations. These repetitive oscillations of the reflection coefficient are characteristic for this plane slope case, see, *e.g.*, Dingemans (1997, §2.6.7–§2.6.8). As can be seen, neither the mild-slope parabolic and cosh-structure model, nor the classical mild-slope equation follow the oscillations in the reflection coefficient well, when compared with the accurate results of Porter & Porter (2006).

While all three mild-slope models have about the same mean trend of the reflection coefficient, averaged over the oscillation length, the parabolic-structure model and mild-slope equation show oscillations – although much too weak – while the cosh-structure model shows hardly any oscillation. This difference in results for parabolic and cosh-structure model was unexpected for us. Since for the Booij test case, with quite low values of relative depth kh of less than 0.86, both models have low errors in their representation of frequency dispersion, Eq. (4.24), we expected the same behaviour with respect to reflection. This is not the case. The most obvious difference between the two variational models is their normalisation of the vertical-structure function $f(z;h,\kappa)$: the parabolic-structure model is normalised to let the parameter ψ represent the vertical velocity at the free surface, while in the cosh-structure model it represents the deviation of the velocity potential from its free-surface value. Therefore, the effects of normalisation on reflection in the mild-slope versions of the variational model are studied below in subsection 4.5.4.

Next, the effects on reflection of not using the mild-slope approximation in the variational models are presented. Figure 4.4 shows the results for the parabolic and cosh-structure models, with coefficients given in Eqs. (4.14) and (4.17). For $\omega^2 L/g$ larger than one, the variational model results are in this Figure indistinguishable

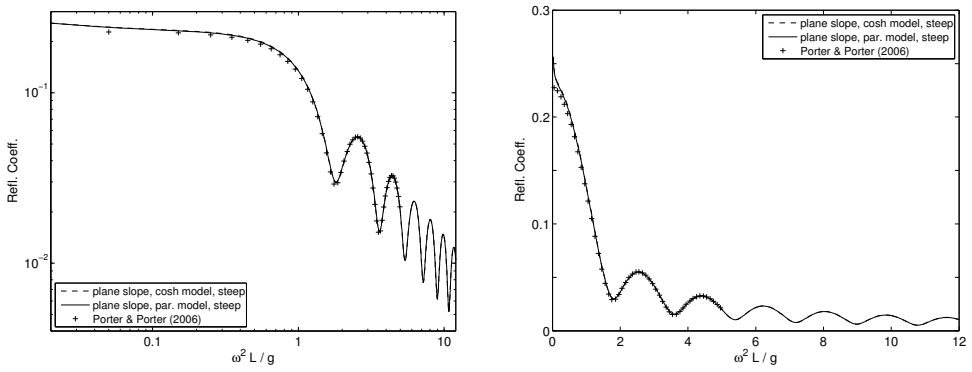

Figure 4.4: Reflection coefficients as a function of $\omega^2 L/g$ for a plane slope: steep slope models. Solid lines: parabolic-structure model for the steep slope formulation, model coefficients given by Eq. (4.14); dashed lines: cosh-structure model for the steep slope formulation, model coefficients given by Eq. (4.17); +: Porter & Porter (2006).

from those of Porter & Porter (2006). Deviations for very steep slopes with $\omega^2 L/g$ smaller than one – corresponding with slopes having a tangent $(h_2 - h_1)/L$ of 0.4 or larger – are due to the neglect of bottom-slope effects on the vertical structure function $f(z; h, \kappa)$ itself, which always has $\partial_z f = 0$ in the presented formulations. Further, without the mild-slope approximation in the Hamiltonian, the results of the parabolic and cosh-structure model are almost indistinguishable, in sharp contrast with the findings for the mild-slope variants of the models.

4.5.3 Smooth slope case

In the Booij test case, the reflection is – for long slopes – dominated by the slope discontinuities at the start and end of the slope. For instance, Porter & Chamberlain (1997) report on wave reflection for this test case, as found with the classical mild-slope equation and with an improvement thereupon, called the modified mild-slope equation. They show that using the jump conditions from the modified mild-slope equation in the classical mild-slope equation already gives good reflection characteristics. To show the effect of the slope discontinuities, we also computed the reflection for the smooth slope as given by Eq. (4.38) and Figure 4.2, using the non mild-slope versions of the parabolic and cosh-structure models. As can be seen in Figure 4.5, reflection is much less for the smooth bed, and also shows exponential decay as a function of slope length L. While for the plane slope $|R|$ decays as L^{-1}, as can be seen from the visual aid by the dash–dot line, the reflection coefficient $|R|$ for the smooth slope decays faster than any power of L. In this sense the Booij test case has an artificial behaviour, not (often) found in nature.

4.5.4 Normalisation effects on reflection

The parabolic-structure model performs better with respect to reflection than the cosh-structure model. One difference between the two models is their normalisation

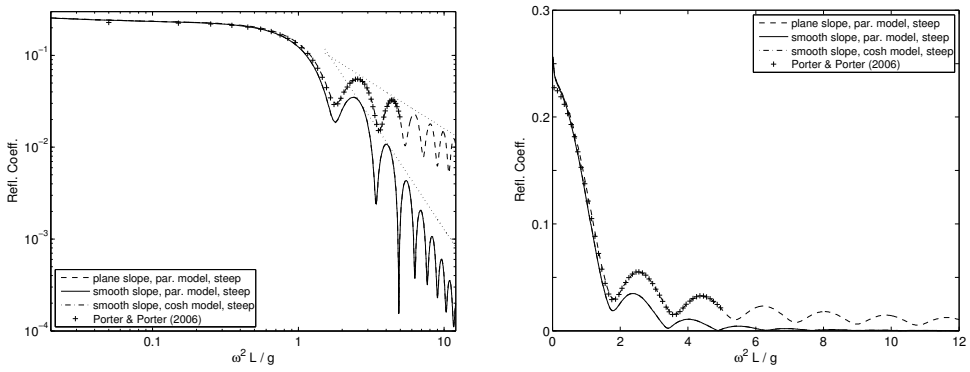

Figure 4.5: Reflection coefficients as a function of $\omega^2 L/g$ for a smooth slope: steep slope models. Solid and dashed lines: parabolic-structure model for the steep slope formulation, model coefficients given by Eq. (4.14); dash-dot lines: cosh-structure model for the steep slope formulation, model coefficients given by Eq. (4.17); +: Porter & Porter (2006).

of the vertical flow-structure $f(z;h,\kappa)$. For the present case of relative low kh this is the most important difference. The parabolic-structure model is normalised in such a way that ψ is the vertical velocity at the free surface ($pd_z f = 1$ at $z = 0$). On the other hand, this is not the case for the cosh-structure model, where ψ has the dimensions of a velocity potential.

To study the effect of normalisation, the vertical structure (4.7c) is used, which combines a cosh vertical structure with ψ representing the vertical velocity at the free surface. In this case, the integrals (4.9) become in the mild-slope approximation:

$$\begin{aligned} P_m^{(cs)} &= \frac{\mathcal{S} - \kappa h \mathcal{C}}{\kappa^2 \mathcal{S}}, \qquad F_m^{(cs)} = \frac{1}{2}\frac{\kappa h + 2\kappa h \mathcal{C}^2 - 3\mathcal{S}\mathcal{C}}{\kappa^3 \mathcal{S}^2}, \\ X_m^{(cs)} &= Y_m^{(cs)} = 0 \qquad \text{and} \qquad K_m^{(cs)} = M_m^{(cs)} = \frac{1}{2}\frac{\mathcal{S}\mathcal{C} - \kappa h}{\kappa \mathcal{S}^2}, \end{aligned} \tag{4.42}$$

with again $\mathcal{S} = \sinh(\kappa h)$ and $\mathcal{C} = \cosh(\kappa h)$.

Figure 4.6 shows indeed that the normalisation has a strong effect. The same normalisation of $f(z;h,\kappa)$, and thus also of ψ, as in case of the parabolic-structure model gives a reflection behaviour similar to the mild-slope equation. The behaviour of $|R|$ is also nearly equal to that of the parabolic-structure model (not shown, but see Figure 4.3). Of course the reflection characteristics are still not good for all these mild-slope versions of the variational model. But these changes due to normalisation tempted us to search for variational mild-slope models with good reflection characteristics. The advantage of the mild-slope models is that they are simpler than the models without this approximation.

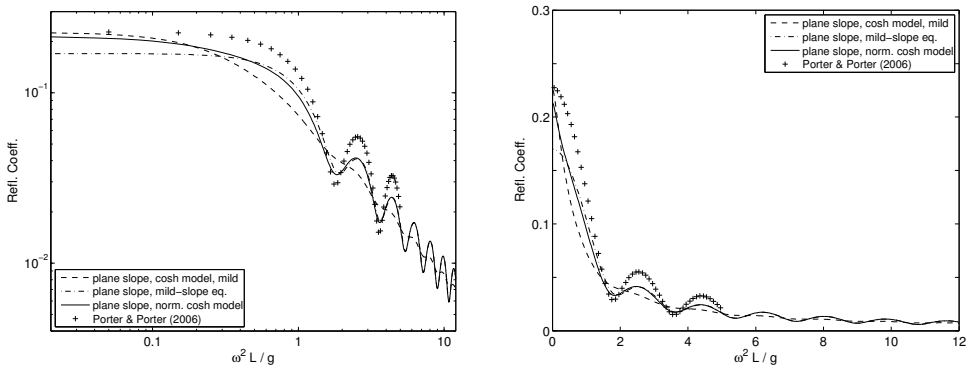

Figure 4.6: Reflection coefficients as a function of $\omega^2 L/g$ for a plane slope using cosh-structure models: effect of normalisation. Dashed lines: cosh-structure model in the mild-slope approximation, model coefficients given by Eq. (4.15); drawn lines: cosh-structure model with normalisation and in the mild-slope approximation, model coefficients given by Eq. (4.42); dash-dot lines: mild-slope equation (4.41); +: Porter & Porter (2006).

4.6 Search for mild-slope models with good reflection characteristics

We now try to find mild-slope models with better reflection characteristics, using different methods of normalisation of the vertical flow-structures.

4.6.1 Parabolic-structure model

For the parabolic-shape functions, we normalise with a yet unknown power of the water depth h^n. This can be seen as the most simple generalisation of Eq. (4.7a). So:

$$f^{(po)} \;=\; \frac{1}{2}\,\frac{(z+h)^2 \;-\; h^2}{h^n}. \tag{4.43}$$

Notice, that as a result of a different normalisation of f, also the dimension and physical interpretation of ψ changes. While for $n = 1$ we can interpret ψ as the vertical velocity at the free surface, for other values of n this is no longer the case. As a result, we get the following steep-slope coefficients, using (4.9):

$$P^{(po)} \;=\; -\frac{1}{3}\,h^{3-n}, \tag{4.44a}$$

$$F^{(po)} \;=\; \frac{2}{15}\,h^{5-2n}, \tag{4.44b}$$

$$X^{(po)} \;=\; \frac{1}{6}\,(\,2n \;-\; 3\,)\,h^{2-n}\,h', \tag{4.44c}$$

$$Y^{(po)} \;=\; -\frac{1}{120}\,(\,16n \;-\; 25\,)\,h^{4-2n}\,h' \quad \text{and} \tag{4.44d}$$

$$K^{(po)} \;=\; \frac{1}{3}\,h^{3-2n} \;+\; \frac{1}{60}\,\left(8n^2 \;-\; 25n \;+\; 20\right)\,h^{3-2n}\,(h')^2. \tag{4.44e}$$

We want to choose n in such a way, that better reflection characteristics will be obtained for the mild-slope model associated with $f^{(po)}$, *i.e.*:

$$P_m^{(po)} = -\frac{1}{3}\,h^{3-n}, \qquad F_m^{(po)} = \frac{2}{15}\,h^{5-2n}, \qquad X_m^{(po)} = Y_m^{(po)} = 0$$
$$\text{and} \quad K_m^{(po)} = \frac{1}{3}\,h^{3-2n}. \quad (4.45)$$

Our optimisation strategy is as follows: instead of optimising n for a best-fit of the reflection coefficient $|R|$, we try to make the difference between the coefficients between the mild-slope (4.45) and steep-slope (4.44) variants as small as possible. This, in the knowledge that if the coefficients are the same, the produced solutions for φ and ψ will also be the same. The differences between mild and steep slope occur in the coefficients $X^{(po)}$, $Y^{(po)}$ and $K^{(po)}$. Note that the bed-slope induced changes in these coefficients are all of the form $\int_{-h}^{0} W(z)\,\partial_x f\,\mathrm{d}z$, *e.g.* with $W(z) = 1$ for $X^{(po)}$, see Eq. (4.9). Several strategies to minimise the differences are feasible. We have chosen the simple approach to equate $X^{(po)} = \int_{-h}^{0} \partial_x f^{(po)}\,\mathrm{d}z$ to zero, expecting that the other coefficients ($Y^{(po)}$ as well as parts of $K^{(po)}$) depending on h' will also be small. Note that $X^{(po)}$ is in general the simplest of these coefficients, see Eq. (4.9). As a result of $X^{(po)} = 0$, we get $n = \frac{3}{2}$ as an optimal value which makes $X^{(po)}$ equal to zero. The associated steep-slope coefficients are:

$$\begin{aligned} P^{(po)} &= -\frac{1}{3}\,h^{3/2}, \qquad F^{(po)} = \frac{2}{15}\,h^{2}, \qquad X^{(po)} = 0, \\ Y^{(po)} &= \frac{1}{120}\,h\,h' \quad \text{and} \quad K^{(po)} = \frac{1}{3} + \frac{1}{120}\,(h')^2. \end{aligned} \quad (4.46)$$

Comparison with the integrals (4.14) for the parabolic-structure model shows that – besides the different powers of h due to the different normalisations, and the associated different physical interpretation of ψ – the coefficients in the terms depending on h' in the new formulation (4.46) are indeed much smaller than in (4.14). So, let us try to see what happens if we neglect these terms, *i.e.* let us try the mild-slope approximation for the optimised case. We then get the following coefficients of a mild-slope model for which we expect reasonable reflection characteristics:

$$P_m^{(po)} = -\frac{1}{3}\,h^{3/2}, \quad F_m^{(po)} = \frac{2}{15}\,h^{2}, \quad X_m^{(po)} = Y_m^{(po)} = 0 \quad \text{and} \quad K_m^{(po)} = \frac{1}{3}. \quad (4.47)$$

Note that without the mild-slope approximations, different normalisations give similar (good) results with respect to linear wave reflection. See Figure 4.4, which shows results for the steep-slope variants of the parabolic and cosh-structure model with different normalisations for f.

4.6.2 Cosh-structure model

For the cosh-structure model, we use a normalisation of the form:

$$f^{(co)} = \frac{\cosh\left(\kappa\,(z+h)\right) - \cosh\left(\kappa\,h\right)}{N(\kappa\,h)}. \quad (4.48)$$

The normalisation factor $N(\kappa\,h)$ is taken to be positive for all $\kappa\,h$. The mild-slope coefficients resulting from this normalisation are:

$$\begin{aligned} P_m^{(co)} &= \frac{1}{\kappa\,N}\,(\,\mathcal{S}-\kappa\,h\,\mathcal{C}\,)\,, \qquad F_m^{(co)} = \frac{1}{N^2}\,\left(-\frac{3}{2}\,\frac{1}{\kappa}\,\mathcal{S}\,\mathcal{C}+\frac{1}{2}\,h+h\,\mathcal{C}^2\right), \\ X_m^{(co)} &= Y_m^{(co)} = 0 \qquad \text{and} \qquad K_m^{(co)} = \frac{1}{N^2}\,\left(\frac{1}{2}\,\kappa\,\mathcal{S}\,\mathcal{C}-\frac{1}{2}\,\kappa^2\,h\right). \end{aligned} \tag{4.49}$$

As for the parabolic-structure model, a form of $N(\kappa\,h)$ is sought which minimizes the steep-slope coefficient $X^{(co)}$. We are not able to find a closed-form solution which makes $X^{(co)}$ equal to zero for all κh, as we can for the parabolic-structure model. However, we can find approximate closed-form solutions which make $X^{(co)}$ small for all κh.

Taking the x-derivative of $f^{(co)}$ we get:

$$\begin{aligned} \partial_x f^{(co)} = \frac{\sinh(\kappa\,(z+h))}{N}\,\left((z+h)\,\partial_x\kappa+\kappa\,\partial_x h\right)+\frac{\sinh(\kappa\,h)}{N}\,\left(h\,\partial_x\kappa+\kappa\,\partial_x h\right) \\ -\frac{\cosh(\kappa\,(z+h))-\cosh(\kappa\,h)}{N^2}\,N'\,\left(h\,\partial_x\kappa+\kappa\,\partial_x h\right), \end{aligned} \tag{4.50}$$

where N' denotes the derivative of $N(\kappa\,h)$ with respect to its argument, which is $\kappa\,h$ in this case. By integrating (4.50) over z, $X^{(co)}$ becomes:

$$\begin{aligned} X^{(co)} \;=\; -\,\frac{1}{\kappa^2}\,\left(\kappa\,h\,\frac{(\mathcal{S}\;-\;\kappa\,h\,\mathcal{C})\;N'}{N^2}\;+\;\frac{\mathcal{S}\;-\;\kappa\,h\,\mathcal{C}\;+\;\kappa^2\,h^2\,\mathcal{S}}{N}\right)\partial_x\kappa \\ -\left(\frac{(\mathcal{S}\;-\;\kappa\,h\,\mathcal{C})\,N'}{N^2}+\frac{1-\mathcal{C}\;+\kappa\,h\,\mathcal{S}}{N}\right)\partial_x h. \end{aligned} \tag{4.51}$$

Using the dispersion relation (4.18) to determine κ as a function of the depth h, the x-derivative of κ is related to that of h by (4.82), written here in the form:

$$\partial_x\kappa \;=\; -\frac{\kappa^2}{\kappa\,h\;+\;\mathcal{S}\,\mathcal{C}}\,\partial_x h. \tag{4.52}$$

Then $X^{(co)}$ becomes:

$$X^{(co)} \;=\; \left(\mathcal{S}\,\mathcal{C}\,\frac{(\kappa\,h\,\mathcal{C}\;-\;\mathcal{S})\,N'}{(\kappa\,h\;+\;\mathcal{S}\,\mathcal{C})\,N^2}-\frac{\mathcal{S}\,(\mathcal{C}\;-\;\mathcal{S}^2)\;+\kappa\,h\,(1\;+\;\mathcal{S}^2\,\mathcal{C})}{(\kappa\,h\;+\;\mathcal{S}\,\mathcal{C})\,N}\right)\partial_x h. \tag{4.53}$$

Now, by setting $X^{(co)}$ equal to zero, we obtain the following differential equation for N, in terms of $q\;\equiv\;\kappa h$:

$$\frac{N'}{N} \;=\; \frac{\mathcal{S}\,(\mathcal{C}\;-\;\mathcal{S}^2)\;+\;q\,(1\;+\;\mathcal{S}^2\,\mathcal{C})}{\mathcal{S}\,\mathcal{C}\,(q\,\mathcal{C}\;-\;\mathcal{S})}, \tag{4.54}$$

where both $\mathcal{S}$ and $\mathcal{C}$ are functions of q. This has a solution for $\log N$ which is not very useful. So we try to find an approximate solution. In order to assess the performance of a normalisation, the following dimensionless quantity is used:

$$\nu = \frac{X^{(co)}\,h}{P^{(co)}\,\partial_x h}. \tag{4.55}$$

Non-dimensionalisation of $X^{(co)}$ using $P^{(co)}$ is motivated by their combined appearance in the continuity equation (4.10a), as well as the independence of $P^{(co)}$ on the bed slope h'. Since $P^{(co)} = P_m^{(co)}$, we get from (4.49), (4.53) and (4.55):

$$\nu \;=\; q\,\frac{\mathcal{S}+\mathcal{SC}(\mathcal{C}-1)\;-q\left(1+\mathcal{S}^2\mathcal{C}\right)}{(\mathcal{S}-q\mathcal{C})\,(\mathcal{SC}+q)} \;-\; \frac{q\mathcal{SC}}{\mathcal{SC}+q}\,\frac{N'}{N}. \tag{4.56}$$

Because we aim for $X^{(co)}$ equal to zero, the deviation of ν from zero is a measure for comparing the performance of different normalisations.

To derive good approximations for $N(q)$, we study the behaviour of N' for large and small q. First, we study the behaviour of (4.54) for large q:

$$\lim_{q\to\infty}\frac{N'}{N} = 1, \tag{4.57}$$

so for large q we have the following asymptotic behaviour of N:

$$N \;\sim\; \mathrm{e}^q. \tag{4.58}$$

For small q, a Taylor series of (4.54) around $q=0$ is made:

$$(\log N)' \;=\; \frac{1}{q} \;+\; \frac{7}{12}\,q \;-\; \frac{13}{72}\,q^3 \;+\; \frac{22573}{302400}\,q^5 \;-\; \frac{92623}{3024000}\,q^7 \;+\; \mathcal{O}\left(q^9\right), \tag{4.59}$$

from which the following behaviour of N for small q is found:

$$N \;=\; q \;+\; \frac{7}{24}\,q^3 \;-\; \frac{1}{384}\,q^5 \;+\; \frac{5501}{1612800}\,q^7 \;+\; \mathcal{O}\left(q^9\right). \tag{4.60}$$

A simple form of $N(q)$ which satisfies to lowest order both limits of q, to zero and infinity, is

$$N_A \;=\; \sinh(q). \tag{4.61}$$

Note that a multiplicative constant factor of N, independent of κ and h, is not important, since N is only a normalisation of the shape function $f(z;\kappa,h)$. The Taylor series expansion of (4.61) around $q=0$ is:

$$\sinh(q) \;=\; q \;+\; \frac{1}{6}\,q^3 \;+\; \frac{1}{120}\,q^5\,\frac{1}{5040}\,q^7 \;+\; \mathcal{O}\left(q^9\right). \tag{4.62}$$

To include more terms of the Taylor series (4.60) while maintaining the correct asymptotic behaviour (4.58), there are many possibilities. Besides the behaviour near $q=0$ and $q\to\infty$ also the intermediate behaviour is important. We found – by trial and error – that multiplying $\sinh(q)$ with a rational function of the form:

$$N_B \;=\; \frac{1+v\left[\cosh(q)-1\right]}{1+w\left[\cosh(q)-1\right]}\;\sinh(q), \tag{4.63}$$

performs well, especially for moderate values of q. Note that $\cosh(q)-1 = \frac{1}{2}q^2+\mathcal{O}(q^4)$ for the limit $q\to 0$.

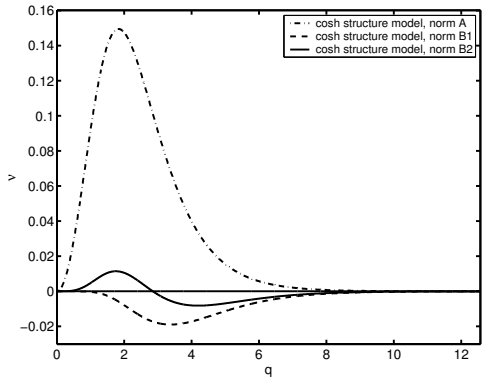

Figure 4.7: Variation of ν as a function of $q = \kappa h$ for different normalisations of the cosh-structure model. The dash-dot line is with N_A, Eq. (4.61); the dashed line is for N_{B_1} with Padé coefficients, Eq. (4.66); and the drawn line is N_{B_2} with minmax coefficients, Eq. (4.68).

We used two approaches to determine the coefficients v and w in (4.63). The first is by making a MacLaurin expansion of N_B in terms of q:

$$\begin{aligned} N_B = q + \left(\frac{1}{6} + \frac{1}{2}v - \frac{1}{2}w\right) q^2 \\ + \left(\frac{1}{120} + \frac{1}{8}v - \frac{1}{8}w - \frac{1}{4}vw + \frac{1}{4}w^2\right) q^3 + \mathcal{O}\left(q^4\right). \end{aligned} \tag{4.64}$$

Now v and w are chosen such as to get the same coefficients for the q^2 and q^3 terms as in (4.60). As a result, we find:

$$v_1 = \frac{37}{40} \qquad \text{and} \qquad w_1 = \frac{27}{40}. \tag{4.65}$$

So

$$N_{B_1} = \frac{3 \,+\, 37\,\cosh q}{13 \,+\, 27\,\cosh q}\,\sinh q. \tag{4.66}$$

The resulting behaviour of ν, see (4.55), as a function of q is shown in Figure 4.7. As can be seen, the absolute value of ν for the normalisation N_{B_1} with these coefficients (v_1, w_1) is much smaller than for N_A with equation (4.61). The second approach is to try to improve further by hand. A more-or-less optimum for ν for any q has been found with:

$$v_2 = 1 \qquad \text{and} \qquad w_2 = \frac{3}{4}. \tag{4.67}$$

Then:

$$N_{B_2} = \frac{\sinh q\ \cosh q}{\frac{1}{4} \,+\, \frac{3}{4}\,\cosh q}. \tag{4.68}$$

The result on ν as a function of q can be seen in Figure 4.7.

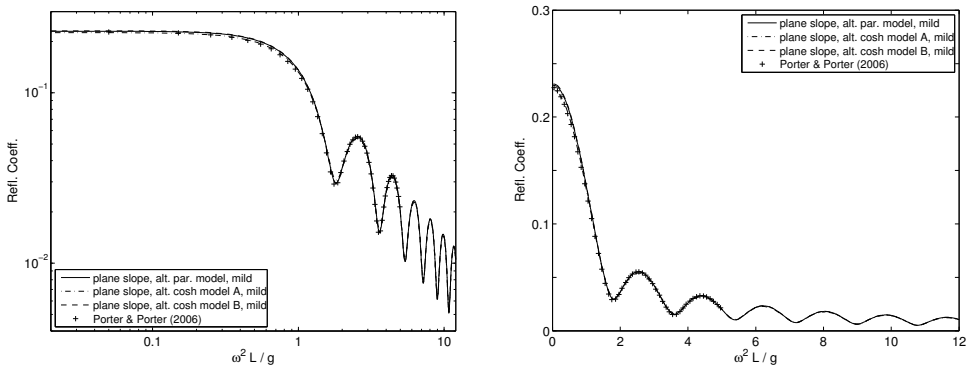

Figure 4.8: Reflection coefficients as a function of $\omega^2 L/g$ for a plane slope: alternative normalisations in mild-slope models. Solid lines: parabolic-structure model with alternative normalisation in the mild-slope approximation, model coefficients given by Eq. (4.47); dash-dot lines: cosh-structure model with alternative normalisation A in the mild-slope approximation, model coefficients given by Eqs. (4.49) and (4.61); dashed lines: cosh-structure model with alternative normalisation B_2 in the mild-slope approximation, model coefficients given by Eqs. (4.49) and (4.68); +: Porter & Porter (2006).

4.6.3 Plane slope case for the mild-slope approximation with optimised normalisations

Figure 4.8 shows the results for the mild-slope variants, both of the parabolic as well as the A and B_2 forms cosh-structure models, Eqs. (4.47) and (4.49) with coefficients (4.61) and (4.67), respectively. As can be seen, the resulting reflection behaviour is very good, compared with the highly-accurate numerical results of Porter & Porter (2006). The coefficients from Eq. (4.61) result in slightly to high reflection in the first trough in the reflection curve near $\omega^2 L/g \approx 1.8$ On the other hand, these mild-slope models result in a better behaviour of $|R|$ for very steep slopes with $\omega^2 L/g < 0.1$, than the models without mild-slope approximation.

4.7 Conclusions

The presented results on wave reflection are for linearised versions of a variational approach to the Boussinesq-like modelling of water waves over bathymetry. The time-dependent linear flow equations for wave propagation in one spatial dimension are given in Equation (4.10). The corresponding harmonic case, with a single angular frequency ω, is given in (4.20), and subsequently solved numerically.

We considered several options for the inclusion of bottom-slope terms. Firstly we neglected all bottom-slope terms in the Hamiltonian density, resulting in the *mild-slope approximation*. Secondly we kept those terms, which resulted in the so-called *steep-slope case*. For both cases results are shown for the plane-slope test case of Booij (1983). Despite that the global average trend of the reflection coefficient – as compared with the accurate numerical results of Porter & Porter (2006) – is followed quite well, the mild-slope models are not capable to represent the reflection

oscillations accurately as a function of slope length. The parabolic-structure model (4.13) shows part of the oscillation, while this oscillation is nearly absent in the cosh-structure model (4.15). This behaviour of the cosh-structure model is found despite the fact that it provides in principle a better representation of the vertical structure of the flow than the parabolic-structure model. As shown later on, this difference in behaviour is due to the different normalisations of the vertical structure as used in both models.

Inclusion of the bed-slope effects in the parabolic and cosh-structure model, see Eqs. (4.14) and (4.17), gives for both models results on linear reflection which are in good agreement with the accurate numerical data of Porter & Porter (2006). Using the same steep-slope models for an infinitely smooth slope, we find that the reflection is much less and decaying much faster (exponentially) with slope length. In this respect Booij's plane-slope case, and many other test cases, are not such a good representation of most situations found in nature. Reflection in Booij's test case is dominated by the discontinuities in bed slope.

We also considered different normalisations for the vertical-structure functions. We found that a optimisation of the normalisation resulted, for the mild-slope case, in a much-improved performance of the reflection properties. With the normalisation (4.68) with coefficients (4.49) for the cosh-structure model the accuracy is as good as was found previously for the steep-slope case. The same holds for the parabolic model with coefficients (4.47). So these provide good reflection results without the additional complexity of the bottom-slope terms in the model.

A different normalisation is believed not to have effects on the behaviour of the model with respect to wave refraction, diffraction and shoaling. At least that is our experience with the parabolic and cosh-structure models, in the mild-slope approximation and with different normalisations (*i.e.* unoptimised for reflection). Although the presented results are for the linear case, we expect similar conclusions to transfer to the case of the corresponding non-linear model, *e.g.* see Appendix 4.A for the normalised cosh-structure model.

Appendix 4.A Non-linear variational model with improved reflection characteristics

4.A.1 Hamiltonian

In practical applications, one uses a non-linear wave model, while in this paper we have studied the reflection characteristics for the linearised version. So for completeness, we present the non-linear version underlying the present reflection analysis. The non-linear cosh-structure model without normalisation can be found in Klopman, van Groesen & Dingemans (2010).

First, the non-linear form of the vertical flow-structure for the velocity potential Φ (4.48) becomes:

$$\Phi(\boldsymbol{x},z,t) \;=\; \varphi(\boldsymbol{x},t) \;+\; f(z;\zeta,h,\kappa)\,\psi(\boldsymbol{x},t) \qquad \text{with} \tag{4.69a}$$

$$f(z;\zeta,h,\kappa) \;=\; \frac{\cosh\left(\kappa\,(h+z)\right) \;-\; \cosh\left(\kappa\,(h+\zeta)\right)}{N(\kappa\,(h+\zeta))}, \tag{4.69b}$$

with $\boldsymbol{x}$ the horizontal coordinates in two horizontal directions, and the normalisation N in one of the forms as given in subsection 4.6.2.

The Hamiltonian $\mathscr{H}$ is the sum of the kinetic and potential energies:

$$\mathscr{H} \;=\; \iint H\;\mathrm{d}\boldsymbol{x} \;=\; \iint \rho\left(\int_{-h(\boldsymbol{x})}^{\zeta(\boldsymbol{x},t)} \frac{1}{2}\,|\boldsymbol{\nabla}\Phi|^2\;\mathrm{d}z \;+\; \frac{1}{2}\,g\,\zeta^2\right)\mathrm{d}\boldsymbol{x}, \tag{4.70}$$

where H is the Hamiltonian density per unit of horizontal area, and again assuming a constant and unit fluid density. Performing the vertical integration of the kinetic energy, the Hamiltonian density H equals, see Klopman *et al.* (2010):

$$\begin{aligned} H = \rho\Bigg[\; & \frac{1}{2}\,(\,h \;+\; \zeta\,)\;|\,\boldsymbol{\nabla}\varphi\,|^2 \;+\; \frac{1}{2}\,F\;|\,\boldsymbol{\nabla}\psi\,|^2 \;+\; \frac{1}{2}\,G\,\psi^2\;|\,\boldsymbol{\nabla}\zeta\,|^2 \;+\; \frac{1}{2}\,K\,\psi^2 \;+ \\ & +\,P\;(\,\boldsymbol{\nabla}\psi\,)\cdot(\,\boldsymbol{\nabla}\varphi\,) \;+\; Q\,\psi\;(\,\boldsymbol{\nabla}\varphi\,)\cdot(\,\boldsymbol{\nabla}\zeta\,) \;+\; R\,\psi\;(\,\boldsymbol{\nabla}\psi\,)\cdot(\,\boldsymbol{\nabla}\zeta\,) \;+ \\ & +\,\frac{1}{2}\,g\,\zeta^2\Bigg], \end{aligned} \tag{4.71}$$

with the vertical integrals given by

$$F(\zeta,h;\kappa) = \int_{-h}^{\zeta} f^2\;\mathrm{d}z, \qquad G(\zeta,h;\kappa) = \int_{-h}^{\zeta} (\,\partial_\zeta f\,)^2\;\mathrm{d}z, \tag{4.72a}$$

$$K(\zeta,h;\kappa) = \int_{-h}^{\zeta} (\,\partial_z f\,)^2\;\mathrm{d}z, \qquad P(\zeta,h;\kappa) = \int_{-h}^{\zeta} f\;\mathrm{d}z, \tag{4.72b}$$

$$Q(\zeta,h;\kappa) = \int_{-h}^{\zeta} (\,\partial_\zeta f\,)\;\mathrm{d}z \qquad \text{and} \qquad R(\zeta,h;\kappa) = \int_{-h}^{\zeta} f\;(\,\partial_\zeta f\,)\;\mathrm{d}z. \tag{4.72c}$$

Next we will derive the equations resulting from the Hamiltonian.

4.A.2 Flow equations

The flow equations become, like in Eq. (4.1):

$$\rho\,\partial_t\zeta = +\frac{\delta\mathscr{H}}{\delta\varphi} \quad \text{and} \quad \rho\,\partial_t\varphi = -\frac{\delta\mathscr{H}}{\delta\zeta}, \quad \text{under the constraint that:} \quad \frac{\delta\mathscr{H}}{\delta\psi} = 0. \tag{4.73}$$

As a result, we get the evolution equations for $\zeta(\boldsymbol{x},t)$ and $\varphi(\boldsymbol{x},t)$:

$$\partial_t\zeta + \boldsymbol{\nabla}\cdot\Big[\,(h+\zeta)\,\boldsymbol{\nabla}\varphi \;+\; P\,\boldsymbol{\nabla}\psi \;+\; Q\,\psi\,\boldsymbol{\nabla}\zeta\,\Big] \;=\; 0, \tag{4.74a}$$

$$\partial_t\varphi + \frac{1}{2}\,|\boldsymbol{\nabla}\varphi|^2 \;+\; g\,\zeta \;+\; \mathcal{R} \;=\; 0 \tag{4.74b}$$

and the elliptic equation for $\psi(\boldsymbol{x},t)$:

$$\Big(G\,|\boldsymbol{\nabla}\zeta|^2 \;+\; K\Big)\;\psi \;+\; Q\,(\boldsymbol{\nabla}\varphi)\cdot(\boldsymbol{\nabla}\zeta) \;+\; R\,(\boldsymbol{\nabla}\psi)\cdot(\boldsymbol{\nabla}\zeta)$$
$$-\;\boldsymbol{\nabla}\cdot\Big(F\,\boldsymbol{\nabla}\psi \;+\; P\,\boldsymbol{\nabla}\varphi \;+\; R\,\psi\,\boldsymbol{\nabla}\zeta\Big) \;=\; 0, \tag{4.74c}$$

with the non-hydrostatic term $\mathcal{R}(\boldsymbol{x},t)$ in the Bernoulli equation (4.74b) given by:

$$\mathcal{R} = \frac{1}{2}\,(\partial_\zeta F)\,|\boldsymbol{\nabla}\psi|^2 \;+\; \frac{1}{2}\,\Big((\partial_\zeta G)\,|\boldsymbol{\nabla}\zeta|^2 \;+\; \partial_\zeta K\Big)\,\psi^2 \;+$$
$$+\;\Big((\partial_\zeta P)\,\boldsymbol{\nabla}\psi \;+\; (\partial_\zeta Q)\,\psi\,\boldsymbol{\nabla}\zeta\Big)\cdot\boldsymbol{\nabla}\varphi \;+$$
$$+\;(\partial_\zeta R)\,(\boldsymbol{\nabla}\zeta)\cdot(\boldsymbol{\nabla}\psi)\,\psi \;-\; \boldsymbol{\nabla}\cdot\Big(G\,\psi^2\,\boldsymbol{\nabla}\zeta \;+\; Q\,\psi\,\boldsymbol{\nabla}\varphi \;+\; R\,\psi\,\boldsymbol{\nabla}\psi\Big). \tag{4.74d}$$

By taking the gradient of the Bernoulli equation, also flow equations in terms of the horizontal gradient of the free-surface potential φ, or 'velocity', $\boldsymbol{u} = \boldsymbol{\nabla}\varphi$ can be constructed.

4.A.3 Vertical integrals and their derivatives with respect to ζ

Here we derive the vertical integrals (4.72), for the normalised flow-structure (4.69). First we introduce the following abbreviations:

$$\begin{aligned} &\tilde{q} \;=\; \kappa\,(h+\zeta), \quad \mathcal{T} \;=\; \tanh\,\tilde{q}, \\ &\Lambda_1 = 3\,\tilde{q} \;-\; 3\,\mathcal{T} \;-\; \tilde{q}\,\mathcal{T}^2 \quad \text{and} \quad \Lambda_2 = \mathcal{T} \;-\; \tilde{q}\,(1 \;-\; \mathcal{T}^2). \end{aligned} \tag{4.75}$$

Further N' denotes the derivative of the normalisation N with respect to its argument, $\kappa\,(h+\zeta)$ in the present case. And likewise N'' denotes the second derivative. Then the vertical integrals (4.72) become:

$$F \;=\; \frac{1}{2}\,\frac{\Lambda_1}{(1 \;-\; \mathcal{T}^2)\,\kappa\,N^2}, \tag{4.76a}$$

$$G = \frac{\kappa\,\tilde{q}\,\mathcal{T}^2}{(1-\mathcal{T}^2)\,N^2} - 2\,\kappa\,\mathcal{T}\,\frac{\tilde{q}-\mathcal{T}}{(1-\mathcal{T}^2)\,N^3}\,N' + \frac{1}{2}\,\kappa\,\frac{\Lambda_1}{(1-\mathcal{T}^2)\,N^4}\,(N')^2, \tag{4.76b}$$

$$K = \frac{1}{2}\,\kappa\,\frac{\Lambda_2}{(1-\mathcal{T}^2)\,N^2}, \tag{4.76c}$$

$$P = -\frac{\tilde{q}-\mathcal{T}}{\sqrt{1-\mathcal{T}^2}\,\kappa\,N}, \tag{4.76d}$$

$$Q = -\frac{\tilde{q}\,\mathcal{T}}{\sqrt{1-\mathcal{T}^2}\,N} + \frac{\tilde{q}-\mathcal{T}}{\sqrt{1-\mathcal{T}^2}\,N^2}\,N', \quad \text{and} \tag{4.76e}$$

$$R = \mathcal{T}\,\frac{\tilde{q}-\mathcal{T}}{(1-\mathcal{T}^2)\,N^2} - \frac{1}{2}\,\frac{\Lambda_1}{(1-\mathcal{T}^2)\,N^3}\,N'. \tag{4.76f}$$

Their derivatives with respect to ζ are:

$$\partial_\zeta F = 2\,\mathcal{T}\,\frac{\tilde{q}-\mathcal{T}}{(1-\mathcal{T}^2)\,N^2} - \frac{\Lambda_1}{(1-\mathcal{T}^2)\,N^3}\,N', \tag{4.77a}$$

$$\begin{aligned}\partial_\zeta G = {} & \kappa^2\,\mathcal{T}\,\frac{2\,\tilde{q}+\mathcal{T}}{(1-\mathcal{T}^2)\,N^2} - 2\,\kappa^2\,\frac{\tilde{q}-\mathcal{T}+2\,\tilde{q}\,\mathcal{T}^2}{(1-\mathcal{T}^2)\,N^3}\,N' \\ & + 8\,\kappa^2\,\mathcal{T}\,\frac{\tilde{q}-\mathcal{T}}{(1-\mathcal{T}^2)\,N^4}\,(N')^2 - 2\,\kappa^2\,\frac{\Lambda_1}{(1-\mathcal{T}^2)\,N^5}\,(N')^3 \\ & - 2\,\kappa^2\,\mathcal{T}\,\frac{\tilde{q}-\mathcal{T}}{(1-\mathcal{T}^2)\,N^3}\,N'' + \kappa^2\,\frac{\Lambda_1}{(1-\mathcal{T}^2)\,N^4}\,(N')\,(N''),\end{aligned} \tag{4.77b}$$

$$\partial_\zeta K = \frac{\kappa^2\,\mathcal{T}^2}{(1-\mathcal{T}^2)\,N^2} - \kappa^2\,\frac{\Lambda_2}{(1-\mathcal{T}^2)\,N^3}\,N', \tag{4.77c}$$

$$\partial_\zeta P = -\frac{\tilde{q}\,\mathcal{T}}{\sqrt{1-\mathcal{T}^2}\,N} + \frac{\tilde{q}-\mathcal{T}}{\sqrt{1-\mathcal{T}^2}\,N^2}\,N', \tag{4.77d}$$

$$\begin{aligned}\partial_\zeta Q = {} & -\kappa\,\frac{\tilde{q}+\mathcal{T}}{\sqrt{1-\mathcal{T}^2}\,N} + 2\,\kappa\,\frac{\tilde{q}\,\mathcal{T}}{\sqrt{1-\mathcal{T}^2}\,N^2}\,N' \\ & - 2\,\kappa\,\frac{\tilde{q}-\mathcal{T}}{\sqrt{1-\mathcal{T}^2}\,N^3}\,(N')^2 + \kappa\,\frac{\tilde{q}-\mathcal{T}}{\sqrt{1-\mathcal{T}^2}\,N^2}\,N'',\end{aligned} \tag{4.77e}$$

$$\begin{aligned}\partial_\zeta R = {} & \kappa\,\frac{\tilde{q}\,(1+\mathcal{T}^2)-\mathcal{T}}{(1-\mathcal{T}^2)\,N^2} - 4\,\kappa\,\mathcal{T}\,\frac{\tilde{q}-\mathcal{T}}{(1-\mathcal{T}^2)\,N^3}\,N' \\ & + \frac{3}{2}\,\frac{\kappa\,\Lambda_1}{(1-\mathcal{T}^2)\,N^4}\,(N')^2 - \frac{1}{2}\,\frac{\kappa\,\Lambda_1}{(1-\mathcal{T}^2)\,N^3}\,N''.\end{aligned} \tag{4.77f}$$

Appendix 4.B An infinitely smooth function only varying in a finite interval

The following function has the properties that it is smooth everywhere, *i.e.* the function and all its derivatives are continuous, while it is only varying over the finite interval $0 < s < 1$, from a value of zero at $s = 0$ to a value of one at $s = 1$:

$$\Upsilon(s) \;=\; \begin{cases} 0 & \text{if } s \leq 0, \\ \dfrac{1}{2}\left\{1 \;+\; \tanh\left(\Xi(s)\right)\right\} & \text{if } 0 < s < 1, \\ 1 & \text{if } s \geq 0, \end{cases} \tag{4.78a}$$

$$\text{with} \qquad \Xi(s) \;\equiv\; \tan\left[\pi\,\left(s - \frac{1}{2}\right)\right]. \tag{4.78b}$$

The main idea is to have a forward transformation, the tangent function in $\Xi(s)$ in this case, mapping the finite interval $s \in (0, 1)$ on the whole real domain $\mathbb{R}$. And a backward transform mapping the real axis $\mathbb{R}$ to the finite interval from zero to one. The backward transform has to go faster to zero and one, than the forward transform goes to infinity: while the tangent function behaves like $(\frac{\pi}{2} - |x|)^{-1}$ near $x = \pm\frac{\pi}{2}$, the hyperbolic tangent approaches its limits ± 1 exponentially fast.

In the steep-slope variants of the variational models used, also the bottom slope and curvature are needed. So we need the first and second derivative of $\Upsilon(s)$. The first derivative of $\Upsilon(s)$ is:

$$\frac{\mathrm{d}\Upsilon}{\mathrm{d}s} \;=\; \begin{cases} \dfrac{\pi}{2}\left\{1 \;-\; \tanh^2\left(\Xi(s)\right)\right\}\left\{1 \;+\; \Xi^2(s)\right\} & \text{if } 0 < s < 1, \\ 0 & \text{elsewhere.} \end{cases} \tag{4.79}$$

And the second derivative is:

$$\frac{\mathrm{d}^2\Upsilon}{\mathrm{d}s^2} = \begin{cases} \pi^2\left\{1 - \tanh^2\left(\Xi(s)\right)\right\}\left\{1 + \Xi^2(s)\right\} \\ \qquad \times\left\{\Xi(s) - \left[1 + \Xi^2(s)\right]\,\tanh\left(\Xi(s)\right)\right\} & \text{if } 0 < s < 1, \\ 0 & \text{elsewhere.} \end{cases} \tag{4.80}$$

Other mappings are also possible, *e.g.* for the forward mapping use $\widehat{\Xi}(s) = (s - \frac{1}{2})/(s^2 - s)$, but for the present application the chosen form has the advantage that it is closer to a linear function over a wider stretch of the interval $s \in (0, 1)$. For another example, using the same technique, see Dingemans (1997, p. 580).

Appendix 4.C Determination of the x-derivatives of $\kappa(x)$

The parameter field $\kappa(x)$ is specified through the use of the linear-theory dispersion relation:

$$\omega_c^2 \;=\; g\,\kappa\,\tanh\left(\kappa\,h\right), \tag{4.81}$$

with ω_c a constant and a characteristic angular frequency for the problem at hand, and chosen beforehand. Taking the derivatives with respect to x we get:

$$\kappa' \;=\; -\,\kappa^2\,\frac{1\,-\,\mathcal{T}^2}{\mathcal{T}\,+\,\kappa\,h\,\left(1\,-\,\mathcal{T}^2\right)}h' \quad \text{and} \tag{4.82a}$$

$$\begin{aligned}\kappa'' \;=\; & -\,\kappa^2\,\frac{1\,-\,\mathcal{T}^2}{\mathcal{T}\,+\,\kappa\,h\,\left(1\,-\,\mathcal{T}^2\right)}h'' \\ & +\,2\,\kappa^3\,\left(1\,-\,\mathcal{T}^2\right)\,\frac{\mathcal{T}\,\left(2\,-\,\mathcal{T}^2\right)\,+\,\kappa\,h\,\left(1\,-\,\mathcal{T}^2\right)^2}{\left[\mathcal{T}\,+\,\kappa\,h\,\left(1\,-\,\mathcal{T}^2\right)\right]^3}\,\left(h'\right)^2,\end{aligned} \tag{4.82b}$$

where $\mathcal{T} \;=\; \tanh\left(\kappa\,h\right)$.

4.8 References

Booij, N. 1983 A note on the accuracy of the mild-slope equation. *Coastal Eng.* **7** (3), 191–203.

Broer, L. J. F. 1974 On the Hamiltonian theory of surface waves. *Appl. Sci. Res.* **29**, 430–446.

Chamberlain, P. G. & Porter, D. 1995 The modified mild-slope equation. *J. Fluid Mech.* **291**, 393–407.

Dingemans, M. W. 1985 Surface wave propagation over an uneven bottom; evaluation of two-dimensional horizontal wave propagation models. *Tech. Rep.*. Delft Hydraulics, Delft, The Netherlands. W301 part 5, 117 pp. & 70 figures.

Dingemans, M. W. 1997 *Water wave propagation over uneven bottoms*, *Adv. Ser. on Ocean Eng.*, vol. 13. World Scientific, Singapore. 2 Parts, 967 pp.

Kajiura, K. 1961 On the partial reflection of water waves passing over a bottom of variable depth. In *Proc. of the Tsunami Meeting, Univ. of Hawaii, IUGG Monograph*, , vol. 24, pp. 206–228.

Klopman, G., Dingemans, M. W. & van Groesen, E. 2005 A variational model for fully non-linear water waves of Boussinesq type. In *Proc. 20th Int. Workshop on Water Waves and Floating Bodies,* Longyearbyen, Spitsbergen, Norway, May 2005.

Klopman, G., van Groesen, E. & Dingemans, M. W. 2010 A variational approach to Boussinesq modelling of fully non-linear water waves. *J. Fluid Mech.* Accepted for publication.

Madsen, P. A., Fuhrman, D. R. & Wang, B. 2006 A Boussinesq-type method for fully nonlinear waves interacting with a rapidly varying bathymetry. *Coastal Eng.* **53** (5-6), 487–504.

Mei, C. C. & Black, J. L. 1969 Scattering of surface waves by rectangular obstacles in waters of finite depth. *J. Fluid Mech.* **38** (3), 499–511.

Miles, J. W. 1977 On Hamilton's principle for surface waves. *J. Fluid Mech.* **83** (1), 153–158.

Porter, D. & Chamberlain, P. G. 1997 Linear wave scattering by two-dimensional topography. In *Gravity waves in water of finite depth* (ed. J. N. Hunt), *Adv. Fluid Mech.*, vol. 10, pp. 13–53. Comput. Mech. Publ.

Porter, R. & Porter, D. 2006 Approximations to the scattering of water waves by steep topography. *J. Fluid Mech.* **562**, 279–302.

Rey, V., Belzons, M. & Guazzelli, E. 1992 Propagation of surface gravity waves over a rectangular submerged bar. *J. Fluid Mech.* **235**, 453–479.

Zakharov, V. E. 1968 Stability of periodic waves of finite amplitude on the surface of a deep fluid. *J. Appl. Mech. and Techn. Phys.* **9** (2), 190–194. Originally in: *Zhurnal Prildadnoi Mekhaniki i Tekhnicheskoi Fiziki* **9**(2), pp. 86–94, 1968.

Chapter 5

Conclusions and recommendations

5.1 Conclusions

A method has been presented to construct Boussinesq-like equations with positive-definite Hamiltonian – the sum of the kinetic and potential energy – for surface gravity waves. The resulting two-dimensional horizontal (2DH) models, Eqs. (2.15), consist of two evolution equations: a mass-conservation equation describing the time development of the free surface elevation, and the evolution of either the free-surface velocity potential or its gradient, a 'surface velocity'. Besides, depending on the number of shape functions used in the flow approximations, one or several elliptic equations have to be solved for 2DH flow parameter fields describing the vertical structure of the flow. These elliptic equations are linear in the flow parameter fields for which they are to be solved, and result in symmetrical positive-definite matrices due to the variational description with a positive-definite Hamiltonian.

All equations contain only low-order spatial derivatives, at most second-order for the formulation in the free-surface velocity potential, and third-order if written in terms of its gradient. No mixed time–space derivatives occur.

The vertical flow structure beneath the free surface is approximated as the sum of the free-surface potential plus a limited number of shape functions controlled by 2DH-varying parameters. All approximations have to be made *before* the resulting flow velocities are applied to the kinetic-energy part of the Hamiltonian. This guarantees that the approximate Hamiltonian stays positive-definite. The used approach transfers several conservation properties from the exact Hamiltonian to the approximate one(s), *e.g.*: mass conservation, energy conservation and – for a horizontal bed – horizontal momentum conservation. Moreover, the resulting flow model is fully non-linear, since no approximations are made in this respect. Note however, that the *non-linear performance* of the model does depend on the approximations made with respect to the vertical structure of the flow velocities, see *e.g.* Figure 1.3.

In this thesis, two variational Boussinesq models (VBM's) have been considered into more detail, both using one shape function for the vertical flow structure: the parabolic VBM – corresponding with the 'classical' parabolic vertical structure for fairly long waves, as used by Boussinesq – and the hyperbolic-cosine (cosh) VBM, with the cosh structure as found in Airy wave theory for waves on arbitrary depth. Both for the parabolic and the cosh model, mainly the quasi-homogeneous ('mild-

slope') approximations have been used in the horizontal-velocity approximations: the effects of bottom slope and the κ-parameter gradient $\boldsymbol{\nabla}\kappa$ (in the cosh VBM) have been neglected in order to simplify the resulting models. Several linear wave characteristics of the models have been studied: dispersion, shoaling and reflection; as well as their non-linear performance in several numerical test cases.

The solution of an elliptic equation has limited impact on the computational efforts, because of the positive-definiteness and symmetry of the associated matrices. Also good preconditioners have been found for the used conjugate gradient method. The additional effort – in terms of CPU time – for solving the elliptic equation, as compared with the CPU time needed for the time evolution of the mass and momentum equations, is about 30% to 50%.

The **parabolic VBM** performs well for relative water depths $kh_0 < \pi$, *i.e.* for wave lengths λ in excess of twice the water depth h_0: the phase speed error is less than 3%, and the wave amplitude errors due to shoaling are less than 10%. For $kh_0 < \frac{1}{2}\pi$ ($\lambda > 4h_0$) the shoaling errors are less than 1%. Linear reflection characteristics of the parabolic VBM are good for the full model – without the quasi-homogeneous approximation – for slopes up to 1:2.5 (one meter bottom change over 2.5 m horizontal stretch), and can be made good for the quasi-homogeneous parabolic VBM by use of a proper normalisation of the vertical shape function. The normalisation affects the neglected terms in the quasi-homogeneous approximation, and is chosen in a way to minimise these neglected terms.

Several non-linear test cases – periodic waves over a horizontal bed, periodic wave deformation by an underwater bar, oblique periodic waves propagating over an elliptic shoal on a plane beach, and propagation of a confined wave group into a region of shallow water or over an underwater bar – show the capacities of the parabolic VBM. Good agreement is found in the comparison with either laboratory experiments or with the results of numerical models solving the full non-linear equations. It must be noted however, that most of the shown cases are for slowly-varying waves. For random waves, with a broader wave spectrum of *e.g.* JONSWAP form, wave lengths easily become short (with respect to water depth) for wave components at a few at times the spectral peak frequency, in the spectral tail. For these cases, as well as for waves at mid sea, the parabolic VBM will perform less well.

The **cosh VBM** can be tuned, through its parameter κ, to have the exact phase and group velocity – according to Airy wave theory – for a certain wave number and at a certain water depth. As a result, linear waves of fixed frequency can be made to have exact shoaling, since the VBM satisfies wave action conservation for slowly-varying waves, as a direct consequence of its variational description and Whitham's average Lagrangian method. With respect to linear wave reflection, the quasi-homogeneous cosh VBM has excellent reflection characteristics using an optimised normalisation of the cosh shape function. The capacities of the cosh VBM with respect to non-linear wave propagation are even better than those of the parabolic VBM (see Figure 1.8, for highly non-linear solitary waves).

5.2 Recommendations

Several efforts are already being made towards the further development and implementation of variational Boussinesq models. Within the Department of Applied Mathematics at the University of Twente – and in collaboration with LabMath-Indonesia – progress is made with respect to *e.g.* finite-element implementations, optimisation of κ in the cosh VBM, internal wave-generation zones (Koop, 2006; van Groesen *et al.*, 2008; Adytia & van Groesen, 2009; Kristina, 2009; Lakhturov & van Groesen, 2010). Also within industry, implementations of VBM equations are under development at the moment.

For waves of infinitesimal amplitude, the cosh VBM has exact phase velocity Ω/k and group velocity $\partial_k\Omega$, *i.e.* the first derivative of the dispersion equation $\Omega(k)$. However, it does not have the correct curvature $\partial_k^2\Omega$, and this parameter is of direct importance for the correct modelling of deep-water wave groups (Zakharov, 1968; Dysthe, 1979). It is not possible to obtain the correct curvature with only one shape function, as has been used in all practical examples shown here. Therefore, it is recommended to investigate an extended cosh model with two shape functions.

For practical applications, it is important to be able to model the effects of wave breaking. The incorporation of breaking waves into the variational Boussinesq model can be undertaken by extending the bore approach as used in the shallow water equations. The challenge is to find jump conditions (Rankine–Hugoniot conditions) across the breaker. The symmetries and associated conservation laws for the underlying variational principles can be of help here (Benjamin & Olver, 1982), as they are for the shallow water equations. Besides equality of the mass and horizontal momentum fluxes across the jump, two additional jump conditions – still to be sought – are needed for a VBM with one shape function.

Bottom friction at the sea bed is also important in many shallow-water applications, and can easily be incorporated, through the addition of a quadratic friction law in the momentum equations. Although the VBM is derived (here) from a potential flow description – *i.e.* a flow which cannot transfer shear stresses – the resulting 2DH equations no longer have this restriction. This is because the bed shear stress has the appearance of as a 'body force' in the VBM momentum equations.

Another aspect of importance for wave propagation over longer stretches is wind input. Often, wave energy lost by whitecapping is re-supplied through the forcing by the wind. While free-surface pressure forcing can be incorporated directly from the start in the variational description, forcing by wind shear can be added afterwards to the VBM momentum equations, in a similar fashion as the bottom shear stress. The challenge here is to obtain the correct in-phase forcing of the wind on the waves.

5.3 References

Adytia, D. & van Groesen, E. 2009 Variational Boussinesq model for simulations of coastal waves and tsunamis. In *Proc. 5th Int. Conf. on Asian and Pacific Coasts, APAC 2009,* 13-16 October 2009, Singapore, Thailand.

Benjamin, T. B. & Olver, P. J. 1982 Hamiltonian structure, symmetries and conservation laws for water waves. *J. Fluid Mech.* **125**, 137–185.

Dysthe, K. B. 1979 Note on a modification to the nonlinear Schrödinger equation for application to deep water waves. *Proc. R. Soc. London A* **369**, 105–114.

van Groesen, E., Adytia, D. & Andonowati 2008 Near-coast tsunami waveguiding: phenomenon and simulations. *Nat. Hazards Earth Syst. Sci.* **8** (2), 175–185.

Koop, O. R. 2006 *Continuous and discontinuous Galerkin finite element methods of variational Boussinesq water-wave models*. Master's Thesis, University of Twente, Department of Applied Mathematics, Enschede, The Netherlands.

Kristina, W. 2009 *Wave reflection over flat and slowly varying bathymetry modeled by effective boundary conditions*. Master's Thesis, University of Twente, Department of Applied Mathematics, Enschede, The Netherlands.

Lakhturov, I. & van Groesen, E. 2010 Optimized Variational Boussinesq Modelling for broad-band waves over flat bottom. *Submitted for publication* .

Zakharov, V. E. 1968 Stability of periodic waves of finite amplitude on the surface of a deep fluid. *J. Appl. Mech. and Techn. Phys.* **9** (2), 190–194. Originally in: *Zhurnal Prildadnoi Mekhaniki i Tekhnicheskoi Fiziki* **9**(2), pp. 86–94, 1968.

Appendix A

Confined wave groups over an underwater bar[1]

In Chapter 2, several numerical experiments with the one-dimensional version of the parabolic VBM are described in §2.6. Here, another case of the propagation and transformation of a confined wave group is considered, with the same initial characteristics as the other cases in §2.6.3: *i.e.* an initial water depth of $h_0 = 12$ m, a carrier wave period of 6 s ($\omega_0 = \frac{1}{3}\pi$ rad/s), a carrier wave amplitude in the group center of $a_0 = 1.0$ m and the gravitational acceleration is $g = 9.81$ m/s^2.

This example considers the propagation of the confined wave group over an underwater bar. This case has also been computed by Dingemans *et al.* (1991), using the evolution equations for the wave envelope and the long waves of Liu & Dingemans (1989). The topography of the underwater bar is given by:

$$h_0(x) \;=\; h_\infty \;-\; \frac{1}{2}\left\{ \tanh\left[\left| \frac{2\,s_a}{\Delta_h} \right| (x - x_a) \right] \;-\; \tanh\left[\left| \frac{2\,s_b}{\Delta_h} \right| (x - x_b) \right] \right\} \Delta_h, \tag{A.1}$$

with h_∞ the water depth far from the bar, Δ_h the height of the bar, s_a and s_b the maximum front and back bar-slopes, and x_a and x_b the associated deflection points. In all results presented, we used $s_a = s_b = 0.01$, $x_a = 7.5$ km and $x_b = 10.5$ km. Besides the case $\Delta_h = 4$ m, as considered in Dingemans *et al.* (1991), we have also computed the case $\Delta_h = 6$ m. The periodic computational domain has a length of 40 km, to prevent disturbances in the domain of interest of fast-traveling long waves. The duration of the computations is for a physical time of 3600 s, *i.e.* 600 carrier-wave periods.

The surface elevations $\zeta(x,t)$, at several moments in time, are presented in Figures A.1(a)–(d). Clearly the generation of free long waves, as well as the deformation of the wave group can be seen. The free long waves compare quite well with the results of Dingemans *et al.* (1991), see Figures A.1(e)–(f): in our computations the maximum elevation is 0.041 m and the minimum is -0.024 m. In Dingemans *et al.* (1991) the maximum and minimum are 0.033 m and -0.024 m. Note that the space

[1] This Appendix has been part of a previous version of the paper presented in Chapter 2:

Klopman, G., van Groesen, E. & Dingemans, M. W. 2010 A variational approach to Boussinesq modelling of fully non-linear water waves. *J. Fluid Mech.* Submitted for publication.

It is omitted from its last revision in order to reduce the paper's length.

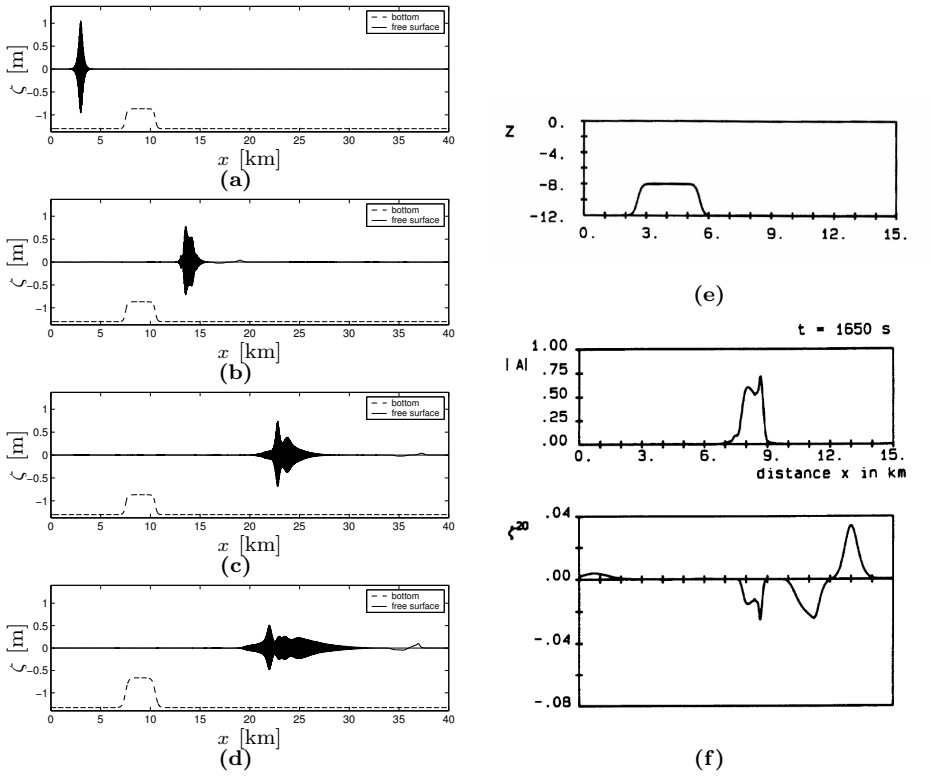

Figure A.1: Confined wave group propagation over an underwater bar: surface elevation $\zeta(x,t)$ as a function of x. Left column: present model; (a) $t = 0$ s, water depth above bar $h_0 = 8$ m, (b) $t = 1920$ s, water depth above bar $h_0 = 8$ m, (c) $t = 3600$ s, water depth above bar $h_0 = 8$ m, (d) $t = 3600$ s, water depth above bar $h_0 = 6$ m; the dashed line indicates the bottom topography (not on scale). Right column: from Dingemans *et al.* (1991); (a) Figure 2, bottom topography and (b) Figure 6, wave envelope amplitude $|A|$ and long wave elevation $\zeta^{(20)}$, in their notation.

x and time t of our computations are shifted in relation to Dingemans *et al.* (1991): the moment $t = 1920$ s is about the same as $t = 1650$ s in Dingemans *et al.* (1991).

As kan be seen from Figures A.1(b) and (f), the shape of the wave group in both models is quite different: in Dingemans *et al.* (1991) the group splits into a higher-amplitude group in front, followed by a lower-amplitude one, and the front of the wave group is very steep. For the parabolic structure model, the opposite occurs: a lower-amplitude group is followed by a higher-amplitude group. Furthermore, the start of the wave train is very smeared. This becomes even more apparent for the case with the higher bar, $\Delta_h = 6$ m, see Figure A.1(d).

To gain more insight into the evolution of the wave groups and the differences with the results of Dingemans *et al.* (1991), we have computed the spatial Fourier transform $A(k,t)$ of the surface elevation $\zeta(x,t)$. In figure A.2, the amplitude spectra $|A(k,t)|$ are plotted, as a function of kh_∞, with h_∞ the water depth in the deeper horizontal parts of the cases considered. The amplitude spectra have been normalised using the maximum of $|A(k,0)|$ at $t = 0$. Besides the carrier wave con-

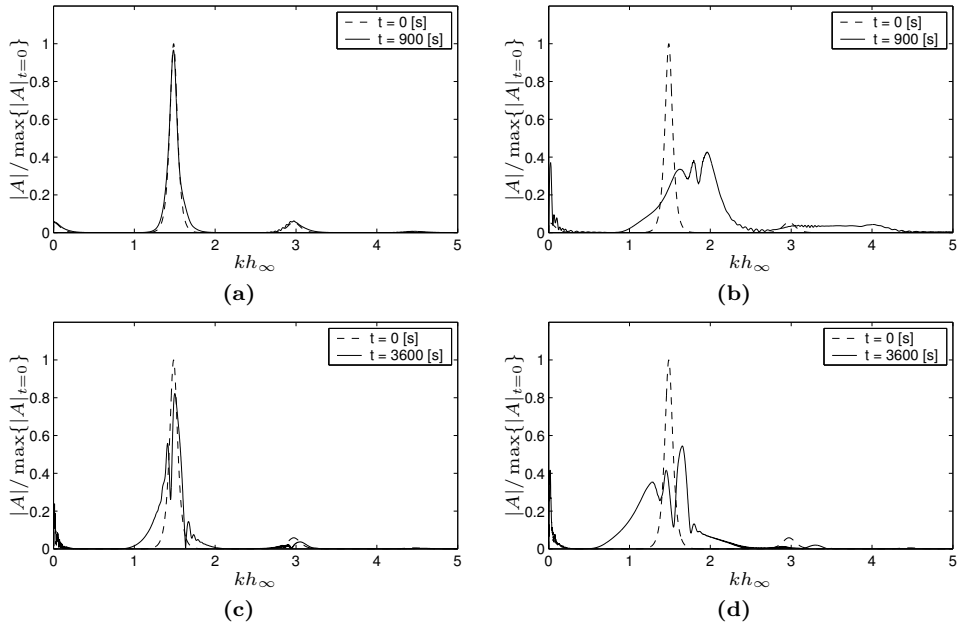

Figure A.2: Amplitude spectra $|A(k,t)|$ of the surface elevation as a function of dimensionless wave number kh_∞, for confined wave groups propagating over an underwater bar. The dashed lines are for the initial situation at $t = 0$ s, and the solid lines for the times indicated below: (a) $t = 900$ s, horizontal bed case, (b) $t = 900$ s, slope case, (c) $t = 3600$ s, underwater bar case with water depth above bar $h_0 = 8$ m, and (d) $t = 3600$ s, underwater bar case with water depth above bar $h_0 = 6$ m.

tributions around $kh_\infty = 1.49$, the non-linear sub-harmonics near $kh_0 = 0$ and super-harmonics near $kh_\infty = 2.98$ are visible. As can be seen from Figure A.2(c) and A.2(d), behind the bar part of the carrier waves have relative wave numbers $kh_\infty < 1.36$, and are therefore in the defocussing class of NLS equations. This is especially true for the higher bar with $\Delta_h = 6$ m.

When looking in detail into the waves at the front of the wave trains at $t = 3600$ s (not shown), the front waves are longer and have $kh_0 < 1.36$. The front waves for the case $\Delta_h = 6$ m are longer than for the case $\Delta_h = 4$ m. This explains why the wave group in Figure A.1(d) has progressed further than the lower-bar case in figure A.1(c), despite the fact that are waves are more slowed down on top of the bar when the water depth is shallower.

In the computations of Dingemans *et al.* (1991) with a NLS-type model for the wave envelope evolution, the carrier-wave frequency ω_0 is a constant in the whole spatial domain. The carrier-wave number $k_0(x)$ is computed using the local water depth $h_0(x)$ and the linear dispersion relationship. So, $k_0(x)$ will be (almost) a constant in the parts of the domain away from the bar. Then, also the coefficients of their NLS-type model, being a function of $k_0(x)$, will be constant. However, as seen from the results with the parabolic structure model, the carrier wave number changes throughout the domain, being smaller (and even in the defocussing regime) in the

front of the wave train. For the higher bar, $\Delta_h = 6$ m, the amplitude spectrum of the wave group, far behind the bar at $t = 3600$ s, even has become quite broad-banded, see figure A.2(d). The spatial and temporal variations of the carrier-wave number k_0 may explain the differences for the evolution of the wave envelope in both models, since they are not accounted for in the approach by Dingemans *et al.* (1991).

While trailing tails have often been observed in the deformation of water-wave solitons due to bathymetry, we here observe the generation of a forerunning front of the wave envelope. This is probably due to the fact, that the deeper parts of the domain are in the focussing regime, but the shallow region on top of the bar is in the defocussing regime. The defocussing on top of the bar causes a spatial separation of longer and shorter waves. And the longer waves stay in the defocussing regime after the bar, forming the forerunning front.

A.1 References

Dingemans, M. W., Petit, H. A. H., Meijer, T. J. G. P. & Kostense, J. K. 1991 Numerical evaluation of the third-order evolution equations for weakly nonlinear water waves propagating over uneven bottoms. In *Proc. Computer Modelling in Ocean Eng. '91,* Barcelona, Spain (ed. A. S. Arcilla, M. Pastor, O. C. Zienkiewicz & B. A. Schreffler), pp. 361–370. Balkema, Rotterdam.

Liu, P. L.-F. & Dingemans, M. W. 1989 Derivation of the third-order evolution equations for weakly nonlinear water waves propagating over uneven bottoms. *Wave Motion* **11** (1), 41–64.